Stony Brook University

Development of New Generation of Ceramics for Environmentally Focused Chemical Separations

A Dissertation Presented

by

Girish Ramakrishnan

to

The Graduate School

in Partial Fulfillment of the

Requirements

for the Degree of

Doctor of Philosophy

in

Materials Science and Engineering

Stony Brook University

August 2015

Stony Brook University

The Graduate School

Girish Ramakrishnan

We, the dissertation committee for the above candidate for the

Doctor of Philosophy degree, hereby recommend

acceptance of this dissertation.

Dr. Alexander Orlov – Dissertation Advisor
Associate Professor, Department of Materials Sciences and Engineering

Dr. Tae Jin Kim - Chairperson of Defense
Assistant Professor, Department of Materials Sciences and Engineering

Dr. Gary Halada - Committee Member
Associate Professor, Department of Materials Sciences and Engineering

Dr. Harold Walker - Committee Member
Professor & Director, Department of Civil and Environmental Engineering

This dissertation is accepted by the Graduate School

Charles Taber

Dean of the Graduate School

Abstract of the Dissertation

Development of New Generation of Ceramics for

Environmentally Focused Chemical Separations

by

Girish Ramakrishnan

Doctor of Philosophy

in

Materials Science and Engineering

Stony Brook University

2015

This dissertation focuses on the use of composite materials for environmental applications. For the first time, application of both fresh and aged concrete as inexpensive adsorbents for nitrogen dioxide (NO2) removal is demonstrated. Concrete is the most widely used composite material of the modern era. Cement manufacturing (a major component of concrete) is considered to be one of the leading contributors to air pollution, resulting in 7% of the global carbon dioxide emissions along with a number of other harmful pollutants such as oxides, mercury and particulates. These emissions aide in the formation of acid rain, smog, and toxic ground level ozone, causing detrimental effects such as respiratory illnesses, visibility reduction, eutrification and global warming. This thesis offers a novel and sustainable solution in mitigating NO_X emissions, by introducing the significant adsorption potential of recycled concrete. The work is based on both commercially available cement paste and already aged

concrete samples, providing truly scalable solutions. The concrete samples aged for different periods of time were exposed to NO_2 to measure their adsorption capacity. The results show that all of the concrete samples (fresh and aged) exhibited excellent NO_2 adsorption capacity, with the fresh concrete samples removing almost 100% of the NO_2. Furthermore, to compare the effects of long term aging, 12 year-old recently demolished concrete samples were obtained and its NO_X removal was shown to be almost 60%. The experimental results provide evidence of nitrate and nitrite species formation from chemical reactions occurring between NO_2 and surface alkaline species. This important discovery can be utilized for NO_2 removal and subsequent NO_X sequestered demolished concrete (NSDC) recycling in new concrete, either as a set accelerating admixture or as a corrosion inhibitor, a big leap towards better sustainability and longevity of the new reinforced concrete structures.

The rest of this thesis focuses on development of a new generation of ceramic membranes utilizing thermal spray techniques to produce highly scalable and extremely cost effective filtration membranes. Thermal spray method of membrane manufacturing has the advantage of economic scalability (up to tens of square meters) along with performance enhancement as compared to conventional wet casting process. In addition to developing a proof of concept for this approach, several strategies on how to improve ceramic membranes' performance via spraying process optimization are also described. Specifically, several thermal sprayed Alumina membrane samples were prepared by varying different process parameters. These samples were characterized using known techniques and subjected to permeability and size exclusion tests to correlate spraying parameters with membranes' performance. The membrane samples showed excellent clean water flux comparable to commercially available membranes and had rejection rates up to 96%. These results show that the membranes produced in this research achieve

outstanding performance at a fraction of the cost of commercially produced membrane, enabling the use of membrane filtrations units in developing countries.

Dedicated to my parents.

Table of Contents

Contents

Table of Contents vii

List of Figures xii

List of Tables xvi

List of Abbreviations xvii

Acknowledgments xix

Publications xx

Prologue xxii

Chapter 1 Introduction 1

1.1 Ceramics for Environmental Applications 2

1.2 Overview of Concrete 5

1.3 Concrete Preparation 9

1.4 Types of Concrete 10

1.5 Emissions due to cement manufacture 12

1.6 NO_X and SO_X emissions 14

1.7 Summary 17

Chapter 2 Use of Concrete for Sequestration 18

2.1 Introduction 19

2.2 Demolished Concrete as Adsorbent 23

2.3 Beneficial Reuse of Demolished Concrete 29

2.4 Summary 30

Chapter 3 Characterization Techniques 32

3.1 Introduction 33

3.2 X-Ray Diffraction (XRD) 33

3.3 Diffuse Reflectance Infrared Fourier Transform Spectroscopy (DRIFTS) 35

3.4 Scanning Electron Microscopy (SEM) 37

3.5 X-ray Absorption Near Edge Structure (XANES) 39

3.6 Flow Reactor Experiments 42

Chapter 4 NO_X Adsorption by Crushed Concrete 44

4.1 Introduction 45

4.2 Sample Preparation 45

4.3 Survey of Different materials for NOx Adsorption 47

4.4 Flow Reactor Measurements 48

4.5 DRIFTs Analysis of NO_X Adsorption 53

4.6 Fixed Bed Breakthrough Curves 56

4.7 Summary 63

Chapter 5 SO_X Adsorption by Crushed Concrete 64

5.1 Introduction 65

5.2 XRD Analysis 66

5.3 DRIFTs reactor experiments 68

5.4 Time Resolved DRIFTs spectra 73

5.5 XANES experiments 75

5.6 Summary 77

Chapter 6 Introduction to Membranes Filtration 78

6.1 Membranes for Water Filtration 79

6.2 Types of Membrane Processes 84

6.3 Membrane Classification 89

6.3.1 According to membrane material 89

6.3.2 According to membrane configuration 91

6.3.3 According to filtration setup 93

6.4 Traditional Methods of Ceramic Membranes Preparation 96

6.4.1 Tape Casting/Rolling 97

6.4.2 Vapor Deposition 98

6.4.3 Extrusion 100

6.4.4 Pressing/sintering 103

6.4.5 Slip casting/sintering 104

6.4.6 Sol-Gel Method 105

6.4.7 Dip Coating 107

6.5 Need for scalable membranes 108

Chapter 7 Thermal Sprayed Membranes for Water Filtration 111

7.1 Introduction to Thermal Spray Technique 112

7.2 Advantages of Thermal Spray over Conventional Methods 114

7.3 Material Selection and Process Parameters 116

7.4 Sample Preparation and Characterization 119

7.5 Morphology and Porosity Analysis 123

7.6 Summary 125

Chapter 8 Optimization of Process Parameters 126

8.1 Thermal Spray Process Parameters 127

8.2 Evaluation of membranes' performance 130

8.3 Dead-end Filtration Theory 131

8.4 Effect of process parameters 136

8.5 Summary 139

Chapter 9 Concluding remarks and future work 140

9.1 Concluding Remarks 141

9.2 Future Challenges 143

Bibliography 145

List of Figures

Figure 1.1: Comparison of global cement consumption 6

Figure 1.2: Global cement production capacity according to region 12

Figure 1.3: Global NO_X and SO_X emissions over the past 40 years according to region 14

Figure 1.4: Environmental and Health impacts of NO_X pollution 16

Figure 2.1: Global urban population according to region from 1960 to 2011 20

Figure 2.2: Strategies for mitigating emissions from cement production plants 21

Figure 2.3: FTIR spectra of Nitrogen and Sulphur species from the NIST database 27

Figure 2.4: Dependence between pH and concrete age for concrete samples 28

Figure 3.1: Schematic of X-ray diffraction instrument 34

Figure 3.2: 3D Cross Section representation of DRIFTS environmental cell 35

Figure 3.3: Schematic diagram of DRIFTS cell 37

Figure 3.4: Schematic of SEM system 38

Figure 3.5: Illustrative X-ray absorption spectrum of a transition metal atom. 40

Figure 3.6: Schematic illustration of an X-ray absorption edge 41

Figure 3.7: Experimental system for testing NO_2 removal from gas phase 43

Figure 4.1: Concrete slab sample 46

Figure 4.2: Crushed concrete samples in a capillary tube 46

Figure 4.3: Evaluation of NO_2 conversion on various building materials. 47

Figure 4.4: Schematic of the (A) flow and (B) fixed bed reactor system 48

Figure 4.5: Schematic diagram of the DRIFTs reactor cell 50

Figure 4.6: Flow reactor results 51

Figure 4.7: Time resolved IR spectra of crushed concrete 53

Figure 4.8: FTIR spectra of Portlandite powder after NO_2 adsorption 55

Figure 4.9: SEM images of concrete 56

Figure 4.10: Fixed bed reactor data: Graphs I & II show breakthrough curves 57

Figure 4.11: XRD comparison of fresh and aged concrete 59

Figure 4.12: NO_2 breakthrough curves 62

Figure 5.1: XRD spectra of Cement and 3 concrete samples showing different phases 67

Figure 5.2: IR spectra C+W sample before (black) and after (red) exposure to SO_2 69

Figure 5.3: IR spectra C+W+F sample before (black) and after (red) exposure to SO_2 71

Figure 5.4: IR spectra C+W+F+Cr sample before (black) and after (red) exposure to SO_2 72

Figure 5.5: Time resolved IR spectra of concrete 74

Figure 5.6: XANES spectra of the reference cement and the SO_2 exposed concrete samples 76

Figure 6.1: Overview of membrane separation process 80

Figure 6.2: Filtration spectrum - Particle size chart for filtration applications 83

Figure 6.3: Schematic representation of microfiltration 84

Figure 6.4: Schematic representation of ultrafiltration 85

Figure 6.5: Schematic representation of reverse osmosis 87

Figure 6.6: Schematic representation of nanofiltration 88

Figure 6.7: Different types of membrane configurations available today 91

Figure 6.8: Schematic of filtration processes (a) dead end vs (b) cross flow 94

Figure 6.9: A generalized flow sheet for preparation of ceramic membranes 96

Figure 6.10: Tape casting process of membrane production 98

Figure 6.11: Vapor deposition process 99

Figure 6.12: Extrusion method 101

Figure 6.13: Pressing method 103

Figure 6.14: Slip casting method 104

Figure 6.15: Sol-Gel method..... 105

Figure 6.16: Dip coating method 107

Figure 7.1: Schematic diagram showing the plasma spray process 113

Figure 7.2: Schematic of the (a) plasma spray process (b) SEM image of spray cross section showing various features..... 116

Figure 7.3: (a) Schematic of the filtration system showing the filtration cell (b) Photo of the actual cell and one of the prepared membranes 118

Figure 7.4: XRD spectra of the prepared membranes..... 120

Figure 7.5: Surface morphology, EDAX Spectra and Cross Section SEM of the prepared membranes 122

Figure 7.6: SEM images of the as prepared 300 µm thick membranes 123

Figure 8.1: Visual representation of dead-end filtration process 130

Figure 8.2: Dead-end filtration cell used for the experiments described in this thesis 131

Figure 8.3: Clean water flux vs thickness for the prepared membranes 133

Figure 8.4: Flux vs Rejection rate..... 136

List of Tables

Table 2.1: Uncontrolled NO_X Emissions (pounds per ton [lb/t]) by Kiln Type 22

Table 2.2: The pH values of seawall concrete as a function of depth 24

Table 3.1: Absorption edges 41

Table 4.1: BET Surface area and Pore size..... 60

Table 7.1: Processing conditions for the thermal spray samples 117

Table 8.1: Porosity and Pore size variation across prepared 300 µm thick membranes..... 138

List of Abbreviations

AFt	Ettringite
AFm	Monosulfoaluminate
APS	Atmospheric Plasma Spray
ASTM	American Society for Testing and Materials
BET	Brunauer-Emmett-Teller
CFS	Controlled Flame Spray
DRIFTS	Diffuse Reflectance Infrared Fourier Transform Spectroscopy
EDX	Energy Dispersive X-ray Spectroscopy
FTIR	Fourier Transform Infrared Spectroscopy
HVOF	High Velocity Oxygen Fuel
LMH	Liters per Meters squared per Hour
MCT	Mercury Cadmium Telluride
MF	Micro Filtration
MFC	Mass Flow Controller
NF	Nano Filtration

NIST	National Institute of Standards and Technology
NO_X	Nitrogen Oxides
NSDC	Nitrogen Sequestered Demolished Concrete
RO	Reverse Osmosis
SCCM	Standard Cubic Centimeters per Minute
SCR	Selective Catalytic Reduction
SEM	Scanning Electron Microscopy
SNCR	Selective Non Catalytic Reduction
SOFC	Solid Oxide Fuel Cell
TS	Thermal Spray
UF	Ultra Filtration
VPS	Vacuum Plasma Spray
VOC	Volatile Organic Compounds
XANES	X-ray Absorption Near Edge Structure
XRD	X-ray Diffraction

Acknowledgments

I would like to start by thanking my advisor, Dr. Alexander Orlov, for giving me the opportunity, support and guidance throughout my time at Stony Brook. I was able to accomplish all that I have only because of his thoughtful counsel and fantastic mentorship. I would also like to thank my committee members for providing extremely insightful inputs for my dissertation and during my thesis defense; their suggestions have vastly improved the quality of this work.

I want to also thank all my collaborators Dr. Sanjay Sampath, Dr. Gopal Dwivedi, Dr. Jyuhuk Moon, and Dr. Daniel Knopf. The discussions and constructive criticism I received from them have greatly enriched my research experience. A special thanks goes to Prof. Vlad Tarabara and his group for their generous help during the initial stages of my research on membranes.

I owe my gratitude to all the members of our group, past and present. We have been through hundreds of morning coffee meetings, BNL sessions and weekend barbecues that I will cherish for the rest of my life. Your friendship and enthusiasm has enabled me to achieve more than I possibly would have both academically and personally.

I am forever indebted to my parents for their unceasing love, support and encouragement; without which I would not be where I am. They gave me the utmost freedom to pursue my dreams and for that I am eternally grateful.

Lastly, I would like to acknowledge my partner in science and in life, Seetha Pothapragada, who has been my pillar of strength during difficult times and has made me better at everything.

Publications

Journal Publications directly related to this project

[1] **Ramakrishnan, G.,** Moon J. and Orlov A., Development of novel inexpensive adsorbents from waste concrete to mitigate SOx emissions. (In Preparation).

[2] **Ramakrishnan, G.**, Dwivedi, G., Sampath, S., Orlov, A., "Development and optimization of thermal sprayed ceramic microfiltration membranes", Journal of Membrane Science, 2015.

[3] **Ramakrishnan, G.** and Orlov A., Development of novel inexpensive adsorbents from waste concrete to mitigate NOx emissions. Building and Environment, 2014. 72: p. 28-33.

[4] **Ramakrishnan, G.**, Zhao S., W.Q. Han and A. Orlov, Simultaneous observation of gas phase and surface species in photocatalytic reactions on nanosize Au modified TiO2: The next generation of DRIFTS systems. Chemical Engineering Journal, 2011. 170(2-3): p. 445-450.

[5] Zhao, S., **Ramakrishnan, G.**, D. Su, R. Rieger, A. Koller, and A. Orlov, Novel photocatalytic applications of sub-nanometer gold particles for environmental liquid and gas phase reactions. Applied Catalysis B-Environmental, 2011. 104(3-4): p. 239-244.

Other Journal Publications

[6] Uchimiya M., Orlov A., **Ramakrishnan G.**, Sistani K., In situ and ex situ spectroscopic monitoring of biochar's surface functional groups, Journal of Analytical and Applied Pyrolysis, 2013.102, 53-59

[7] Jones K., Uchimiya M., Orlov A., **Ramakrishnan G.**, Castaldi M.J., LeBlanc J., Hiradate S., Enrichment of Carboxyl Surface Functional Groups on Low Pyrolysis Temperature Pecan Shell Biochars (In Preparation)

[8] Jones K., **Ramakrishnan G.**, Uchimiya M., Orlov A., New applications of x-ray tomography in pyrolysis of biomass: biochar imaging, Energy & Fuels 2015. 29 (3), 1628-1634

[9] Ging J., Tejerina-Anton R., **Ramakrishnan G.**, Nielsen M., Murphy K., M Gorham J.M., Nguyen T., Orlov A.; Development of a conceptual framework for evaluation of nanomaterials release from nanocomposites: Environmental and toxicological implications; Science of The Total Environment, 2014. 473, 9-19

[10] Orlov A., **Ramakrishnan G.**, Ging J., Hubert A, Feka P, Korach C. S., Evaluating safety and stability of CNT nanocomposites exposed to environmental conditions, Proceedings of the Technical Proceedings of the 2012 NSTI Nanotechnology Conference and Expo, Santa Clara, CA, 2012. 335-337

Conference Proceedings

[11] **Ramakrishnan, G.**, G. Dwivedi, S. Sampath and A. Orlov, Innovative Application of Plasma Spray Process: Manufacture of Economic and Scalable Ceramic Microfiltration Membranes. Abstracts of Papers of the American Chemical Society, 2014.

[12] **Ramakrishnan, G.** and A. Orlov, Studies of gas phase NO2 removal using fresh and recycled concrete. Abstracts of Papers of the American Chemical Society, 2013. 246.

[13] **Ramakrishnan, G.**, S. Peethamparan and A. Orlov, Utilizing demolished concrete as efficient NO2 adsorbent and beneficial concrete admixture. Abstracts of Papers of the American Chemical Society, 2013. 245.

[14] **Ramakrishnan, G.**, S. Zhao and A. Orlov, Simultaneous observation of gas phase and surface species in photocatalytic reactions: The next generation of DRIFTS applications. Abstracts of Papers of the American Chemical Society, 2010. 240.

Prologue

The research presented in this thesis is organized in two related but distinct parts with the overall focus on ceramics and composite materials for environmental applications. The first part consists of chapter 1 through chapter 5 concentrating mainly on concrete and its use as an adsorbent for sequestration of environmentally hazardous air pollutants. Chapter 6 through chapter 9 describes the second part of this thesis, investigating the use of thermal sprayed Alumina membranes for the purpose of water filtration. Finally, chapter 10 gives a short synopsis of the research in this thesis and provides a brief conclusion.

Chapter 1 provides a brief introduction about the ceramics used in environmental applications with the versatility of concrete as a construction material being the main focus. The production of concrete, the harmful emissions caused thereby and its negative effects on the environment and human health are also explained. Chapter 2 elaborates on how concrete has been used as an adsorbent and its application for sequestration of different hazardous materials including CO_2 and Mercury. This chapter provides a basis for the research described in chapters 4 and 5.

Chapter 3 contains detailed descriptions of various characterization techniques (such as X-Ray Diffraction, Scanning Electron Microscopy, Diffuse Reflectance Infrared Spectroscopy, etc) and experimental methods used throughout the thesis (as described in Chapters 4, 5, 8 and 9). The chapters themselves contain short methods sections, which present crucial information regarding methodology specific to that particular chapter, as well as references to specific sections within this chapter for further information.

Chapter 4 discusses the uptake of NO_2 on concrete, its feasibility and the possible reaction mechanism. Further, the prevalence of SO_2 and NO_2 in most practical situations necessitates study of the interactions between concrete and SO_2. Chapter 5 expands discussion on these interactions and provides additional background on significance of NO_2 interactions relevant to this research.

Chapter 6 outlines the fundamentals of membrane filtration, explaining various types of membranes, membrane materials, processes, filtration configurations and manufacturing techniques.

Chapter 7 describes different thermal spray processes and parameters involved in preparing a spray sample, elaborating on how each of these parameters affect the final membrane in terms of its chemistry and morphology. Chapter 8 presents an evaluation of the filtration testing of the membranes, with emphasis on the efficiency and the efficacy of the different thermal sprayed membrane samples. These results are correlated with the processing conditions for each of the membranes to determine the optimal processing parameters for producing membranes with the best filtration performance.

Lastly, Chapter 9 summarizes the research given in this thesis providing a brief synopsis of the insights gained over the previous chapters and conclusions reached. It also elaborates on the future challenges this research might face and provides a few possible approaches in overcoming them.

Chapter 1

Introduction

1.1 Ceramics for Environmental Applications

Ceramics cover a broad range of materials making a precise definition difficult to achieve. However, ceramics can be briefly described as nonmetallic, inorganic and refractory materials. They can be further classified into two segments, namely, traditional and advanced [15]. Clay, silicate glass and cement are considered as traditional ceramics, whereas carbides, oxides, nitrides and other non-silicate glasses fall under advanced ceramics. There are numerous advantages of using ceramics over metals and alloys. Ceramics in general have better mechanical properties such as improved stiffness and hardness combined with reduced weight when compared to high strength alloys like steel . They also possess greater corrosion and heat resistance and can be considered as viable replacements for many polymers [16]. Lastly, ceramic materials display a wide variety of properties which facilitate their use in many different product areas.

Ceramics find applications in most engineering fields though their significance has only been truly realized in the last 50 years or so. These materials possess unique properties with high melting temperatures, excellent compressive strengths, low heat and electrical conductivity, etc. Since the 1970s the ceramic industry has developed into one of the most competitive and innovative markets, as new techniques and understanding have thrust these materials to the frontier of technology. This industry today is worth tens of billions of dollars and is growing further with rapid advance in research and development discovering new applications [17].

Traditionally ceramics have been used for thousands of years. The traditional ceramics industry originated long ago. Today there are many segments of this industry. Some of the

products of traditional ceramics include pottery, tableware, sanitary ware, tiles, structural clay products, refractories, blocks, and electrical porcelain. The most common raw materials for manufacturing and processing traditional ceramic materials are clays, Silica, Dolomite, Feldspar, Calcite, Talc etc. These precursors are easily available and are generally very cheap to acquire. Now, each raw material contributes a certain property such as dry strength, plasticity, shrinkage, etc. to the ceramic body. A careful selection of materials is therefore needed to impart the desired properties required for the final output. Since most of the final products are prepared using powders it is essential to pay special attention when preparing these powders. The important parameters governing the final product requirements include particle size, particle shape, size distribution and surface area. Unlike the advanced ceramics industry, the purity of ceramic powder is not an issue in traditional ceramics[16].

In the advanced ceramics industry, special types of ceramics are used mainly for electrical, electronic, optical, and magnetic applications. Here the requirements for the precursor powders are quite different from those in the traditional ceramics industry. In fact the raw material processing plays a critical role. Advanced production techniques are employed to assure that the produced ceramic powders possess sufficient purity. Typically, ceramic powders are produced using chemical reactions like the sol-gel process or liquid gas reactions. These processing techniques are generally very expensive and as such factored into the final product [18].

One of the most prolific areas of applications for ceramic materials is the electronics industry. Due to their piezoelectric and semiconductor properties ceramic materials like Barium Titanate ($BaTiO_3$) are used to build capacitors, oscillators, sensors etc. Pumps, microphones and

sonar are other areas where the unique characteristics of ceramics materials such as ferroelectricity have been applied. Functional ceramics such Lead Zirconate Titanate, Lead Titanate, Barium Titanate and many others are utilized in the industry due to their unique properties [19].

Numerous other applications like magnetic ceramics and bio ceramics have expanded the use of these materials beyond the traditional sense. Magnetic ceramics are used for the production of antennas and inductors, while bio ceramics like alumina with high density and purity are used for dental implants, eye glasses and hip and knee replacement. Further, advanced ceramics provide an interesting alternative to wherever abrasive materials are used due to their excellent corrosion and wear resistance. The transport, mixing and or grinding of such abrasive and corrosive particles requires a high level of protection for the inherent equipment. Ceramic components ensure long life for parts that are subject to high stress during operation of such machinery. In the field of environmental technology such as water treatment plants and waste recycling centers, ceramic materials can withstand extreme temperatures and mechanical stresses. These applications for generating energy in power plant engines and turbines or in systems for photovoltaics, solar thermal energy conversion, wind and water power are ideally suited for the use of ceramic materials. Technical ceramics ensure increased performance capability of plants, environmentally friendly efficient use of resources in energy distribution and supply from both conventional and renewable energy sources [20].

However, one of the largest applications by volume for ceramic/composite materials is in the building and construction segment as elaborated in the next section.

1.2 Overview of Concrete

Concrete is the most widely used ceramic/composite material of modern times. Concrete is made by mixing 4 simple components namely cement, sand, rock and water. It is however one of the most complex materials that is still being studied today despite its use for over 1000 years [21]. In the last year alone the total concrete consumption was over 100 million tons for the U.S. which is 5 times the consumption of steel by weight. Around the world, the ratio of concrete usage versus steel is more than 1:10. In the year 2010, the steel production grew by a factor of 8 whereas concrete production increased by a factor of 25 [22]. Overall in the last few years, over 6 gigatons of concrete has been consumed by the developing world as shown in Figure 1.1. There is no other man made material that can rival concrete in terms of the amounts used. The current estimates put concrete usage at around 15 billion tons every year [23]. Steel is tougher and stronger that concrete, though there are certain important qualities that make concrete one of the most useful materials in engineering today. There are three reasons that make concrete such a widely used engineering and construction materials.

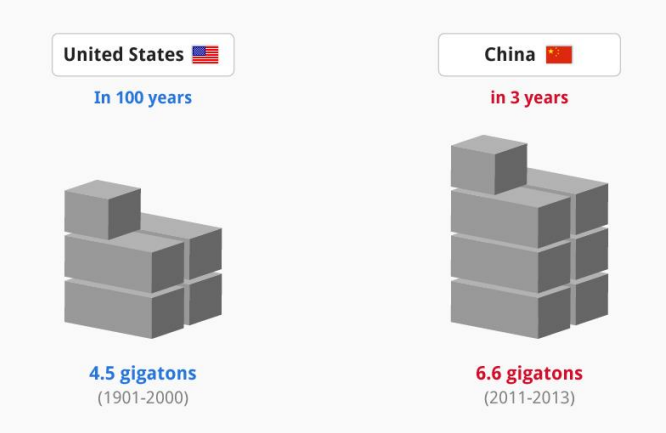

Figure 1.1: Comparison of global cement consumption (Mineral Industries of China 1990-2013, USGS)

The most important reason for the success of concrete is it excellent water resistance property [24]. Where regular steel, wood or other construction materials would face serious corrosion and damage, concrete is able to withstand water without major deterioration. This is one of the main reasons why it is used in buildings and structures that transport and store water (dams etc.). Even early Romans used concrete for their aqueducts and waterfront walls and there are believed to be concrete's earliest known applications. Dams, pavements, canal linings, etc. are some of the most commonly seen sights where concrete is used around the world.

Reinforced concrete is another application where concrete containing steel bars is used for structural purposes [25]. Many structures like pikes, foundations, beams, floors, roofs, columns, pipes, walls etc. are constructed out of prestressed reinforced concrete. The use of steel as reinforcement in concrete is based on the assumption that multiple materials acting together would be better at resisting tensile forces. The process of introducing a precompression force to the reinforcing steel bars is called prestressing. This is done to counter the tensile stress that the reinforced concrete will experience during normal usage in order to prevent cracking. Most of

the concrete based structural elements used today have reinforced and prestressed concrete. Owing to its outstanding durability under aggressive conditions, especially in water, many industries and natural environments have extensively used concrete.

Another reason for the large scale use of concrete is its ability to be formed or cast into a variety of shapes and sizes. A batch of freshly made concrete has a viscous and plastic like consistency which can be used to pour it into a premade framework or mold. Once the concrete has solidified after a few hours or days depending on the size of the mold it can be removed out and the mold can be reused. This gives concrete the kind of versatility in terms of element shapes and sized that is very hard for other materials to match [21].

Lastly, the most critical reason for the extensive use of concrete, when considering both the engineering and economic perspectives is its availability and its cost. Pound for pound it is one of the cheapest and easily available materials that engineers can use. The key constituents for preparing concrete are a) cement, b) water and c) aggregates all of these components are available across the world and are generally inexpensive. Depending on the components' transportation cost, in certain geographical locations the price of concrete may be as high as U.S. $75 to $100 per cubic meter; at others it may be as low as U.S. $60 to $70 per cubic meter (2014 PCA Market Forecast). Further, the main reasons that promote the use of concrete over steel in the construction area are given below:

Maintenance: Concrete does not corrode, needs no surface treatment, and its strength increases with time; therefore, concrete structures require much less maintenance. Steel structures, on the other hand, are susceptible to rather heavy corrosion in offshore environments,

require costly surface treatment and other methods of protection, and entail considerable maintenance and repair costs.

Fire resistance: The fire resistance of concrete is perhaps the most important single aspect of offshore safety and, at the same time, the area in which the advantages of concrete are most evident. Since an adequate concrete cover on reinforcement or tendons is required for structural integrity in reinforced and prestressed concrete structures, the protection against failure due to excessive heat is provided at the same time.

Resistance to cyclic loading: The fatigue strength of steel structures is greatly influenced by local stress fields in welded joints, corrosion pitting, and sudden changes in geometry, such as from thin web to thick frame connections. In most codes of practice, the allowable concrete stresses are limited to about 50 percent of the ultimate strength; thus the fatigue strength of concrete is generally not a problem.

It should be noted that though concrete generally consists of 4 simple components there are a large number of additives and admixtures available to tune the properties of the final concrete according to the requirements of the application. Further, the preparation of concrete for each of these applications varies substantially. The next section provides a simplified overview of the concrete preparation process.

1.3 Concrete Preparation

Aggregate is the granular material, such as sand, gravel, crushed stone, crushed blast-furnace slag, or construction and demolition waste that is used with a cementing medium to produce either concrete or mortar. The term coarse aggregate refers to the aggregate particles larger than 4.75 mm (No. 4 sieve), and the term fine aggregate refers to the aggregate particles smaller than 4.75 mm but larger than 75 μm (No. 200 sieve). Gravel is the coarse aggregate resulting from natural disintegration by weathering of rock. The term sand is commonly used for fine aggregate resulting from either natural weathering or crushing of stone. Crushed stone is the product resulting from industrial crushing of rocks, boulders, or large cobblestones. Iron blast-furnace slag, a by-product of the iron industry, is the material obtained by crushing blast-furnace slag that solidified by slow cooling under atmospheric conditions. Aggregate from construction and demolition waste refers to the product obtained from recycling of concrete, brick, or stone rubble.

When sand cement and water are mixed together the resulting mixture is called Mortar. It is like concrete without the coarse aggregate. Another mixture of cement and sand (fine aggregate) called grout is formed when enough water is added such that the mixture retains its consistency during pouring and does not segregate into its constituents. Lastly, shotcrete refers to a mortar or concrete mixture which is pneumatically transported through a hose and projected onto a surface at high velocity.

The chemical reactions occurring between the minerals and water give cement its binding property. This process is called hydration. Cement is called hydraulic when the hydration

products are stable in an aqueous environment. Portland cement is the most commonly used hydraulic cement in the world mainly consisting of reactive calcium silicates. The C-S-H paste formed during the hydration process of Portland cement is the key ingredient responsible for the adhesive characteristic of cement and it is stable in aqueous environments. There is another component that is generally not mentioned in the definition of hydraulic cements. These components are called admixtures and are widely used in most modern concrete mixtures.

Materials other than the defined concrete mixture (cement, water, aggregates) which are added to the cement mix are called admixtures. These materials are generally added to the concrete mix either before or during the mixing process. Admixtures are today used widely as they provide a number of benefits. Depending on the type of the admixture they can impart a variety of properties to the concrete mix and the final concrete itself. Chemical admixtures can modify the setting and hardening characteristic of the cement paste by influencing the rate of cement hydration while, water-reducing admixtures can plasticize fresh concrete mixtures by reducing the surface tension of water. Air entraining admixtures can improve the durability of concrete exposed to cold weather; and mineral admixtures such as pozzolans (materials containing reactive silica) can reduce thermal cracking in mass concrete.

1.4 Types of Concrete

Based on unit weight, concrete can be classified into three broad categories. Concrete containing natural sand and gravel or crushed-rock aggregates, generally weighing about 2400 kg/m^3 (4000 lb/yd^3), is called normal-weight concrete, and it is the most commonly used

concrete for structural purposes. For applications where a higher strength-to-weight ratio is desired, it is possible to reduce the unit weight of concrete by using natural or pyro-processed aggregates with lower bulk density. The term lightweight concrete is used for concrete that weighs less than about 1800 kg/m^3 (3000 lb/yd^3). Heavyweight concrete, used for radiation shielding, is a concrete produced from high-density aggregates and generally weighs more than 3200 kg/m^3 (5300 lb/yd^3) [26].

Strength grading of cements and concrete is prevalent in Europe and many other countries but is not practiced in the United States [21]. However, from standpoint of distinct differences in the microstructure-property relationships it is useful to divide concrete into three general categories based on compressive strength:

- Low-strength concrete: less than 20 MPa (3000 psi)
- Moderate-strength concrete: 20 to 40 MPa (3000 to 6000 psi)
- High-strength concrete: more than 40 MPa (6000 psi).

Moderate-strength concrete also referred to as ordinary or normal concrete is used for most structural work. High-strength concrete is used for special applications. It is not possible here to list all concrete types. There are numerous modified concretes which are appropriately named: for example, fiber reinforced concrete, expansive-cement concrete, and latex-modified concrete. The composition and properties of special concretes are beyond the scope of this dissertation.

1.5 Emissions due to cement manufacture

With the widespread use of concrete however the concrete industry has become one of two largest producers of carbon dioxide (CO_2), creating up to 7% of worldwide man-made emissions of this gas, of which 50% is from the chemical process and 40% from burning fuel [27].

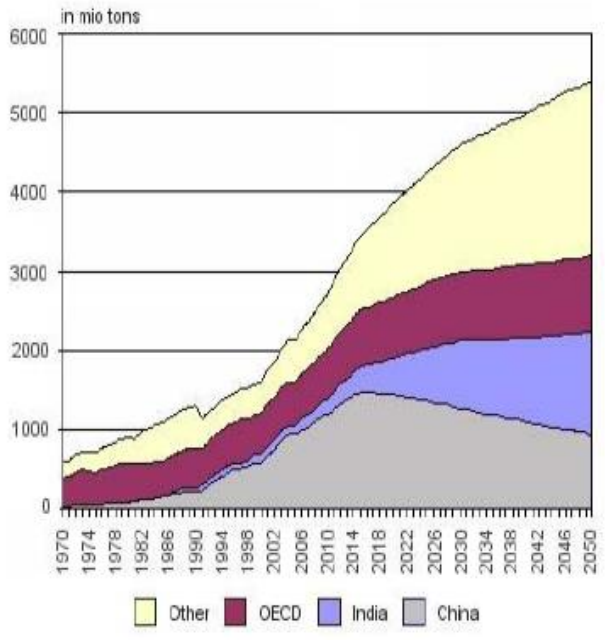

Figure 1.2: Global cement production capacity according to region from 1970 to 2010 and projections from 2011 to 2050 (International Energy Agency)

The CO_2 produced for the manufacture of one ton of structural concrete (using ~14% cement) is estimated at 410 kg/m^3 (~180 kg/ton @ density of 2.3 g/cm^3) (reduced to 290 kg/m^3 with 30% fly ash replacement of cement) [28]. The CO_2 emission from the concrete production is directly proportional to the cement content used in the concrete mix; 900 kg of CO_2 are emitted for the

fabrication of every ton of cement [29]. Cement manufacture contributes greenhouse gases both directly through the production of CO_2 when calcium carbonate is thermally decomposed, producing lime and CO_2, and also through the use of energy, particularly from the combustion of fossil fuels. The 2010 world's yearly cement production of 1.6 billion tons as shown in Figure 1.2 accounts for about 7% of the global loading of CO_2 into the atmosphere with the projected production increasing to almost 6 billion tons by 2050. Portland cement, the principal hydraulic cement in use today, is not only one of the most energy-intensive materials of construction but also is responsible for a large amount of greenhouse gases. Producing a ton of Portland cement requires about 4GJ energy, and Portland cement clinker manufacture releases approximately 1 ton of CO_2 into the atmosphere.

Further, cement manufacturing produces a number of other emissions. One of the most significant environmental health and safety issue of cement manufacturing is NO_X and SO_X emission [30]. Cement industry is potentially the largest anthropogenic source of air pollution. The typical gaseous emissions to air from cement production include NO_X, SO_X, CO, CO_2, H_2S, and VOCs, dioxins, furans and particulate matters [31, 32]. These major pollutants can be classified in two categories- gaseous and particulates. Fuel combustion process is the source of gaseous emissions which include oxides of nitrogen, oxides of sulfur, oxides of carbon and volatile organic compounds and hydrogen sulfide.

1.6 NO_X and SO_X emissions

Recent studies determine relationship between cement air pollution and human health diseases. Pollutants from cement plants are causing harmful effects on human health and environment [33]. The emissions of NO_X and SO_X are shown in the Figure 1.3 and while the levels are decreasing in many developed countries it is still a major environmental hazard in most other developing countries. Oxides of sulphur are formed from the combustion of fuels which contain Sulphur and via the oxidation of Sulphur containing raw materials [34].

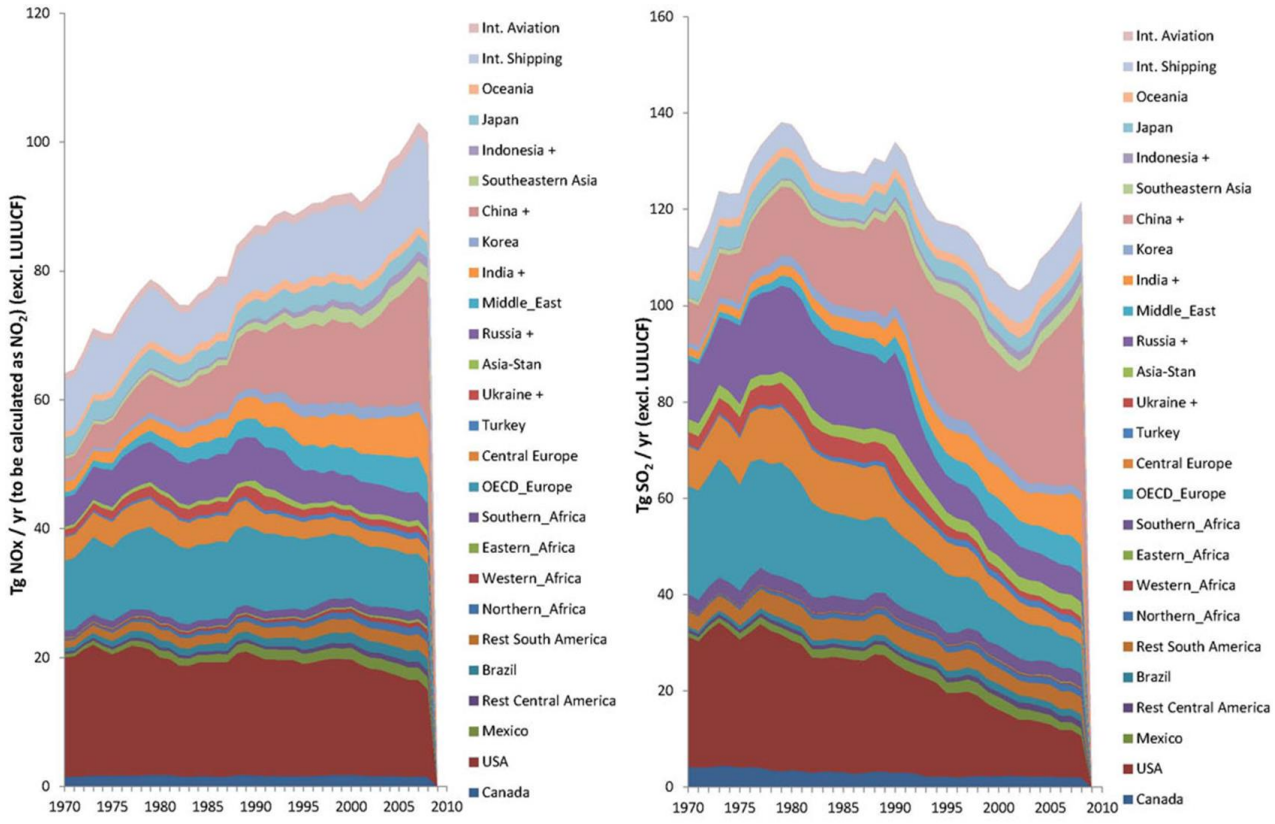

Figure 1.3: Global NO_X and SO_X emissions over the past 40 years according to region (EDGAR v4.2 Nov 2011)

SO_2 emissions generated from sulfur in the raw materials are lesser than SO_2 emissions generated from sulfur in the fuel [33]. In rotary kiln raw material oxidized to form SO_2 and SO_3 at temperatures between 370 ^oC and 420 ^oC. Sulfur dioxide (SO_2) is formed by thermal decomposition of calcium sulfate in clinker. SO_3 is present as anhydrite and can easily be decomposed to SO_2 and O_2. These sulfur oxides react with water vapor and other chemicals at high altitudes in the presence of sunlight to form sulfuric acids. The acids formed usually dissolve in the suspended water droplets, which can be washed from the air on to the soil by rain or snow. This is known as acid rain. Respiratory illnesses such as bronchitis are seen to increase with sulfur oxide levels [35-37]. Increased level of SO_X in the atmosphere can also degrade agricultural productivity and destruction of some plants.

Nitrogen oxides are produced in the combustion flame of a rotary kiln, which enter the atmosphere with the exit gases, and undergo many reactions in the atmosphere. Majorly NO_X are formed by thermal oxidation, which happens in temperature range between 1,200-1,600 °C. Due to high temperature significant amounts of thermal Nitric Oxide (NO) is generated in the Kiln. Combustion of nitrogen-bearing fuels such as certain coals also produces gaseous nitrogen (N_2), or NO [38]. As temperature increases, NO formation also increases. About 90% of the nitrogen oxides are produced in the form of nitric oxide (NO) and the remaining 10% are in the form of nitrogen dioxide (NO_2). Produced NO converts to NO_2 at the exit of the stack at atmospheric conditions [39]. NO_X causes a wide variety of health and environmental impacts because of various compounds and derivatives in the family of nitrogen oxides, including nitrogen dioxide, nitric acid, nitrous oxide, nitrates, and nitric oxide. Similar to Sulphur dioxide, NO_X reacts with water and other compounds to form various acidic compounds. When these acidic compounds

that are deposited to the earth's surface, they can impair the water quality of different water bodies and acidify lakes and streams. Acidification (low pH) and the chemical changes result in lowering the reproductive capabilities of fish and other aquatic species. Acid rain can also harm forest ecosystems by directly damaging plant tissues [40]. NO_X and volatile organic compounds react in the atmosphere in the presence of sunlight to form ground-level ozone, which causes smog in cities and rural areas. This ground level ozone causes respiratory disease and other health problems [41]. Nitrogen dioxide affects body functions such as difficulty in breathing, chronic lung diseases, such as chronic inflammation and irreversible structural changes in the lungs, which with repeated exposure, can lead to premature aging of the lungs and other respiratory illness (Figure 1.4) [42].

Figure 1.4: Environmental and Health impacts of NO_X pollution (EPA 2009)

1.7 Summary

Concrete is one of the most prolific construction materials available to man today. It is the predominant material used to build anything from the most basic projects to the grandest structures constructed. Cement, the main component in concrete, is manufactured on such a massive scale that it contributes to 5-7% of the annual global CO_2 production. Further, emissions such as NO_X, SO_X, Mercury and particulate matter from cement production have caused significant deterioration of human health and environment worldwide. With the need for infrastructure growing at an exponential rate, especially in developing countries like China and India, this problem is only likely to get worse. In fact, it is estimated that by 2050 the use of concrete will have reached 4 times the level that of in 1990. This chapter gives an overview of cement/concrete, its types, its manufacturing process and the emissions resulting in the production of cement.

Chapter 2
Use of Concrete for Sequestration

2.1 Introduction

As mentioned in the previous chapter, NO_X and SO_X pollution are a significant environmental and health concern. To summarize, it is one of the major contributors towards acid rain, eutrophication, visibility problems and cause formation of toxic substances affecting health [43]. NO_X (which includes such Nitrogen Oxides as NO and NO_2) is also the precursor to ground level ozone, formed by light induced reactions between volatile organic matter and NO_X, which can cause lung tissue damage and reduce lung function [44-48]. Given that now, for the first time in human history more people live in urban rather than rural environments, the higher pollution levels in densely populated areas affects more people than ever before (Figure 2.1). Furthermore, in developing countries like India and China, with less stringent environmental standards coupled with rapid urbanization, atmospheric pollution results in millions of people being exposed to unsafe levels of smog and ozone [49-52].

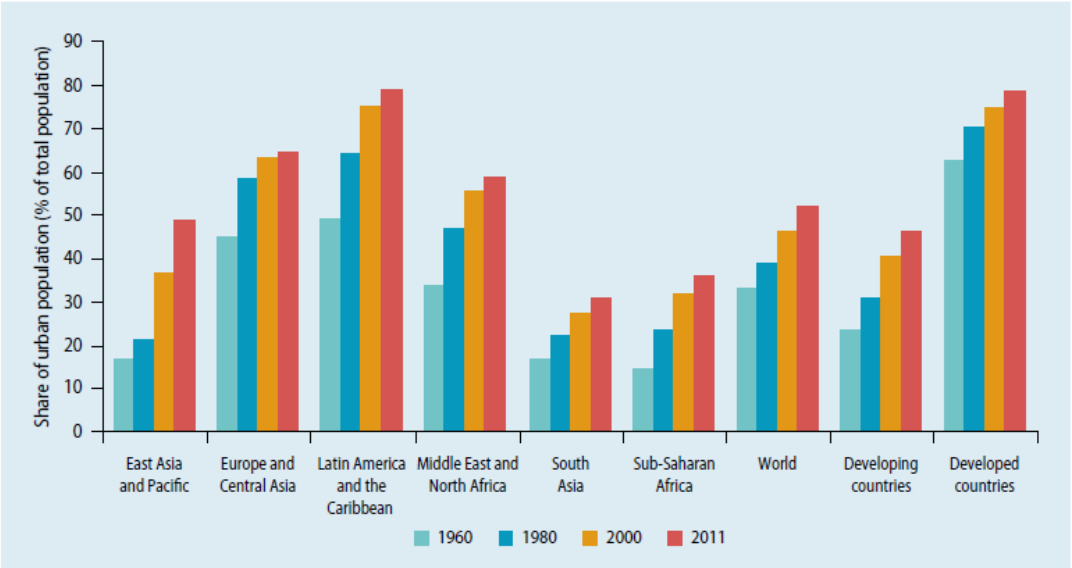

Figure 2.1: Global urban population according to region from 1960 to 2011 (Global Monitoring Report 2013)

Moreover, with 80% of the US population now living in urban areas it is of prime importance to understand and mitigate these priority pollutants [43].

Sulfur dioxide and nitrogen oxides are the major precursors of acid rain, which has acidified soils, lakes and streams, accelerated corrosion of buildings and monuments, and reduced visibility. Sulfur dioxide also is a major precursor of fine particulate soot, which poses a significant health threat. Among many sources of emissions cement kilns (Table 2.1) are very significant contributors. They emit over 219,000 tons/year of NO_X, which amounts to approximately 20% of all industrial emissions [53, 54].

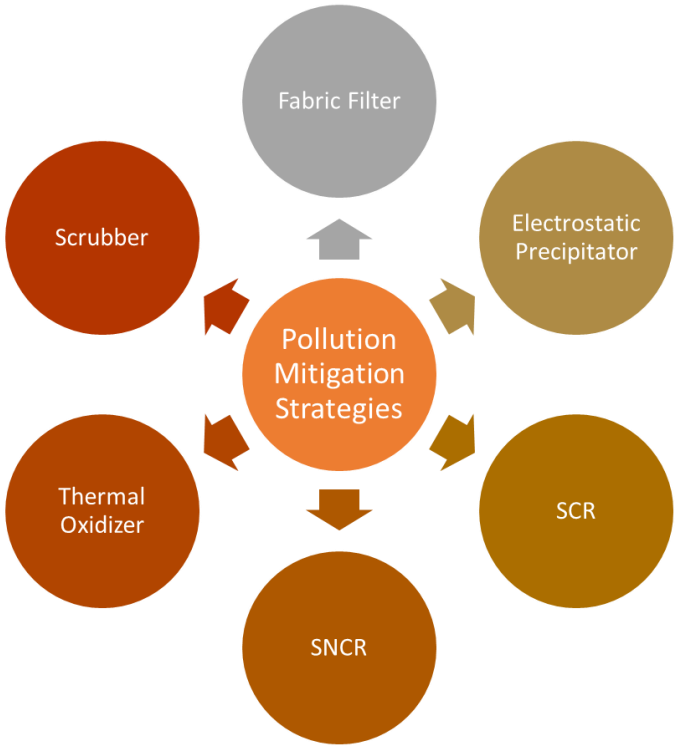

Figure 2.2: Strategies for mitigating emissions from cement production plants

High temperatures reached in cement kilns are favorable for NO_X emissions and cannot be avoided. However, there are several strategies to reduce these emissions as shown previously in Figure 2.2, which include: (1) process modifications, where energy efficiency and related productivity of the process are optimized; (2) combustion optimization and control approaches, which lead to reduction in NO_X formation, and (3) pollution control technologies where NO_X can be effectively removed. The latter utilizes several technologies such as selective catalytic reduction (SCR) and selective non-catalytic reduction (SNCR).

Kiln Type	Range	Average /Percent higher than pH/PC kiln	AP-42/ Percent higher than pH/PC kiln
Wet	3.6-19.5	9.7/155	7.4/76
Long Dry	6.1-10.5	8.6/126	6.0/43
Preheater	2.5-11.7	5.9/55	4.8/14
PH/PC	0.9-7.0	3.8/…	4.2/---

Table 2.1: Uncontrolled NO_X Emissions (pounds per ton [lb/t]) by Kiln Type (US EPA)

Additionally, adsorbents can be relatively economical, easy to implement, and require fairly straightforward setup/control procedures. Activated charcoal is one of the most widely used adsorbents for both gas and liquid phase pollutant removal. However, it can be an expensive option to implement for large scale pollution sources, such as power plants, foundries and kilns, where the flow rate and amount of pollution are very substantial. Alternatively, cement and concrete are cheap and effective adsorbent for emission reduction at such large scales, but very little research has been done on this front. With such limited research, the only known approach is to add activated carbon to concrete as an adsorbent [55]. Without any additives it has been shown that $Ca(OH)_2$ (15-20% of concrete) is an excellent adsorbent for both mercury and arsenic with good regeneration capacity. Concrete has also been used for CO_2 sequestration with a modest amount of success [56]. This work expands on this approach further and provides new avenues for using concrete as an inexpensive and efficient adsorbents. While the removal of pollutants namely NO_X by the use of photocatalytic additives such as TiO_2 (Titanium Dioxide) in concrete has been extensively studied the interaction between NO_X and concrete itself has not been systematically examined [57-72]. Although there are a limited number of studies [73-75] focused on interactions of other pollutants with building materials, such as CO_2, Mercury and others (such as Arsenic and Toluene), further investigation on such interactions with regards to

NO_X and SO_X is required. Another important knowledge gap, is in establishing relation between age dependent composition of building materials and pollutant interactions [76]. Given a very substantial diversity of urban surfaces in terms of their age, ranging from months to hundreds of years, this research believes that it is an important topic to be studied further. This thesis investigates the interaction of NO_2 and SO_2 with both fresh and aged concrete. Also, an innovative approach of utilizing a waste concrete material is proposed, which, based on the preliminary studies, can offer a new method of removing NO_2 and SO_2 in a cheap and sustainable way. The data presented in chapter 4 is also aimed at possibly establishing a quantifiable data for materials' age related uptake of these criterial pollutants.

2.2 Demolished Concrete as Adsorbent

It has been established that concrete is the most commonly used construction material in the world which is made by proportioning and mixing the right amounts of Portland cement, aggregates and water to achieve a specified strength or performance. Portland cement is the binding component in the mixture, which, when reacted with water, will produce the most important binding component of the hardened concrete, calcium silicate hydrate gel (C-S-H), which will coexist along with calcium hydroxide ($Ca(OH)_2$) by-product and ettringite/monosulfoaluminate (AFt/AFm) phases. A freshly prepared concrete has a pH of about 13.2, whereas an old concrete exposed to ambient temperature and humidity may have a pH of approximately 9. A more detailed data described below show Table 2.2 that pH is lower at the surface and higher in the core of the concrete.

Depth/cm	Average pH	Standard deviation
0	8.8	0.26
1	11.87	0.05
3	11.97	0.05
5	12.02	0.10
8	12.05	0.12

Table 2.2: The pH values of seawall concrete as a function of depth (Source: Heng et al., 2004)

This phenomenon is mainly due to carbonation process happening at the surface of the concrete. This process is attributed to absorption of CO_2 from the atmosphere. The CO_2 uptake by concrete is a function of various environmental conditions, such as CO_2 concentration, relative humidity, temperature, and pressure [77]. It is also a function of such concrete properties as: (a) composition; (b) the initial pH; (c) water content; (d) microstructure, and (e) specific surface area.

Although it is not trivial to specify all the chemical reactions taking place in the cement paste, a simplified reaction mechanism can be presented as following [76]:

$$2(CaO)_3SiO_2 + 6H_2O \rightarrow (CaO)_3(SiO_2) + 2(H_2O)_3 + 3\,Ca(OH)_2 \quad (2.1)$$

$$2(CaO)2SiO_2 + 4H_2O \rightarrow (CaO)_3(SiO_2)_2(H_2O)_3 + Ca(OH)_2 \quad (2.2)$$

$$3CaO.Al_2O_3 + 3\,(CaO.SO_3 \cdot 2H_2O) + 26\,H_2O \rightarrow 6CaO \cdot Al_2O_3 \cdot 3SO_3 \cdot 32H_2O\ (\text{Ettringite/AFm}) \quad (2.3)$$

$$2(3CaO \cdot Al_2O_3) + 6CaO \cdot Al_2O_3 \cdot 3SO_3 \cdot 32H_2O + 4\,H_2O \rightarrow 3\,(4CaO \cdot Al_2O_3 \cdot SO_3 \cdot 12H_2O)\ (\text{calcium monosulfoaluminate/AFm}) \quad (2.4)$$

$$Ca(OH)_2 + CO_2 \rightarrow CaCO_3 + H_2O \quad (2.5)$$

Reaction (2.5) is especially important to understand the surface neutralization of concrete, as high initial concentration of $Ca(OH)_2$, in addition to the presence of alkali (Na_2O and K_2O) from the cement, determines a significant basic character of fresh concrete (pH > 13.2). Further, thermodynamics and kinetics would dictate the preferential reaction pathways making it necessary to have a step-by-step study and understand which one of the reactions would occur in a multi pollutant environment. Unfortunately, there is very limited literature data [78] on NO_2 reaction with $Ca(OH)_2$. While there is some data available regarding SO_2 reaction with concrete phases, it is still very rudimentary and needs further investigation. This thesis studies the formation of both sulfur and nitrogen species in concrete during and after uptake. In order to observe and study the formation of these surface species an in-situ DRIFTs cell was used to gather real time spectral data. This data was then compared to the reference spectrum available through the NIST database for the various possible products that could emerge during the adsorption and subsequent reaction. Using the collected spectral data, the NIST reference and

the data available in the literature enables us to interpret the possible reaction mechanisms that occur during the adsorption. The reference IR spectra for some of these phases are shown in Figure 2.3. However due to the complex nature of concrete there would be several intermediate or unknown phases that would not correspond to any of the available IR spectra. It becomes necessary to understand the mechanism of evolution and the thermodynamic feasibility of such phases. In this thesis the Gibbs free energy of the reaction for some of these phases and their thermodynamic favorability examined.

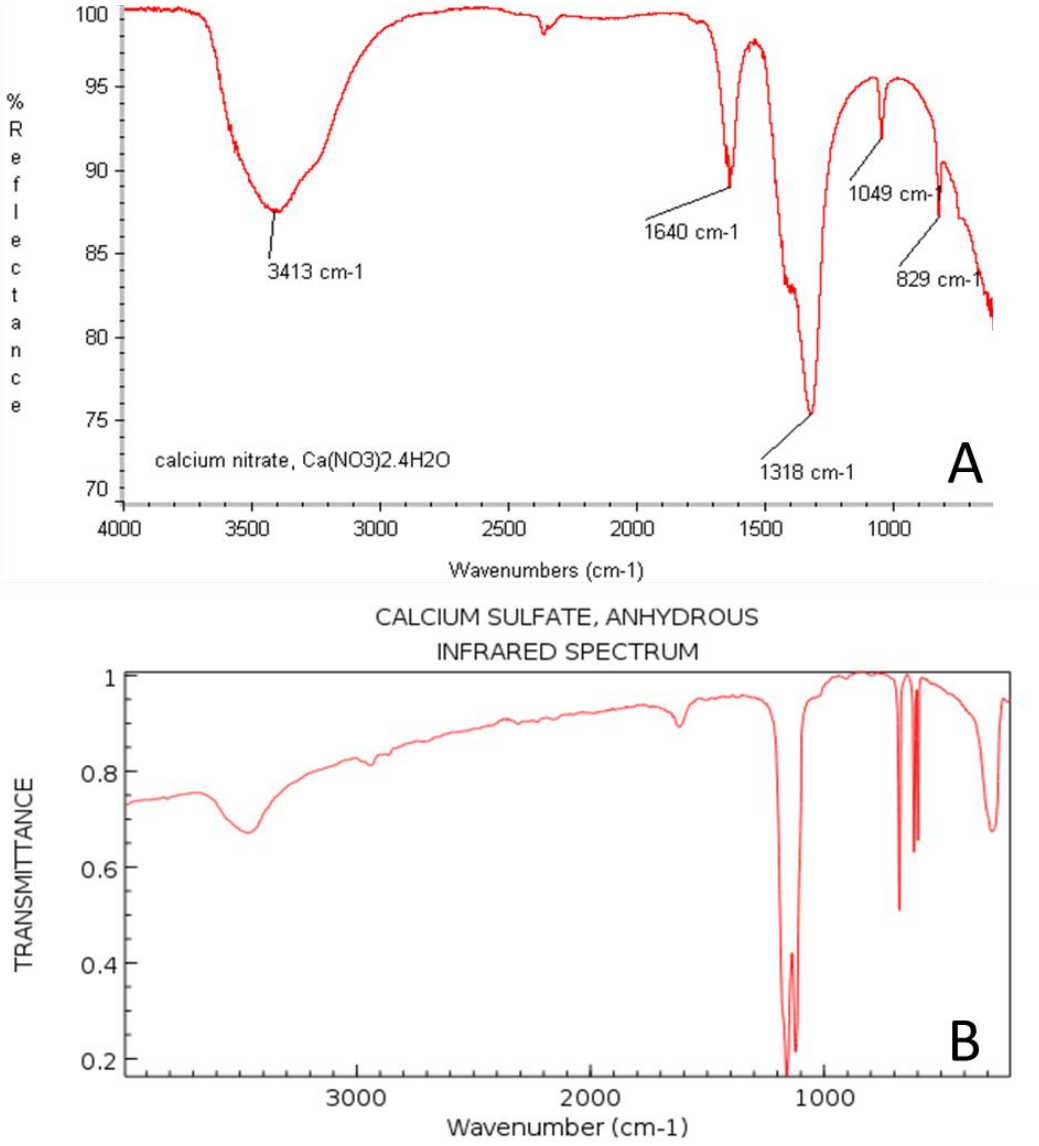

Figure 2.3: FTIR spectra of Nitrogen and Sulphur species from the NIST database used as reference in the thesis

It is important to note that the surface acidity is by itself a function of environmental conditions, concrete composition and concrete age. For example, Heng *et al.* [76] collected numerous concrete powder samples at various locations in Japan and measured their pH values. These results are shown previously in Figure 2.4. They indicate that neutralization of $Ca(OH)_2$

occurs over the period of several years, which results in a significant decrease of the concrete pH. Here, these issues have been addressed by processing the concrete to expose new reactive surfaces for further uptake.

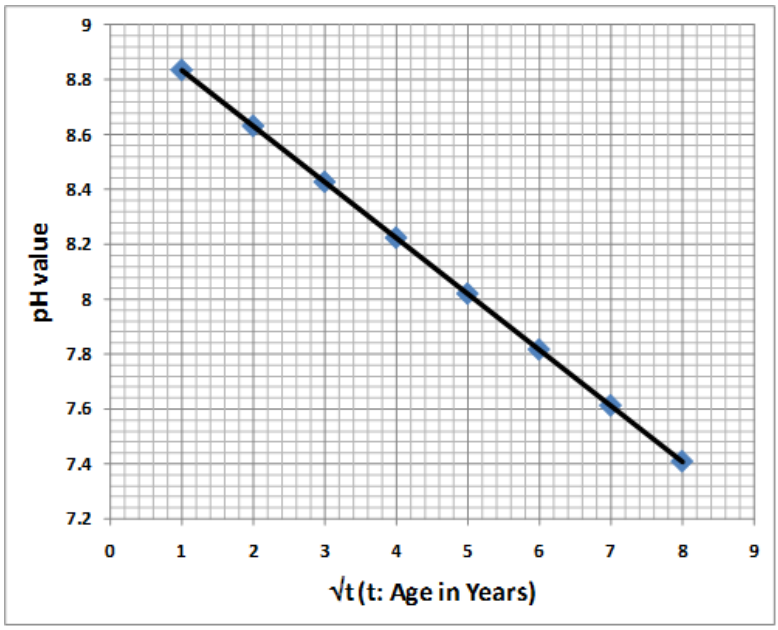

Figure 2.4: Dependence between pH and concrete age for concrete samples from different areas in Japan. (Heng et. al. 2004)

Another potential route of NO_2 sequestration is the absorption of NO_2 by AFt/ AFm phases forming nitrate AFt phase ($Ca_6Al_2O_6(NO_3)_6 \cdot 32H_2O$) or nitrate/nitrite AFm phases ($Ca_4Al_2(OH)_{12}(NO_3)_2 \cdot 4H_2O$/ $Ca_4Al_2(OH)_{12}(NO_2)_2 \cdot 4H_2O$). Limited thermodynamics modeling data available in the literature gives calculated Gibbs free energies -6778 and -6606 *kJ/mol* for nitrate and nitrite AFm formation respectively, indicating a feasibility of the alternative pathway [79].

2.3 Beneficial Reuse of Demolished Concrete

Using concrete to store hazardous waste or to sequester CO_2 has been a very prolific and promising area of research [80-82]. In addition, coatings of concrete with photocatalysts or dispersing them within concrete have also been used for NOx and VOCs mitigation via catalytic removal of hazardous contaminants under solar light. However, there have been no attempts in adopting demolished concrete for removal of air pollutants. One of the primary reasons could be that environmental considerations alone do not offer strong enough incentives to implement such technologies. In contrast to the above mentioned approaches, this thesis looks at sustainability and improved functionality benefits of reusing demolished concrete as adsorbent, thus addressing the major bottleneck in adoption of concrete for pollution mitigation. Moreover, in contrast to research focused on using concrete for CO_2 removal [83, 84], this thesis is focused on mitigating the NO_2 and SO_2 emissions, which are causing immediate environmental and health problems. Finally, in contrast to several studies of using catalyst (TiO_2) modified concrete [58, 85], this thesis proposes a much simpler and cheaper method of pollutant removal without using any catalysts.

There are many sources of these emissions including cement kilns, incineration plants, boilers, process heaters, glass furnaces, power plants and automobiles [86]. Several known strategies to reduce emissions include: (a) process modifications where energy efficiency and related productivity of the processes are optimized; (b) combustion optimization and control approaches, which lead to reduction of SO_X and NO_X formation, and (c) pollution control techniques where SO_X and NO_X can be effectively removed after it is formed in the combustion

zone. The latter approach utilizes several technologies, such as selective catalytic reduction (SCR), selective non catalytic reduction (SNCR) and adsorption/absorption as shown in Figure 2.2. While process modification and combustion control are much better approaches than post-combustion treatment, a supplementary strategy is to couple these approaches with post-combustion pollution control. It has been noted that emission controls using SCR and SNCR methods are generally expensive and can be rather complicated given the need to constantly monitor the catalysts for deactivation and poisoning [87, 88].

The need for developing innovative solutions to address emissions are clearly mentioned in section 2.1.One of the most prevalent problem with NO_2 emissions is the formation of ground level ozone as stated earlier [89, 90]. It is a significant problem nationwide as millions of Americans live in areas that do not meet the health standards for ozone [43]. High concentrations of sulfur dioxide (SO_2) can result in breathing problems with asthmatic children and adults who are active outdoors. Short-term exposure has been linked to wheezing, chest tightness and shortness of breath. Other effects associated with longer-term exposure to sulfur dioxide, in conjunction with high levels of particulate soot, include respiratory illness, alterations in the lungs' defenses and aggravation of existing cardiovascular disease.

2.4 Summary

This chapter explores the potential of demolished concrete as an economical and effective adsorbent for use in pollution remediation. Literature shows that concrete has a moderate degree of success in CO_2 sequestration. Further, cement and phases of concrete like $Ca(OH)_2$ have been

employed for adsorption of other pollutants like mercury, arsenic etc as well. The data from the literature also shows that aged environmentally exposed concrete surfaces can have a significant uptake However, the research in this area is clearly insufficient with evident lack of data when it comes to the interaction of concrete surfaces with respect to criteria pollutants such as NO_X and SO_X. The evaluation of the adsorptive capabilities of demolished concrete is examined in chapters 4 and 5 to address this need for critical information

Chapter 3

Characterization Techniques

3.1 Introduction

In this chapter the experimental methods used for the characterization of ceramic and composite samples are described. These include techniques such as Scanning Electron Microscopy (SEM), X-Ray Diffraction (XRD), Energy Dispersive X-ray Spectroscopy (EDX), Brunauer-Emmett-Teller porosity analysis (BET) for the concrete samples. The concrete samples were further characterized using X-Ray Fluorescence (XRF), Diffuse Reflectance Infrared Fourier Transform Spectroscopy (DRIFTS), X-ray Absorption Near Edge Structure (XANES), Flow and Packed bed reactors.

3.2 X-Ray Diffraction (XRD)

In order to explain the relationship between crystal planes which appear to reflect X-ray bays and the angles of incidence, W.H. Bragg proposed the following equation

$$n\lambda = 2d\,\mathrm{Sin}\theta \qquad 3.1$$

The X-ray wave interference phenomenon is now called X-ray Diffraction (XRD). This was later proved as the existence of periodic atomic structure of crystals [91].

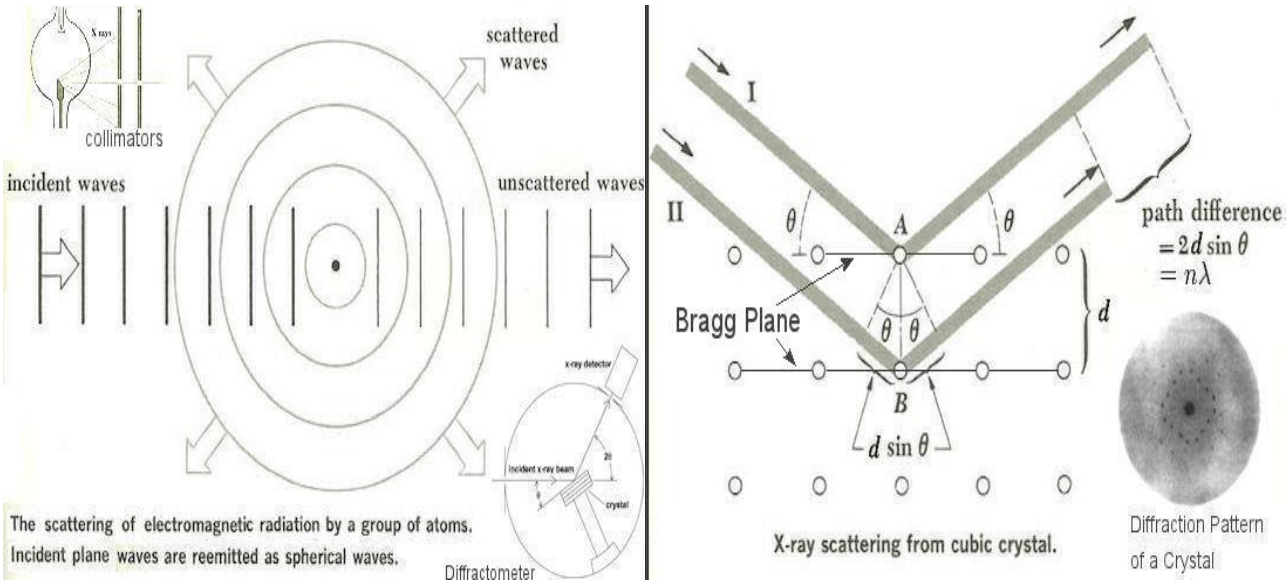

Figure 3.1: Schematic of X-ray diffraction instrument (Perspectives of Modern Physics; A Beiser)

A crystal has the atomic planes which can cause an incident beam of X-rays to interfere with one another when they leave the crystal as shown in Figure 3.1. This phenomenon, which is known as X-ray diffraction, can in principle:

1. Measure the average spacing between layers of the atoms (d-spacing)

2. Determine the orientation of a single crystal or grain

3. Discover the crystal structure for unknown materials

4. Calculate the size, shape and internal stress of a small region of the crystal

The most important use of XRD is to obtain the XRD pattern and compare data with known standards in order to identify the sample phase. It is a fast, nondestructive way for phase identification and high accuracy for d-spacing calculations. The technique can be used in single crystals and amorphous materials.

3.3 Diffuse Reflectance Infrared Fourier Transform Spectroscopy (DRIFTS)

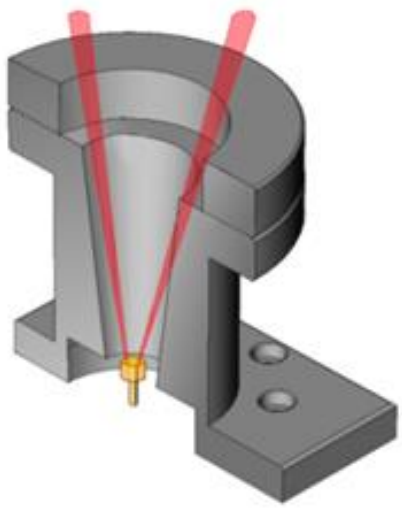

Figure 3.2: 3D Cross Section representation of DRIFTS environmental cell

Diffuse reflectance infrared Fourier transform spectroscopy is a technique that collects and analyzes scattered IR energy. It is used for analysis of fine particles, powder sand films [92].

When the beam of IR enters the sample, it can be either reflected off the surface or transmitted through the sample. The beam that reflects off the surface is typically lost. The beam that passes through a particle can either be reflected by the next particle or be transmitted through the next particle again. This phenomenon of transmission-reflectance can occur many times in the sample. Finally, all scattered IR light is collected by a spherical mirror which is focused onto the IR detector. Because the detected IR light is partially absorbed by the particles of the sample surface, it carries the information of the sample under IR region [93].

The system is based on Nicolet 6700 FTIR equipped with Smart Collector. The Smart Collector also contains an environmental chamber, which gives the capability to conduct the in-situ experiments under controlled temperature and pressure. The surface reactions were monitored using a FTIR spectrometer equipped with diffuse reflectance cell (DRIFTS). The diffuse reflectance cell assembly consists of an environmental chamber that allows us to change gas composition, flow rates and temperatures (up to 900 °C) to simulate the flue-gas composition as described earlier. The infrared beam (Figure 3.2 and Figure 3.3) will be focused by a series of mirrors onto the surface of the sample. In that arrangement the reflected components of the radiation pass through the ZnSe windows of the sample chamber and are focused by the hemispherical mirror onto another series of mirrors to the detector. The detector is a liquid nitrogen cooled mercury-cadmium-telluride (MCT) detector. The resultant interferogram will be then mathematically processed to separate absorbance data for each wavelength component. The outlet of the DRIFTS cell was coupled to either NO_X or SO_X analyzer, or both. The DRIFTS results provide a feedback mechanism concerning the effect of exposure on the surface composition.

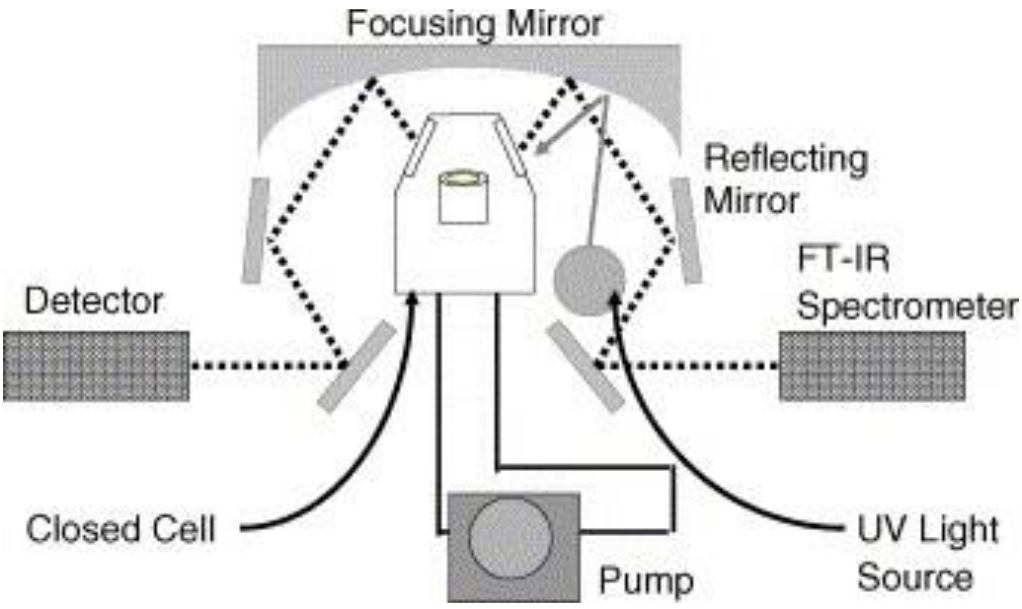

Figure 3.3: Schematic diagram of DRIFTS cell (Harrick Scientific Ltd)

3.4 Scanning Electron Microscopy (SEM)

There are many types of electron microscopes today and Scanning Electron Microscope (SEM) is one of them. A high energy beam of electrons, images the sample surface by scanning it in a raster pattern. The electrons interact with the atoms that make up the sample producing signals that contain information about the sample's surface topography, composition and other properties such as electrical conductivity [94, 95]. Most scanning electron microscopes today use digital controls, signal acquisition and processing techniques of raw grayscale images. They can also determine the elemental composition of the sample materials when used in conjunction with the closely-related technique of energy dispersive X-ray spectroscopy (EDS).

These electron microscopes generally operate under high vacuum. A field emission gun is typically used as a source to generate the high energy electron beam. This beam is then accelerated using a high voltage like and passed through a series of apertures and electromagnetic lenses to produce a collimated beam of electrons as shown if Figure 3.4. This beam then scans the surface of the specimen by the scanning coils. Electrons are emitted from the specimen by the action of the scanning beam and collected by a suitably positioned detector.

As a powerful technique, SEM has been extensively used for imaging new materials, especially at micro and nano scales. SEM is a valuable tool for probing the structure and morphology of such materials.

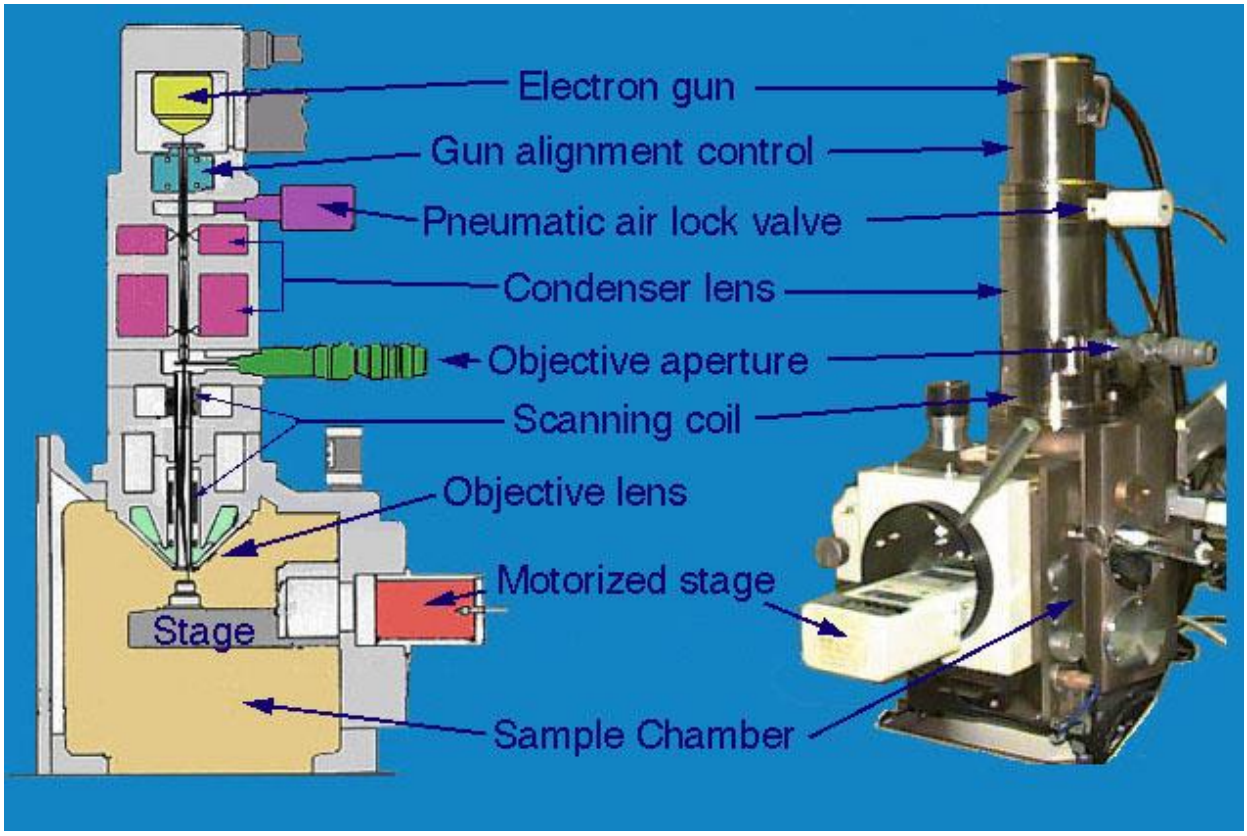

Figure 3.4: Schematic of SEM system (Frostburg University, General Chemistry Online)

3.5 X-ray Absorption Near Edge Structure (XANES)

X-ray Absorption Near Edge Structure (XANES), also known as Near edge X-ray Absorption Fine Structure (NEXAFS), is generally defined as the analysis of the spectra obtained in X-ray absorption spectroscopy experiments [96]. This technique is element specific and is sensitive to local bonding spectroscopic analysis determining the partial density of the empty states of a molecule [97].

X-rays are ionizing electromagnetic radiations that have sufficient energy to excite a core electron of an atom to an empty below the ionization threshold called an excitonic state, or to the continuum which is above the ionization threshold. Different core electrons have distinct binding energies; consequently, if one plots the X-ray absorbance of a specific element as a function of energy, the resulting spectrum will appear similar to Figure 3.5.

As stated above, a core hole is the space a core electron occupied before it absorbs an X-ray photon and ejected from its core shell. The electronegative core holes are extremely unstable owing to their energetic nature having an average lifespan of ~1 femtosecond. These core holes are created through processes in which either a core electron absorbs an X-ray photon (X-ray absorption) or absorbs part of the X-ray photon's kinetic energy (X-ray Raman scattering). The successor process is the decay of a core hole which can take place either through Auger electron ejection of X-ray Fluorescence.

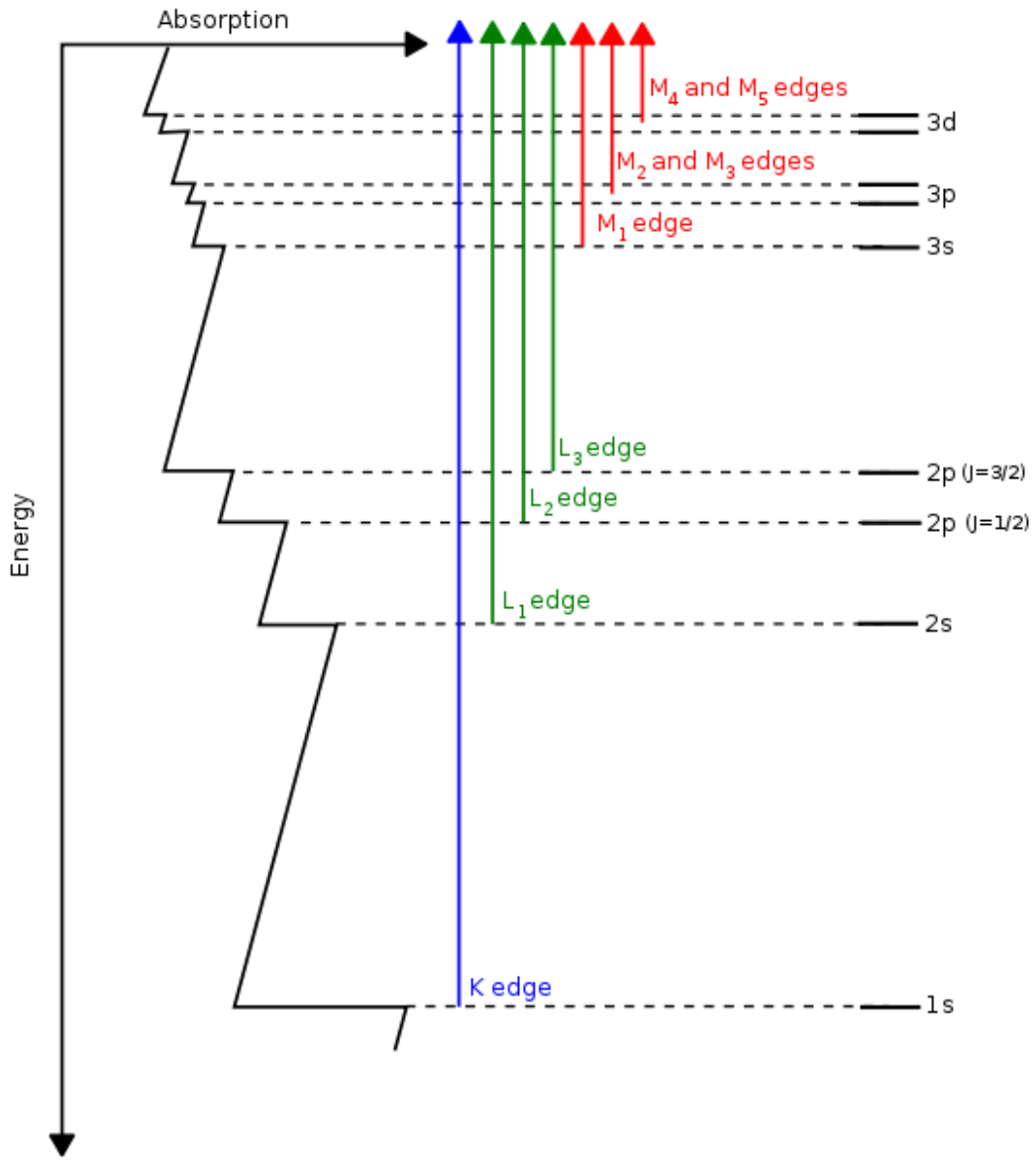

Figure 3.5: Illustrative X-ray absorption spectrum of a transition metal atom. Three major transitions K, L, and M edge transitions are identified, the L edge fine structures are also shown (Source: Wikipedia)

When the energy of X-ray radiation scans through the binding energy regime of a core shell, there is a sudden increase of absorption. This phenomenon corresponds to absorption of the X-ray photon by a specific type of core electrons (e.g. 1s electrons of Cu).giving rise to the

absorption edge. The name of the absorption edges are given according to the principle quantum number, n, of the excited electrons (Table 3.1).

K edge	1s			
L edge	2s	2p		
M edge	3s	3p	3d	
N edge	4s	4p	4d	4f

Table 3.1: Absorption edges (Wikipedia)

The energies of absorption edges in X-ray absorption spectra reveal the identity of the corresponding absorbing elements. However, more useful information can be obtained by a closer examination of a given absorption edge (Figure 3.6).

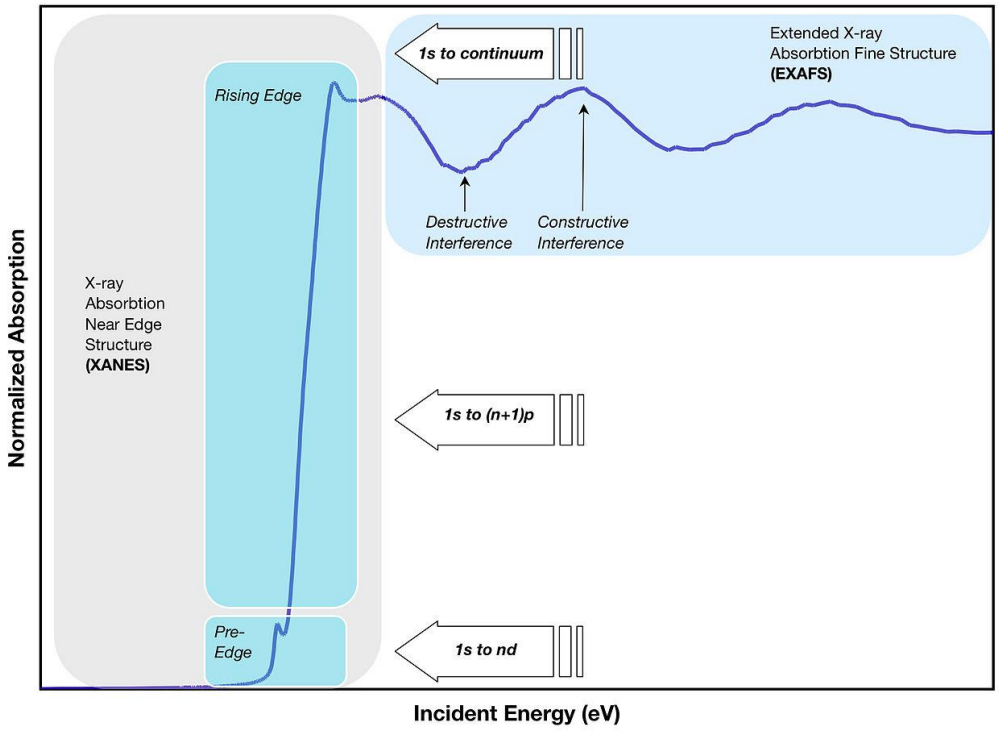

Figure 3.6: Schematic illustration of an X-ray absorption edge (Source: Wikipedia)

Illustrated by Figure 3.6, the absorption edge is often much more complex than simply an abrupt increase in absorption illustrated in Figure 3.5. There are weak transitions below the absorption edge, namely pre-edge structures, as well as significant absorption features in the immediate neighborhood of the absorption edge and well above the edge. The structure found in the immediate neighborhood of the absorption edge, conventionally within 50 eV of the absorption edge, is referred to as X-ray Absorption Near Edge Structure (XANES). Beyond XANES, the oscillatory structure caused by the interference between the outgoing and the back-scattered photoelectron waves is referred to as Extended X-ray absorption Fine Structure (EXAFS), which can extend to 1000 eV or more above the absorption edges [98].

3.6 Flow Reactor Experiments

In addition to the above characterization techniques, concrete samples were also tested in flow and packed bed reactors. The schematic of the experimental setup is shown in Figure 3.7. The flow experiments were conducted in a custom built quartz reactor while the packed bed experiments were carried out in a quartz capillary tube. Both reactors were fed synthetic air and NO_2/SO_2 flows from the compressed gas cylinders that were controlled by mass flow controllers (MFC). Given that water vapor is always present in the atmosphere, the mixture of air and NO_2/SO_2 was humidified by passing a part of the synthetic air from compressed gas cylinder through a water bubbler. The relative humidity of air was controlled by varying the flow of dry and humid air. The resulting humidity was measured by a humidity probe (Vaisala HMP50 Humidity Probe) positioned downstream.

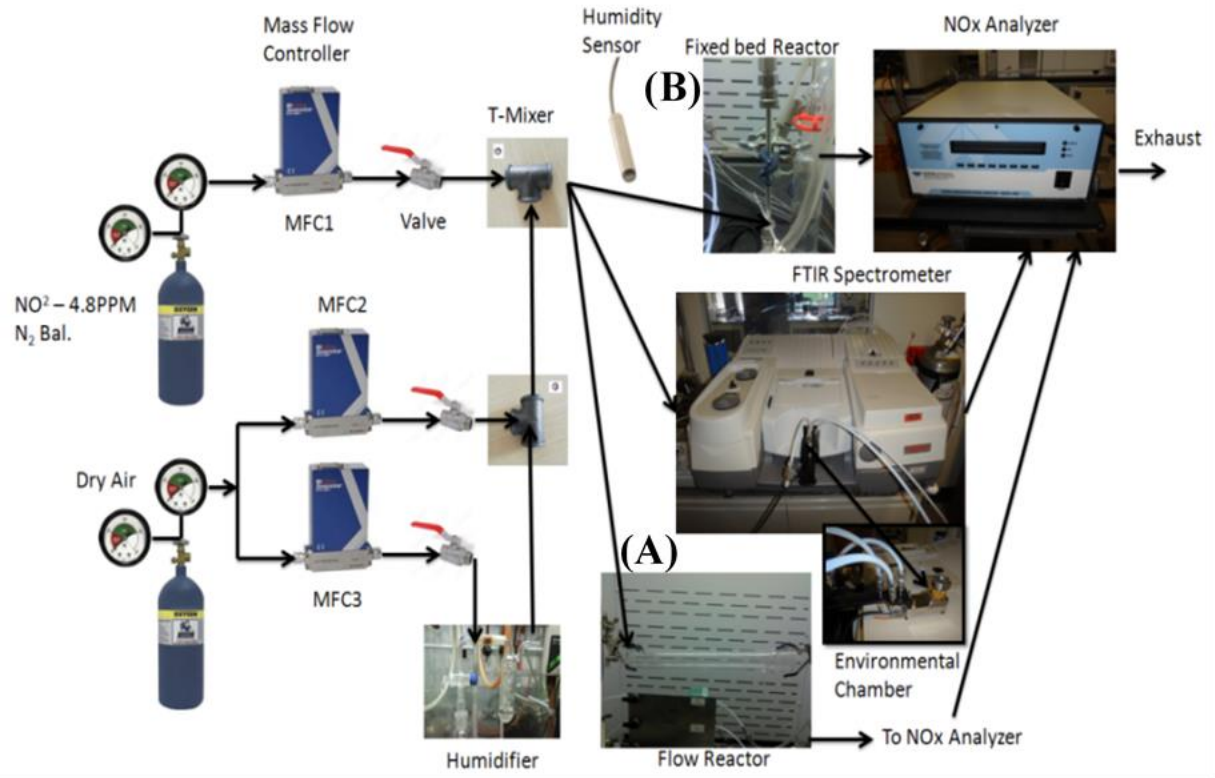

Figure 3.7: Experimental system for testing NO_2 removal from gas phase (A) shows a flow reactor and (B) shows a modified reactor for powder samples.

The samples of concrete were placed inside the sealed reactor and exposed to humidified NO_2/SO_2 and air mixture. The exhaust was connected to a gas analyzer to measure the outflow concentration. The NO_2 conversions were continuously measured by NO_X analyzer (Model 200E, Teledyne API Ltd) and recorded on computer hard drive through the data capture program. The quartz reactor where powdered samples for the packed bed experiments were loaded is shown in the (Figure 3.7 B).

Chapter 4

NO_X Adsorption by Crushed Concrete

4.1 Introduction

In order to study the interaction of concrete with NO_X, several concrete samples were prepared and aged for different periods of time (up to 12 months). These samples were used in both slab and powder form for the adsorption experiments. The concrete slabs were supported on polycarbonate trays while the powders were prepared by pulverizing aged/fresh/waste concrete samples and separating them into different particle size fractions using certified sieves. These samples were loaded both on to capillary tubes for the packed bed experiments and in the DRIFTs environmental cell for IR experiments.

4.2 Sample Preparation

Concrete samples were prepared for all experiments according to ASTM specifications (ASTM C150 and C192). Commercially available Portland cement mixture consisting of Portland cement, limestone filler, sand, gravel, flyash and water (Quikrete Companies Inc.) was used for all the NO_X experiments described in this thesis. The prepared samples were slump tested as per ASTM standards to ensure consistency and workability.

Figure 4.1: Concrete slab sample

Figure 4.2: Crushed concrete samples in a capillary tube

All the cement samples were prepared with deionized water according to specifications and poured into polycarbonate sample trays (3x30cm) as shown in Figure 4.1. The samples were allowed to cure at 20 °C in 50% RH for 28 days to attain strength. To produce the powder fractions as shown in Figure 4.2 concrete slabs were pulverized and passed through a set of standard sieves. The waste concrete samples were obtained from the Stony Brook Campus operations. NO_2 in N_2 (4.68 ppm initial concentration) and SO_2 in N_2 (10 ppm initial concentration) gas mixtures obtained from Praxair Gases was used for the all experiments described here. Lastly, reference samples such as $Ca(OH)_2$ (i.e. portlandite) C-S-H (Calcium Silicate Hydrate gel), synthesized (AFm) and $CaCO_3$ were purchased from Alfa Aesar to establish a reference uptake and provide baseline for the DRIFTS experiments.

4.3 Survey of Different materials for NOx Adsorption

In order to understand the importance of concrete surfaces as compared to other building materials, namely asphalt, masonry, glass and steel; scoping experiments were conducted with these materials. Here aged concrete slab has been used, which was exposed to the outdoor atmosphere (Stony Brook University) for 12 years. Similarly, asphalt and masonry samples were used, which became available due to Stony Brook University buildings and roads demolition/renovation efforts. The results are shown in Figure 4.3. They indicate that both fresh (1 month old) and aged (12 years old) concrete samples remove NO_2 from the gas phase.

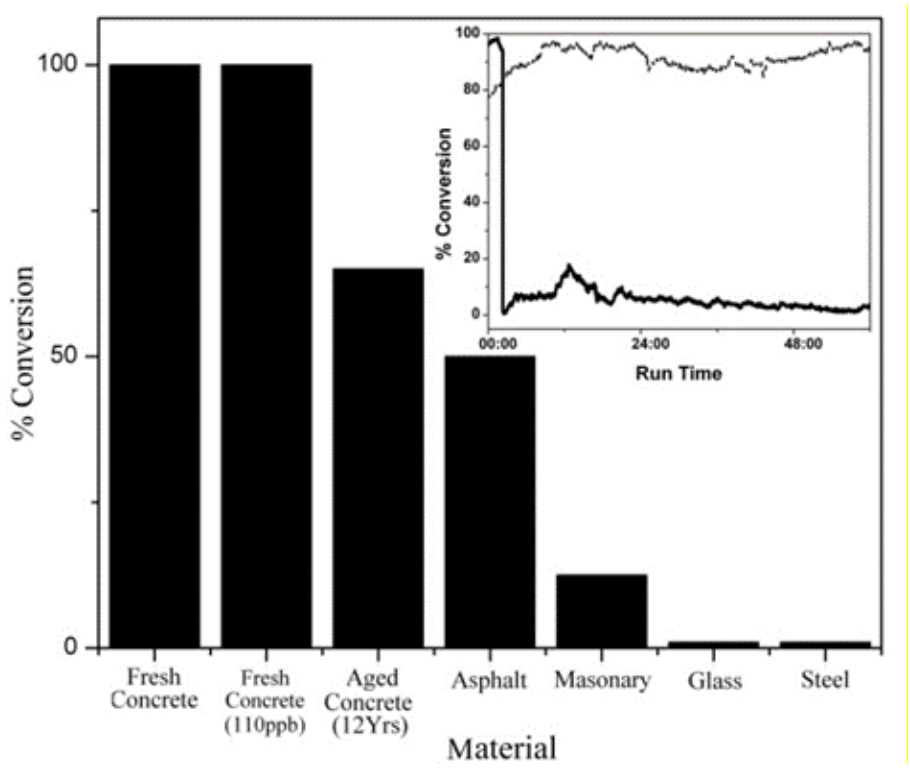

Figure 4.3: Evaluation of NO_2 conversion on various building materials. Inset shows NO_2 removal by fresh concrete exposed to 110 ppb NO_2.

4.4 Flow Reactor Measurements

The flow reactor consisted of a quartz tube connected to synthetic air and NO_2 cylinders via mass flow controllers (MFC). The synthetic air was humidified by passing synthetic air through a gas bubbler and mixing it with dry air to achieve target humidity. The ratio of humidified and dry air were determined based on data provided by a humidity probe (Vaisala HMP50 Humidity Probe) positioned downstream.

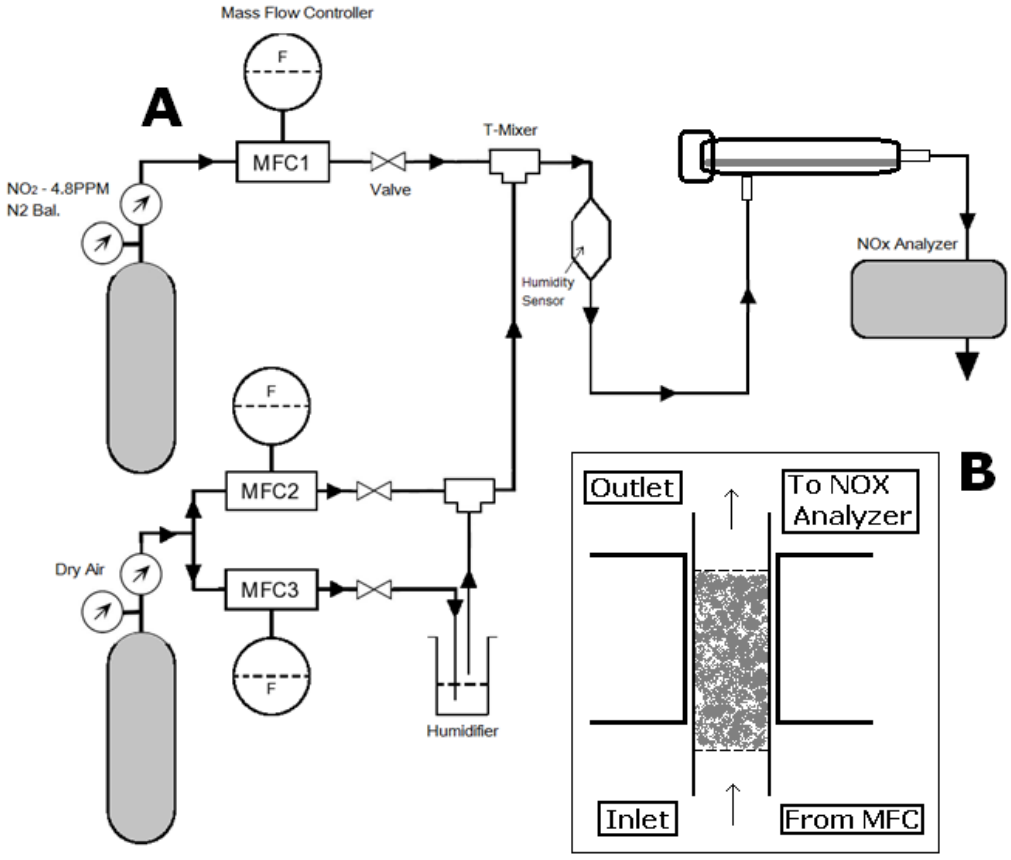

Figure 4.4: Schematic of the (A) flow and (B) fixed bed reactor system

The sample trays were placed inside a sealed reactor and exposed to humidified NO_2/air mixture. The NO_2 concentration was continuously monitored at the outlet by NO_X analyzer (Model 200E, Teledyne API Ltd) and recorded on computer hard drive through the data capture program. Powdered/granular samples were loaded in an alternative reactor configuration which consists of a capillary column of 2 mm diameter (Figure 4.4 A and B). The column was loaded with the crushed concrete, where the size fraction used was selected by passing a sample through a set standard sieves. The experiments with fresh and aged (12 year) concrete utilized size fractions of 0.25mm (60 mesh) and 0.4mm (25 mesh). The concrete samples 1.5 g were exposed to a mixture of 20 sccm (standard cubic centimeter per minute) of NO_2 and 20 sccm of humidified synthetic air for 2 hours, with relative humidity maintained at 50%. The measured NO_2 concentration at the column inlet was 180-190 ppb, where it was measured by NO_X analyzer (Teledyne M200E).

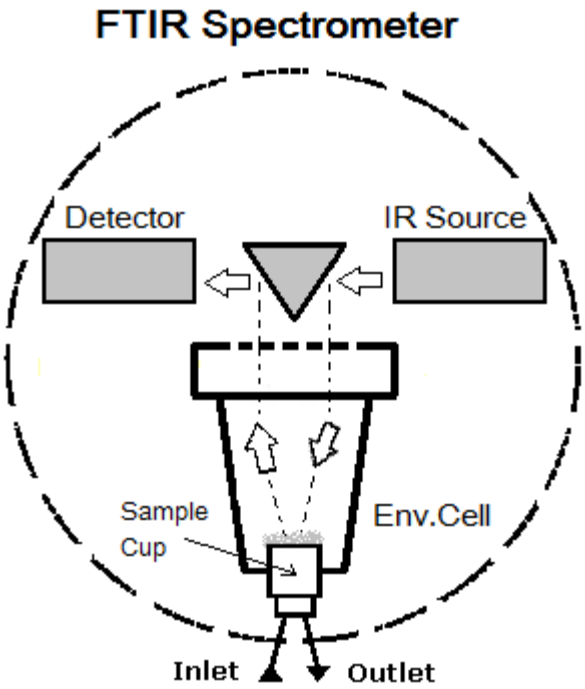

Figure 4.5: Schematic diagram of the DRIFTs reactor cell

Diffuse Reflectance Infrared Fourier Transform (DRIFTS) measurements were performed using the environmental cell integrated into Nicolet 6700 FTIR (Thermo Fisher Scientific Inc.). This setup shown in Figure 4.5, where gas composition and temperature can be easily adjusted, is capable of monitoring surface mediated adsorption/reactions with a time resolution down to 0.5 sec. The detector utilized for these experiments was liquid nitrogen cooled mercury-cadmium-telluride (MCT) detector. The temperature inside the cell was measured by thermocouple (Thermo Scientific temperature controller) and was maintained at 27 °C. The spectral data recorded during the DRIFTS experiments was within the 4000–600 cm^{-1} with spectral range with a resolution of $4cm^{-1}$. Similarly to column experiments, the outlet of DRIFTS cell was connected to chemiluminescent NO_X analyzer (Teledyne API). The concrete sample was tested for 5 days with the 2.4 ppm of NO_2 at 50% humidity. The sample amount was

about 250 mg. Calcium hydroxide powder purchased from Alfa Aesar (99.5% purity) was exposed in the flow reactor to NO_2 at 2.5ppm for over 24 hrs. Subsequently, this powder was analyzed using FTIR to determine formation of nitrate and nitrite phases.

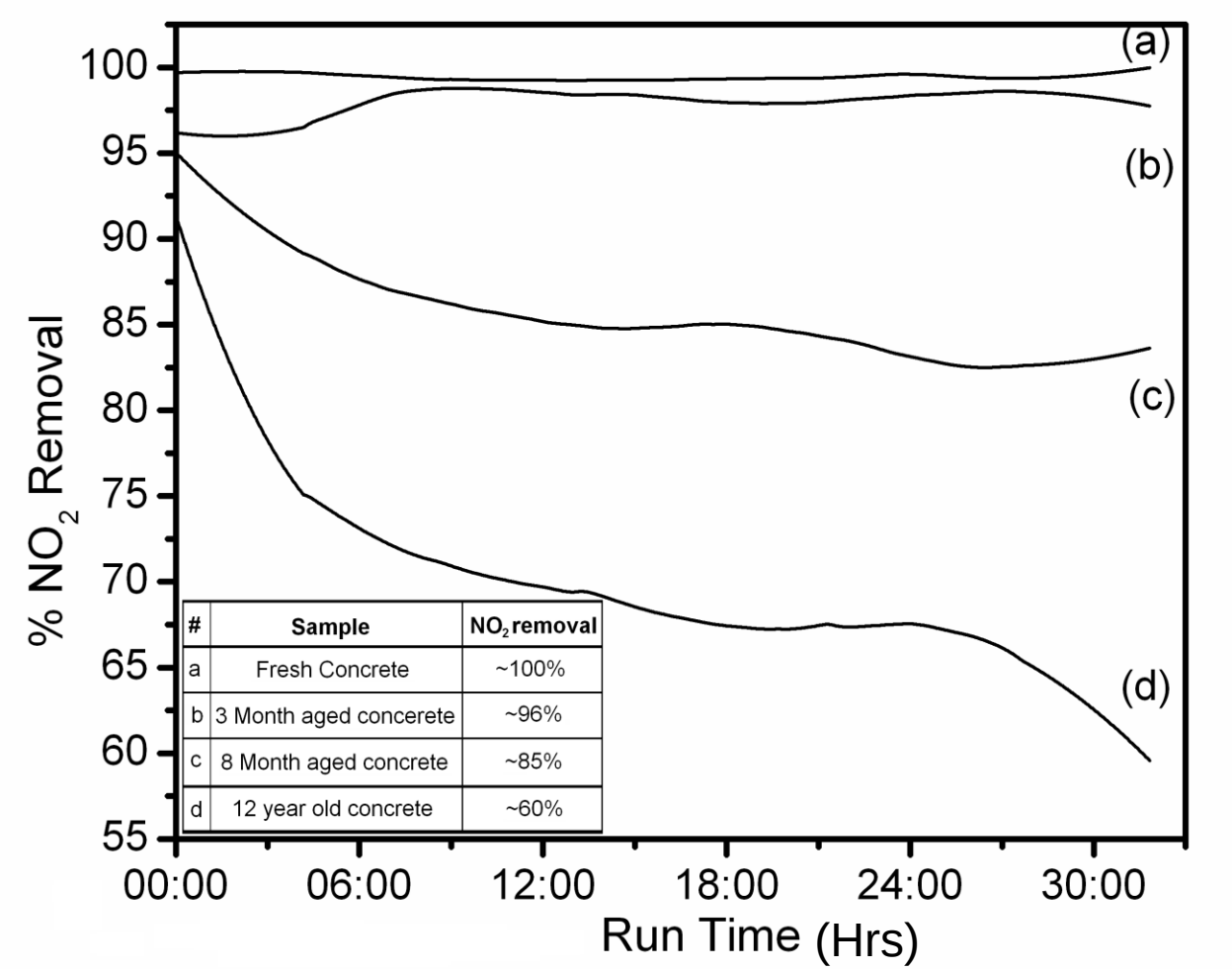

Figure 4.6: Flow reactor results (a) fresh concrete shows highest activity with almost 100% removal of NO2,(b) concrete aged for 3 months displays a slight drop in NO2removal, (c) 8 months aged concrete has a clear reduction in NO2 removal dropping at about 85% within 12 hours, (d) 12 year old concrete retains around 60% NO2 adsorption.

The NO_2 uptake experiments performed for concrete slabs the indicated that freshly prepared samples had the highest adsorption capacity as compared to old concrete samples. Figure 4.6 shows a comparison of NO_2 removal for concrete samples of different age. There is a clear trend of decrease in uptake with increase in concrete age. The fresh concrete sample showed 100% NO_2 removal throughout the experiment. However, even 12 year old sample exhibited almost 60% NO_2 removal at the end of experiment, which is quite striking. The control experiment with empty polycarbonate tray showed a negligible uptake. Also, much smaller uptake in the absence of moisture was observed, indicating that water plays an important role in NO_2 removal. Further fresh concrete under low humidity conditions at 0% RH was tested and it was found that the uptake was about 5-10% of the uptake at 50% RH. It gives indication they are a mix of both heterogeneous and homogenous reactions occurring simultaneously [99-102] and therefore both gas/liquid and liquid/solid processes need to be considered to explain the NO_2 uptake. It is important to note that age dependent NO_2 uptake is related to surface composition of concrete. For example, it is known that surface acidity of concrete depends on the environmental conditions and the age of the concrete [76]. It is known that fresh concrete has significant surface concentration of $Ca(OH)_2$ which is converted to $CaCO_3$ upon exposure to atmospheric CO_2 [99]. This also leads to surface neutralization of concrete over during the exposure of surfaces to the environment, which results in a significant decrease in the pH of concrete. A possible reaction mechanism, which might explain the decreased NO_2 uptake as a function of age is described below:

$$2Ca(OH)_2 + 4(NO_2) \rightarrow Ca(NO_3)_2 + Ca(NO_2)_2 + 2H_2O \qquad 4.1$$

In this reaction, $Ca(OH)_2$ reacts with NO_2 to form calcium nitrate and calcium nitrite. This reaction is thermodynamically feasible having a Gibbs Energy of -437 kJ/mol. It has also been suggested that the calcium nitrite will further decompose to calcium nitrate in the following manner [99]:

$$3Ca(NO_2)_2 + 2H_2O \rightarrow Ca(NO_3)_2 + 4NO + 2Ca(OH)_2 \qquad 4.2$$

4.5 DRIFTs Analysis of NO_X Adsorption

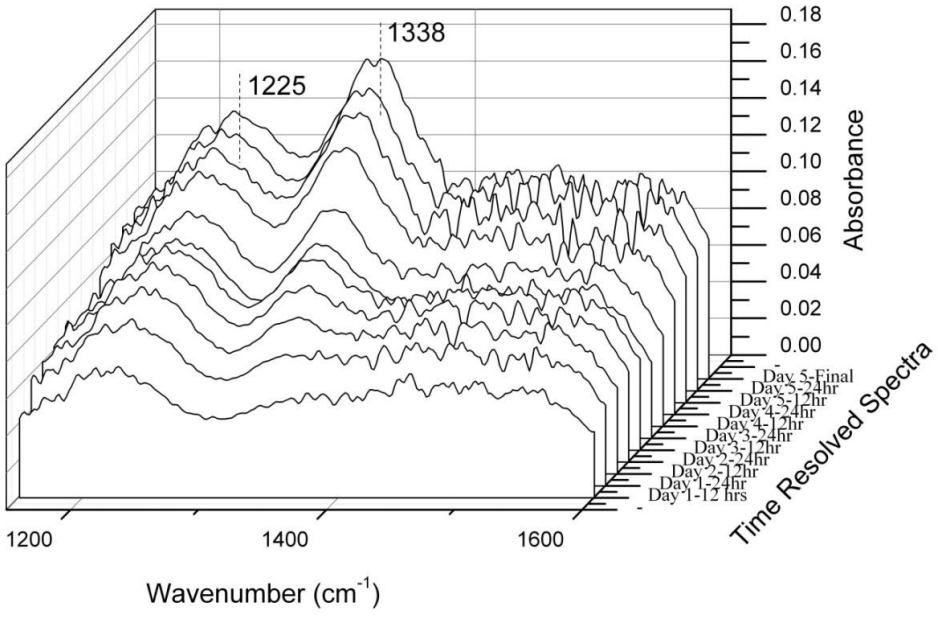

Figure 4.7: Time resolved IR spectra of crushed concrete after 5 days of NO_2 exposure showing nitrite and nitrate peaks at 1225 and 1338 cm^{-1}

In order to determine surface adsorbed reaction products DRIFTs (Diffuse Reflectance Infrared Fourier Transform) analysis of fresh concrete sample were performed. The DRIFTS

experiment was conducted using powdered fresh concrete sample. The increase in the intensity of peaks at 1340 and 1225 cm^{-1} over the duration of the experiment suggests the formation of nitrate and nitrite species as evidenced by the time resolved IR spectra in Figure 4.7 [103]. This might be attributed to reactions (1) and (2) describing $Ca(OH)_2$ reaction with the NO_2 in presence of moisture, which can lead to formation of calcium nitrate and calcium nitrite. In order to verify a feasibility of such mechanism, portlandite $Ca(OH)_2$ phase of concrete was exposed to NO_2. Figure 4.8 shows the IR spectra of the sample after exposure to NO_2 for over 24hrs. The peaks at 1650 and 1340 cm^{-1} are indicative of formation of calcium nitrate phase, consistent with standard spectra for calcium nitrate (NIST Chemistry Web book).

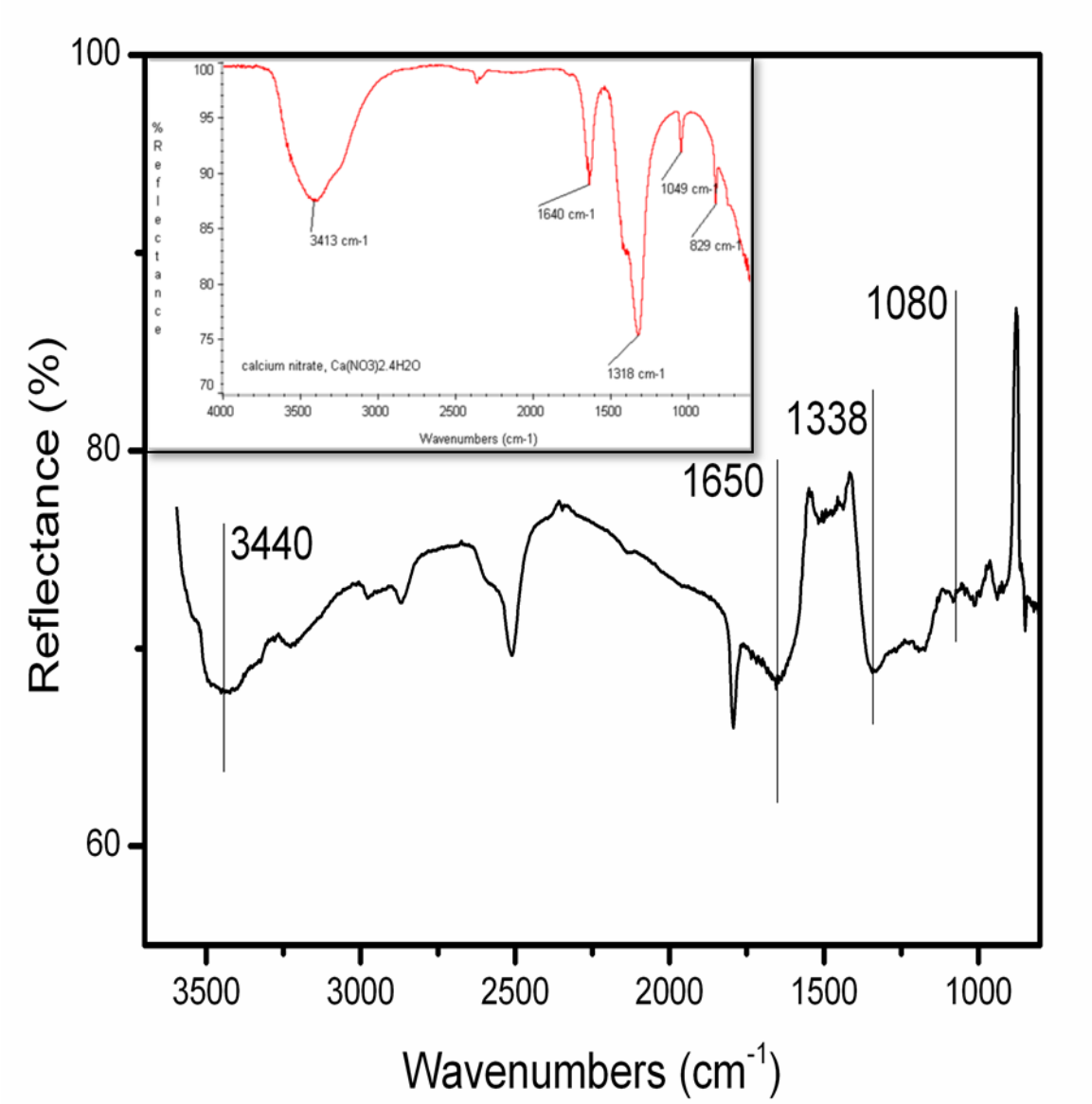

Figure 4.8: FTIR spectra of Portlandite powder after NO_2 adsorption showing nitrate peaks, Inset shows the reference spectra for Calcium Nitrate.

4.6 Fixed Bed Breakthrough Curves

The NO_2 removal efficiency in a packed bed reactor configuration using crushed concrete was tested. Both fresh and old concrete samples were crushed and passed through a set of standard sieves with the 30 mesh (0.5 mm square opening) and 60 mesh (0.25 mm square opening) fractions being selected for experiments. SEM images of all 4 samples showed similar microstructure (Figure 4.9).

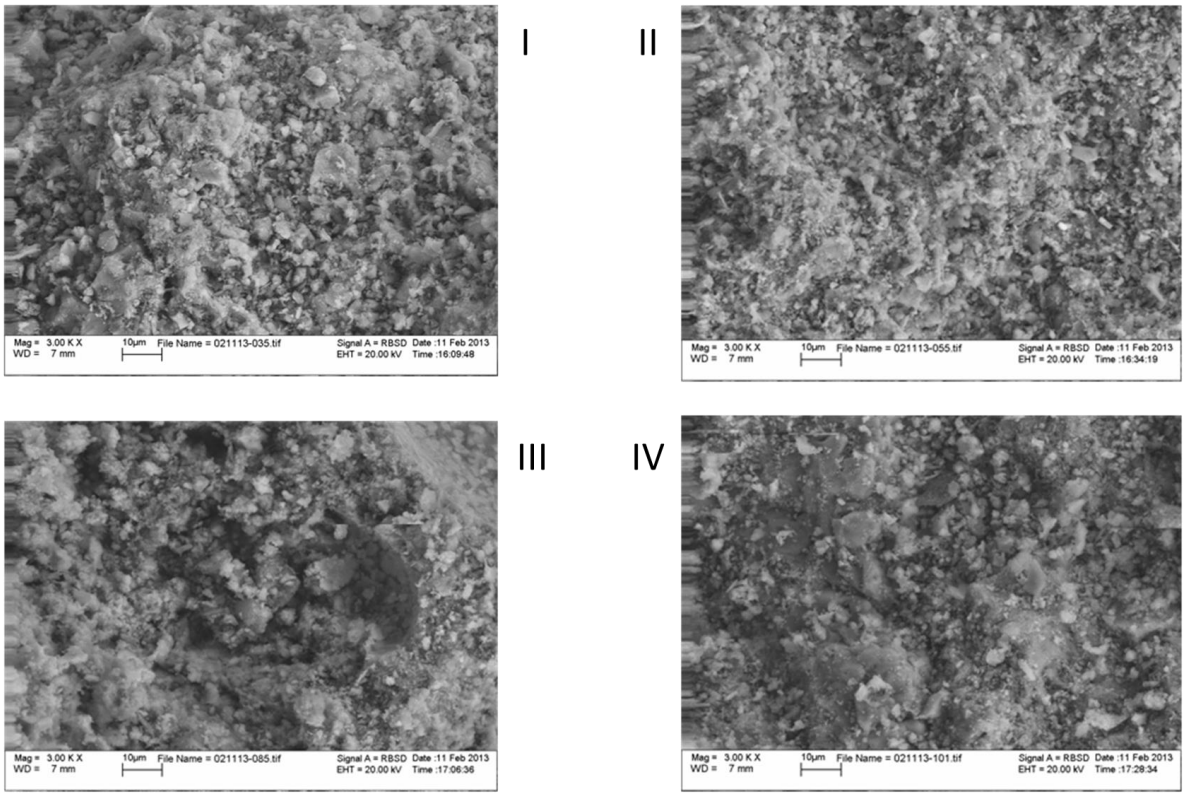

Figure 4.9: SEM images of concrete: I & II show fresh concrete and III & IV show old concrete

Figure 4.10 shows NO_2 uptake on fresh and old concrete (12 years) sample. As expected from the reaction mechanism and greater basicity of the fresh sample surface, fresh sample had

much higher NO_2 removal capacity as compared to that of the old concrete sample. There are also some other notable trends. As expected, the breakthrough for the old concrete samples occurred faster; however, the samples still maintained nominal absorptive capacity. Although the fresh sample had more capacity to adsorb NO_2 in a short run, however, in a long run the slow uptake trend was almost the same as that for old sample.

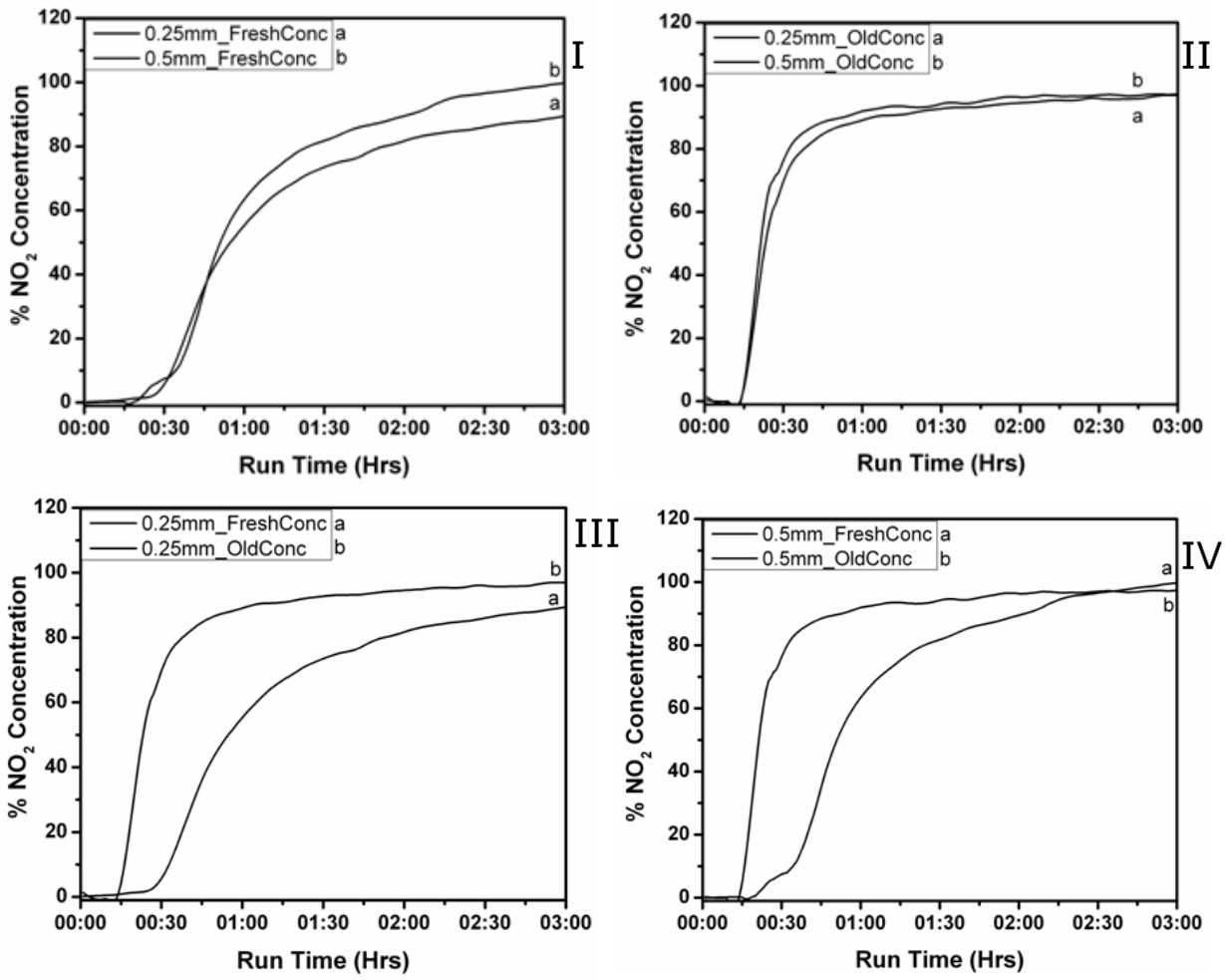

Figure 4.10: Fixed bed reactor data: Graphs I & II show breakthrough curves of fresh concrete and old concrete pellets for (a) 0.25mm (b) 0.5mm sizes. Graphs III & IV compare the two concrete samples

against the same particle size with Graph III comparing fresh (a) and old (b) concrete samples of 0.25mm particle size and Graph IV comparing 0.5mm particle size.

These results are the similar to those seen in the concrete slab experiments described earlier where the NO_2 uptake by old concrete sample was still notable. A mechanistic explanation of these results might be related to $Ca(OH)_2$ content in the old concrete which is reduced over time due to formation of $CaCO_3$ as a result of reaction with CO_2. It is feasible that reaction of NO_2 with $Ca(OH)_2$ will lead to formation of $Ca(NO_3)_2$ and $Ca(NO_2)_2$, as noted in the DRIFTS results. In order to understand the surface and pore size effects on adsorption, BET surface area and average pore size analysis (Quantachrome NOVA 2200e) was performed and results are shown in Table 4.1. Before discussing the data, it is important to note the limitation of this analysis as the old concrete was obtained from industrial sources whereas fresh concrete was prepared in our lab, which might lead to some differences in chemical composition of the samples. Although XRD analysis (Figure 4.11) shows that the bulk composition of two samples is not significantly different, the surface composition might still be quite dissimilar. XRD spectra also shows that there is no portlandite phase visible at 18^0 in the 12 year old concrete, which could be due to the conversion of the $Ca(OH)_2$ to $CaCO_3$. Nevertheless, the analysis of BET data described below still can be instructive. It shows that although the surface areas of two samples are not dramatically different, with 12 year old concrete sample having a slightly higher surface area, the biggest difference is observed in average pore size. A smaller pore size for old concrete might account for diffusion limitations for NO_2 to reach the inner pores and thus resulting in rather slow uptake for the entire course of the experiment.

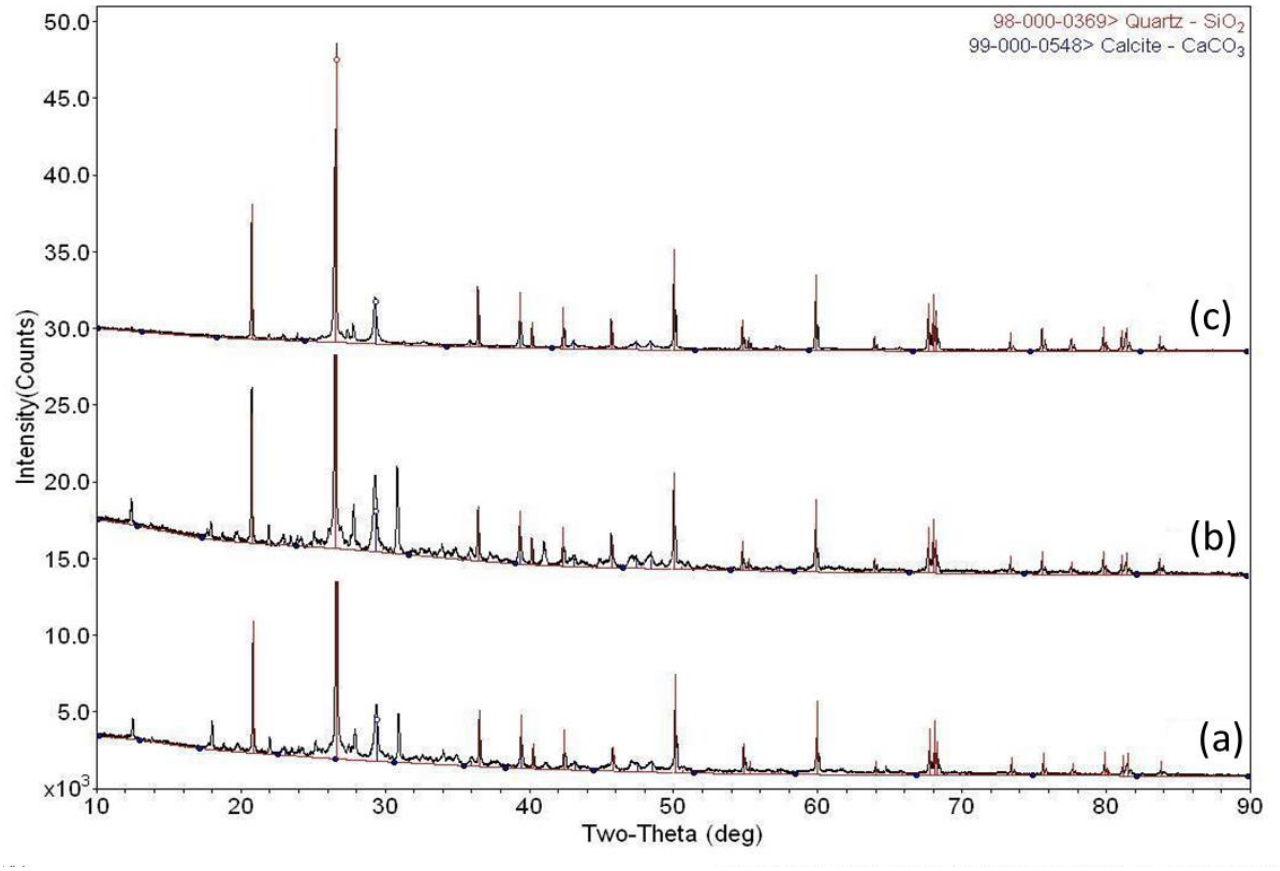

Figure 4.11: XRD comparison of fresh and aged concrete with (a) 3 month old concrete, (b) 8month old concrete, and (c) 12 year old concrete.

The higher concentration and surface availability of $Ca(OH)_2$ in fresh concrete may be the reason for the high initial uptake observed in the experiments. This trend is observed in both the slab and the fixed bed experiments for fresh concrete. It is also known that the portlandite phase in concrete is slowly converted to $CaCO_3$ over the years due to carbonatation, leading to smaller NO_2 uptake. However, with the slight increase in the porosity which was believed to be due to the process of conversion of calcium hydroxide to calcium carbonate (Table 4.1) allows for more reaction sites available for NO_2 uptake inside the concrete matrix, explaining the

relatively steady adsorption in the later stages of the experiments as seen in the slab and the fixed bed experiments for old concrete. The porosity as a function of concrete age in early stage drying of concrete has been studied [104, 105], however the trends in long term porosity changes of individual phases still need further investigation. In fresh concrete once the surface sites are saturated the diffusion limitations into the bulk of the sample where adsorption sites are still available will be governing the uptake.

#	Sample	Surface Area (m^2/g)	Pore Size (A)	Adsorbed Mass of NO_2 (g)
1	Fresh Concrete 0.50mm particle size	5.97	25.175	0.198
2	Fresh Concrete 0.25mm particle size	5.581	15.75	0.202
3	Old Concrete 0.50mm particle size	6.4	16.61	0.091
4	Old Concrete 0.25mm Particle size	7.22	16.638	0.105
5	Portlandite 0.25mm particle size	7.2	15.7	-
6	Portlandite Powder	32	-	-

Table 4.1: BET Surface area and Pore size

Further, the total adsorbed NO_2 for each of the concrete samples is listed in the Table 4.1. The values were calculated up to the breakthrough point for each of the curves given in Figure 4.10. The breakthrough point occurs when the concentration detected at the outlet of the capillary tube filled with the concrete sample was half of the initial concentration of the NO_2 supplied. The breakthrough curve is represented by the following equation, where C_f is the final NO_2 concentration at the end of the experiment, C_0 is the NO_2 concentration at the start of the experiment and r is the initial adsorption rate.

$$C_t = \frac{C_f * C_0 * e^{rt}}{C_f + C_0(e^{rt} - 1)} \quad 4.3$$

This data together with the breakthrough curves further supports the earlier observations regarding the adsorptive capacity of fresh concrete vs old concrete. From the data we can see that the total adsorbed amount of NO_2 for old concrete is almost half that of fresh concrete which is similar to the concrete slab experiments showing a 40% drop in the NO_2 adsorption.

Given the hypothesis that $Ca(OH)_2$ is a possible reason for substantial difference in NO_2 uptake, portlandite $Ca(OH)_2$ was also tested as a possible active phase of the sample. The packed bed results for portlandite are as shown in Figure 4.12. Both the powder and pellet forms of portlandite showed excellent removal of NO_2. The adsorption capacity of these samples was higher than that of fresh concrete, which is expected given that only fraction of fresh concrete derived from Portland cement, is portlandite. The powder sample demonstrated 1005 NO_2 for around 2.5 hours before saturation concentration was reached. On the other hand the pellet sample showed significantly lower uptake and faster deactivation. However, in contrast to powder sample, the pellet sample did not reach the full saturation for over 12 hrs. One possibility in the observed differences might be related to surface areas of the sample as both samples had the same chemical composition.

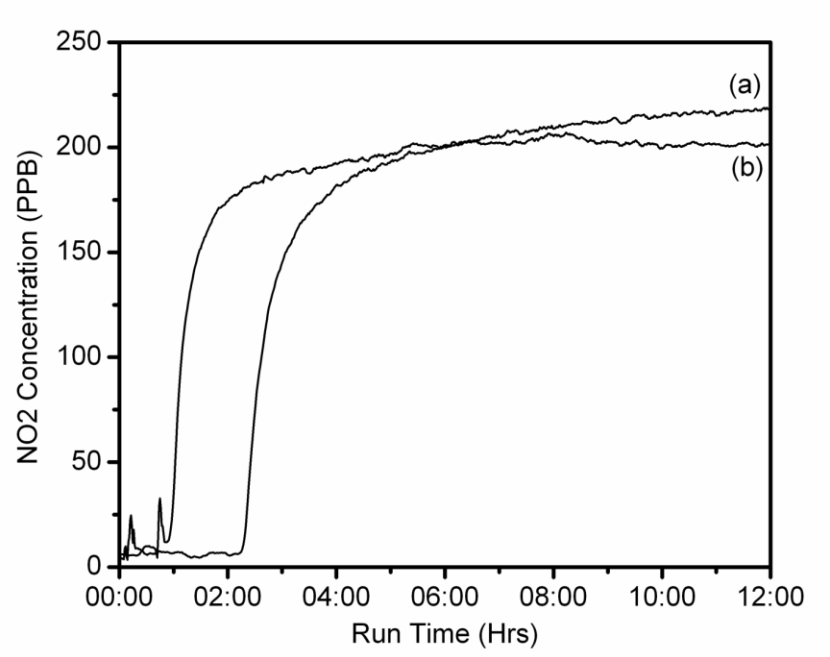

Figure 4.12: NO_2 breakthrough curves for a) Portlandite Powder b) Portlandite pellets (60 mesh)

The surface area of both samples was analyzed using a BET analysis. The surface area of the powder sample accessible to N_2 was found to be 4 times higher than that of the pellet sample, which might account for a higher removal capacity of powder sample at the beginning of the experiment. However, a longer saturation period for the pellet sample might be due to either diffusion limitations for NO_2 to access active sites in the inner part of the pellets, or due to slow breakdown of the pellets due to their exposure to moisture. The data from the earlier DRIFTs experiment together with the above analysis confirms that peaks at 3442, 1650, 1340 and 1080cm^{-1} albeit being slightly blue-shifted can be attributed to nitrate species produced due to NO_2 reaction with portlandite.

4.7 Summary

Here experiments were conducted to understand the feasibility of using concrete as an adsorbent for NO_2 removal. A number of concrete specimen aged for different times were tested and subjected to NO_2 gas in different experimental conditions. The data from these experiments show that fresh concrete is an excellent adsorbent of NO_2 in the given experimental conditions. However, it was also observed that old concrete (12 years aged) still retains a significant portion of its adsorptive capacity removing a sizeable amount of NO_2 from the flow stream. The FTIR analysis of the samples point towards the formation of nitrate and nitrite species on the surface of the exposed concrete. This suggests the possibility of a chemical reaction occurring between the pollutant gas and the hydrated surface.

Chapter 5

SO_X Adsorption by Crushed Concrete

5.1 Introduction

In the previous chapter the adsorption of NO_2 by crushed concrete was discussed. It is well known that NO_X and SO_X are commonly observed together in realistic conditions such as flue gas emissions, power plant discharge, etc. [106, 107]. To understand how SO_X adsorption on concrete occurs in the presence of both gases, we need to first know how each of them interact individually. While there have been studies in the combined adsorption of NO_X and SO_X on Ca based sorbents, these results from these studies have been mostly inconclusive [108-111]. Some researchers have reported that the presence of NO_2 in the flue gas could improve the SO_2 removal capacity of Ca-based sorbents. On the other hand, the effect of SO_2 on NO_2 removal was also studied by some researchers. It was found that slightly higher NO_X removal occurred in both spray drier and baghouse system with the increase of SO_2 concentration [112]. Further, it was also pointed out that the presence of SO_2 in the flue gas could enhance NO_2 removal by Ca-based absorbent at the bag-filter conditions [113]. Lastly, many of the reported experimental data was done under dry or semi dry conditions, and there has been very little research conducted under humid ambient temperature conditions. Thus to gain better insight of SO_2 removal by concrete this subject was investigated further.

In this chapter interactions of SO_2 with concrete using experimental methods like DRIFTs, and XANES was studied. The prepared samples were also characterized using XRD to understand the initial conditions of the concrete sample. Different concrete samples were prepared to study the effects of concrete composition, including proportion of such on components as cement, water, fine and coarse aggregates; on SO_2 adsorption. In order to

understand the effect of each component in concrete the samples prepared for these experiments consisted of a) cement and water (C+W) b) cement, water and fine aggregates (C+W+F) and c) cement, water, fine aggregates and coarse aggregates (C+W+F+Cr).

5.2 XRD Analysis

X-Ray Diffraction analysis of the cement constituents as well as 3 cement samples of different composition was conducted in order to evaluate phases formed during hydration and subsequent hardening. The dried samples from the surface layers were ground by micro mill grinder (Scienceware Ltd) to a fine powder (< 63 μm. The powder was packed into a sample holder for examination in a Philips 1710 X-ray diffractometer using monochromatic CuKα radiation operating at a voltage of 50 kV and current of 30 mA. A scanning speed of 2°2θ/min and a step size of 0.01° were used to examine the samples in the range of 5–80°2θ.

The Figure 5.1a showing XRD patterns of cement clinker demonstrates that it is comprised of four major phases: alite, belite, aluminate and ferrite. Cement also contains minor contributions of gypsum and few other calcium sulfates. Once the cement is hydrated, it forms the C-S-H gel constituting up to 50 to 60% of the overall volume of concrete sample.

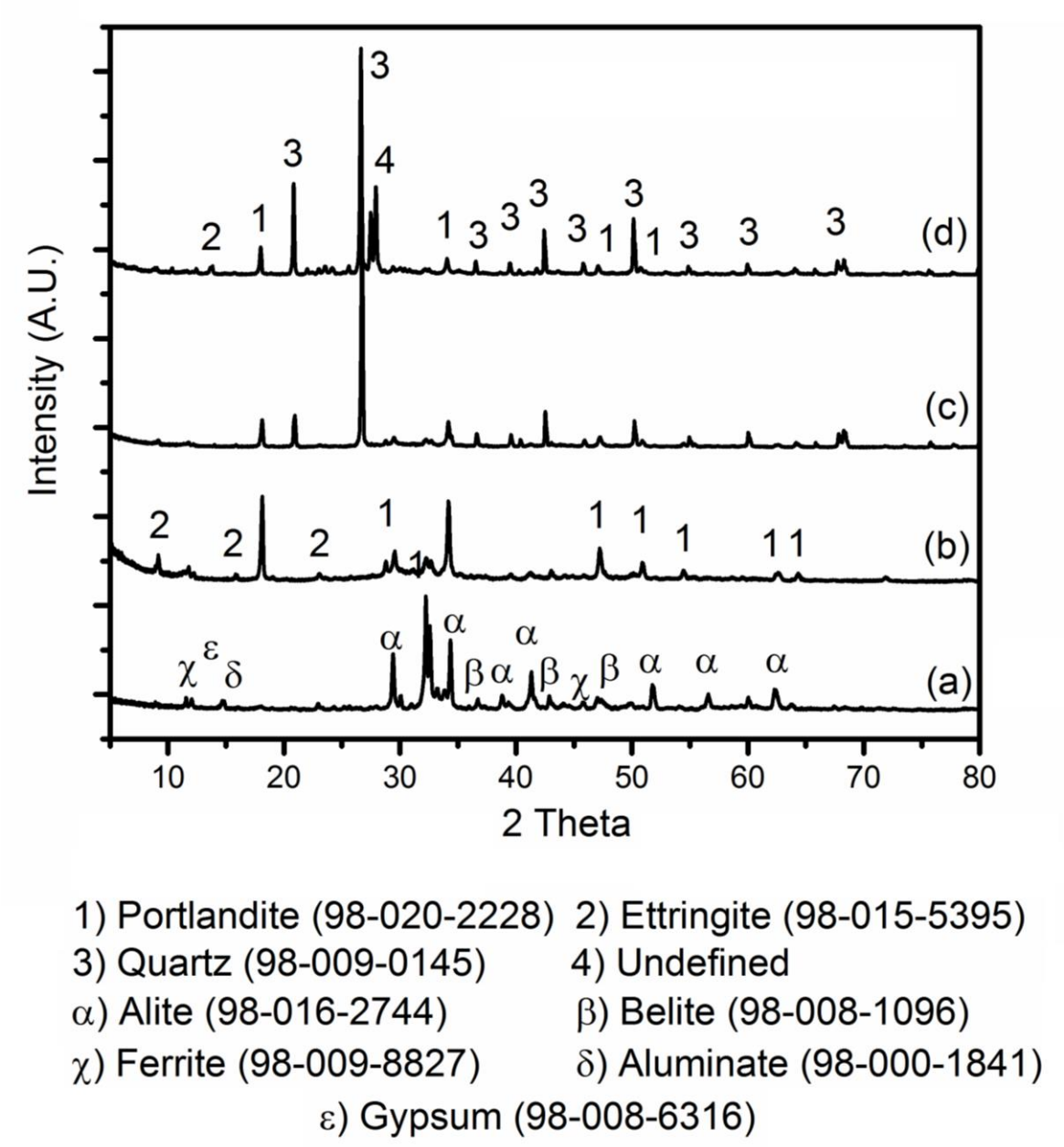

Figure 5.1: XRD spectra of Cement and 3 concrete samples showing different phases.The spectra correspond to the samples as follows (a) cement, (b) C+W, (c) C+W+F and (d) C+W+F+Cr; where C is cement, W is water, F is fine aggregate and Cr is coarse aggregate.

However, the C-S-H phase is very difficult to measure directly due to its amorphous nature and its indeterminate composition. The identification of cement phases present in concrete has additional challenges given poorly crystalline nature of calcium silicate hydrates, which manifest in weak diffraction peaks. These peaks also tend to suffer from interference from very pronounced diffraction peaks originating from such constituents as calcium hydroxide (or from contributions from other minerals).

As only cement and water were used to prepare the first sample show in Figure 5.1 b, we observe that it mainly constitutes of portlandite and ettringite phases. With further addition of fine aggregates, primarily sand, to the C+W+F and C+W+F+Cr samples we notice the strong diffraction peak at around 27° signifying the quartz phase (Figure 5.1c, d). Many of the other features in these two spectra are unfortunately overwhelmed by quartz phase contribution, resulting in loss of valuable information. Finally, in the Figure 5.1 d though most phases have been identified there are a few undefined phases which could be attributed to the coarse aggregates present in this sample. These coarse aggregates have an extremely heterogeneous chemistry comprising of a number of minerals and are difficult to accurately identify.

5.3 DRIFTs reactor experiments

The SO_X uptake of the prepared concrete samples was tested in the DRIFTs environmental chamber. As mentioned earlier, the DRIFTs cell is capable of monitoring surface mediated adsorption/reactions with a time resolution down to 0.5 sec. The detector utilized for these experiments was liquid nitrogen cooled mercury-cadmium-telluride (MCT) detector. The

temperature inside the cell was measured by thermocouple (Thermo Scientific temperature controller) and was maintained at 27 ˚C. The synthetic air was humidified by passing synthetic air through a gas bubbler and mixing it with dry air to achieve target humidity. The ratio of humidified and dry air were determined based on data provided by a humidity probe (Vaisala HMP50 Humidity Probe) positioned downstream. Pulverized samples were loaded in the environmental cell and were exposed to a mixture of 20 sccm (standard cubic centimeter per minute) of SO_2 and 20 sccm of humidified synthetic air for 8 hours, with relative humidity maintained at 50%. The measured SO_2 concentration inside the cell was ~5 ppm.

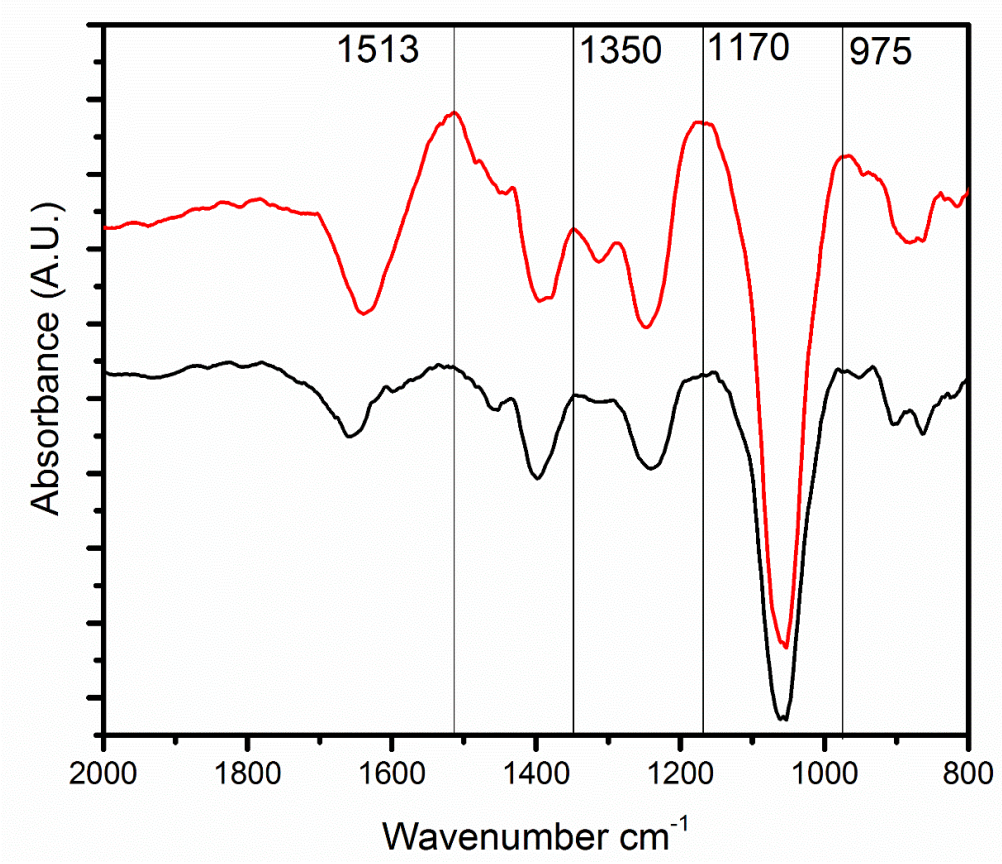

Figure 5.2: IR spectra C+W sample before (black) and after (red) exposure to SO_2 for 8 hours

Figure 5.2 shows the DRIFTs spectra of the C+W (cement + water) samples before and after exposure to SO_X for 8 hours. The initial and the final spectra are compared so as to determine the change of surface composition due to SO_2 uptake on the concrete sample in the presence of moisture. IR peaks at 1513, 1425, 1350, 1285, 1150, and 975 cm^{-1} were affected by SO_X exposure, with intensity of the peaks increasing over time. The prominent peak detected at 1170 cm^{-1} in the final spectra shows the highest change in its intensity as compared to other peaks. According to several studies [114, 115], this band could be assigned to the SO_4^{-2} (sulfate) species. A comparison with the NIST database for calcium sulfate spectra shows the presence of a double peak in this region. Further, the minor peak at 975 cm^{-1} can be ascribed to the SO_3^{-2} (sulfite) species. This is confirmed by both literature data [114, 115] and NIST spectra for calcium sulfite, which is believed to be the product of SO_2 reacting with the portlandite component in concrete. Another interesting observation is the evolution of the double peak 1500 cm^{-1}. The peak sharpens and intensifies after SO_2 exposure. While it resembles the characteristic peak attributed to sulfite species, albeit slightly blue shifted, unambiguous assignment of this peak to these species is probably premature. Lastly the broad band at 1400-1200 cm-1 as seen in Figure 5.2 resolve into two distinct peaks after exposure to SO_2 at 1350 and 1285 cm^{-1}.

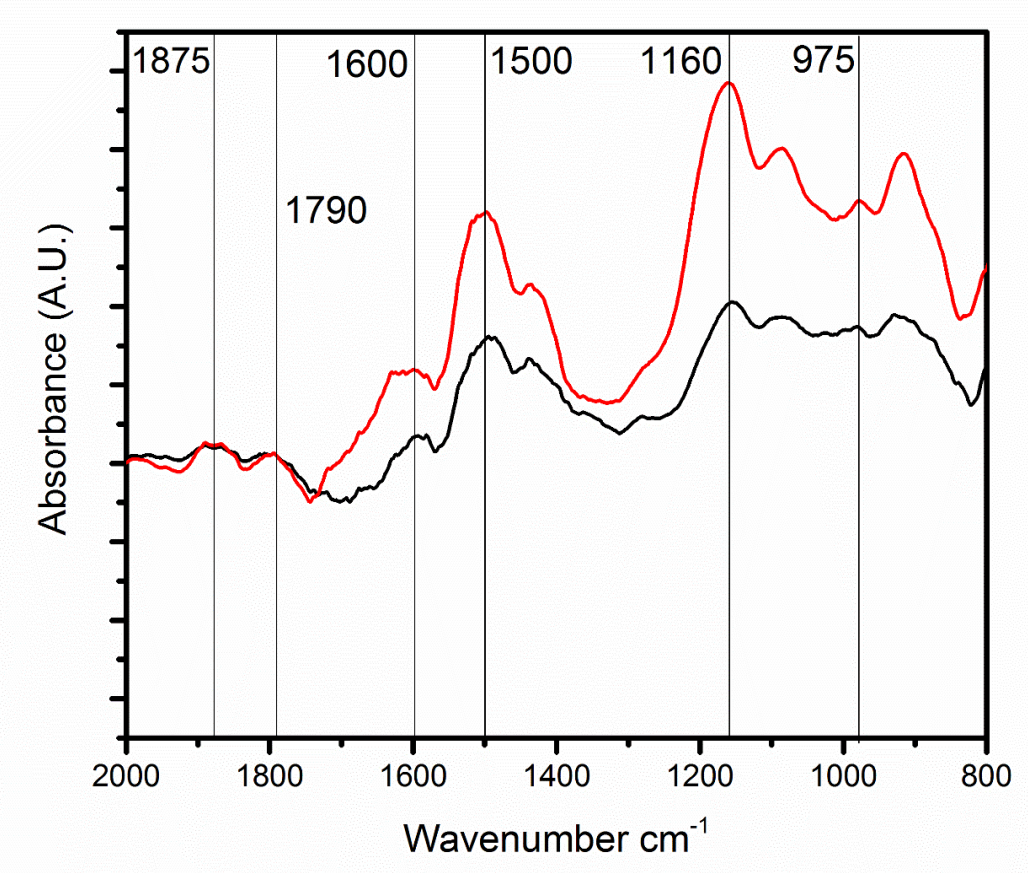

Figure 5.3: IR spectra C+W+F sample before (black) and after (red) exposure to SO_2 for 8 hours

Figure 5.3 represents the IR spectra of the C+W+F (Cement + Water + Fine Aggregate) sample. It is evident that these spectra are more complex that the previous sample. However, many of the characteristic peaks seen earlier are observed here as well. As discussed previously, the peaks at 1165 and 975 cm^{-1} showing marked changes in intensity can be assigned to sulfate and sulfite species respectively. Moreover, similarly to Figure 5.2, 1500 cm^{-1} is present as well. Both the intensity and the blue shift seem to again suggest the presence of sulfite species. Finally, three minor peaks at 1875, 1790 and 1600 can correlated to addition of fine aggregates and to either formation of intermediate phases or the adsorption of water (O-H bending).

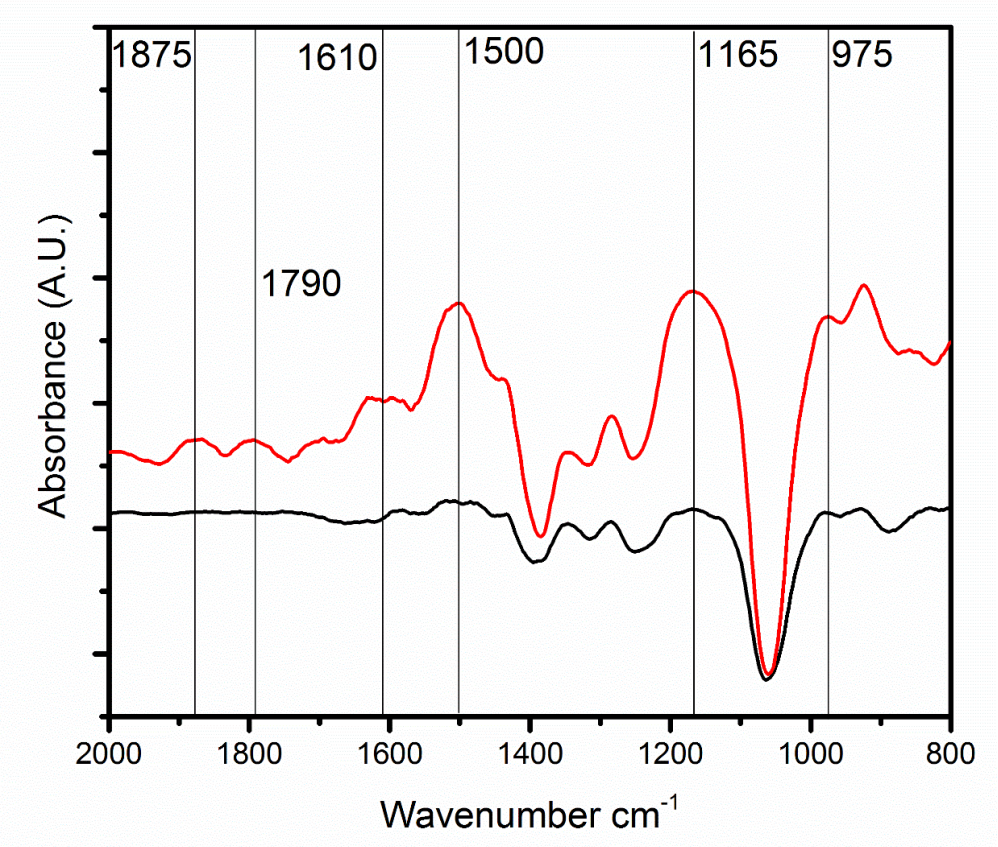

Figure 5.4: IR spectra C+W+F+Cr sample before (black) and after (red) exposure to SO_2 for 8 hours

Figure 5.4 shows the IR spectra of the C+W+F+Cr sample analyzed using the DRIFTs cell. This sample shows similar features as described in the prior section. Peaks at 1160 and 975 cm^{-1} along the broad band at 1500 cm^{-1} are all present. The increase in the intensity of the sulfite peak at 975 cm^{-1}, however, seems to have smaller intensity than that shown in Figure 5.2 and 5.3. The two peaks amid 1400-1200 cm^{-1} are also visible although both of them seem to be present even before exposure to SO_2. This could suggest that the increase in peak intensity might be more due to bonded water molecules rather than to SO_2 adsorption and subsequent reaction.

$$Ca(OH)_2 + SO_2 \rightarrow CaSO_3 \cdot \frac{1}{2}H_2O + \frac{1}{2}H_2O \qquad 5.1$$

$$Ca(OH)_2 + SO_2 + \frac{1}{2}O_2 \rightarrow CaSO_4 \cdot \frac{1}{2}H_2O + \frac{1}{2}H_2O \quad 5.2$$

In general, all samples contained peaks at 1160 and 975 cm^{-1}, which can be assigned to sulfate and sulfite groups. The equations 5.1 and 5.2 as shown above represent the possible reaction mechanisms for the formation of sulfate and sulfite groups. There are also differences between the samples, such as in the peak at 1600 cm^{-1} range, where the possible bonded water peaks are observed (hydroxyl groups) for both C+W+F and C+W+F+Cr. In addition, there are two undefined peaks at 1875 and 1790 cm^{-1}, which can be attributed to fine aggregates or unknown phases present in the concrete samples as these were only seen in the C+W+F and C+W+F+Cr samples. In contrast, the C+W sample seems to have a strong negative peak in this region. Lastly, the observed peak at 1500 cm^{-1} was not unidentified and not attributed to the surface species it represents.

5.4 Time Resolved DRIFTs spectra

Figure 5.5 shows the time resolved DRIFTs spectra of the concrete samples exposed to SO_X. A gradual increase in the sulfate (SO_4^{-2}) peaks was observed and shown in Figure 5.3 (a), (b) and (c). From the Figure 5.3 it appears that the C+W+F and C+W+F+Cr samples show stronger intensity of sulfate peaks than that for the C+W sample. However, the peak at 1500 cm^{-1} in the C+W samples has contributions from other peaks, resulting in underestimation of SOx adsorbance on the C+W sample. Lastly, a more prominent presence of sulfite peaks at 965 and 920 cm^{-1} in the C+W and C+W+F samples (Figure 5.3 a & b) was seen.

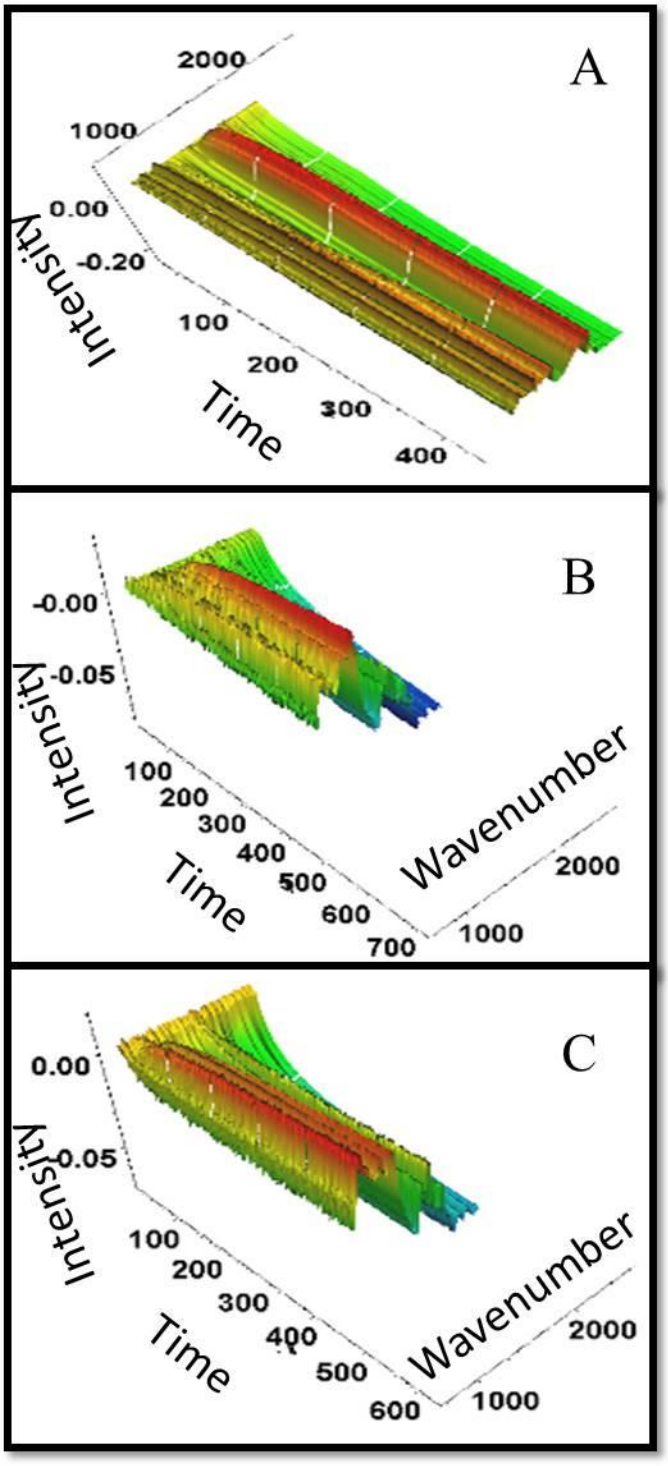

Figure 5.5: Time resolved IR spectra of concrete after 8 Hrs. of SO2 exposure showing sulfate and sulfite peaks between 1625 and 1690 cm-1and ~1150 cm-1. (A) C+W (B) C+W+F and (C) C+W+F+ Cr

5.5 XANES experiments

Chemical form and electronic structure of various systems can be determined using the X-ray absorption near edge spectroscopy (XANES). Different materials including asphalt have been analyzed using XANES to study the sulfur speciation [116-119] in these systems. The technique has been recognized as an effective method for characterizing the local environment of sulfur. However, construction materials have not been ordinarily analyzed using the XANES technique owing to their heterogeneous nature [120-122].

Here, the adsorption of SO_X on different concrete samples and its subsequent surface reactions are studied. To corroborate the DRIFTs results of the formation of sulfur species on the surface and to detect changes in the local environment, spatially resolved XANES is utilized. Further, these spectra are compared to the XANES spectrum of unexposed cement and water mixture.

The sulfur K-edge XANES were recorded in the X15B beamline at the National Synchrotron Light Source (NSLS) of Brookhaven National Laboratory. X15B was equipped with a Si(111) monochromator, with an energy resolution of 0.2 eV at the sulfur K-edge. The XANES spectra were acquired in fluorescence mode and the sulfur K-edge fluorescence was isolated from the detector spectrum. The entire sample environment was purged at 1 atm with helium gas. The spectra for both unexposed cement and SO_X exposed concrete samples were collected by scanning incident energy from 2450 to 2526 eV, with a step size of 0.2 eV and an exposing time of 0.1 s for each step. X-ray fluorescence microscopy method was applied for observing heterogeneous sulfur distribution and selecting several spot positions for XANES measurement.

Ten measurements on an identical position were repeated to achieve one averaged XANES spectrum.

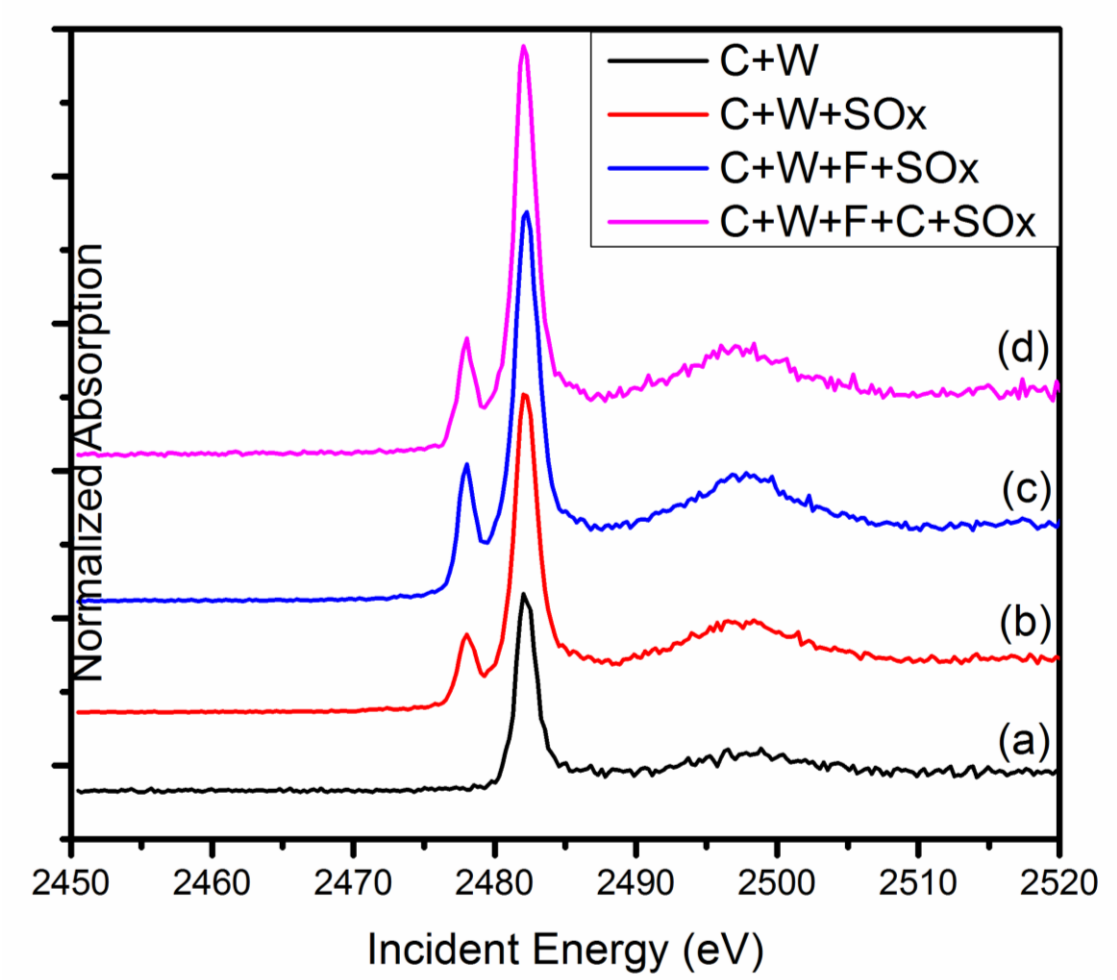

Figure 5.6: XANES spectra of the reference cement and the SO_2 exposed concrete samples

The XANES technique has been widely used to characterize sulfur species because it is nondestructive and very sensitive to the electronic structure that allows it to reveal oxidation state and local symmetry of absorbing site [117, 118, 123]. Figure 5.6 shows the K-edge XANES spectra for the reference concrete and samples exposed to SO_2 for 8 hrs. The XANES spectra for the concrete samples is dominated by a signal arising from sulfate-type moieties near 2482 eV

[124, 125]. This is present in all of the analyzed samples indicating the presence of inherent SO_4^{-2} species in the concrete itself. Further, there is no change in the position of this absorption edge indicating that the oxidation state of elemental sulfur has not changed. However, the increase in the peak intensity on the exposed samples can be interpreted as evidence of formation of surface SO_4^{-2} due to SO_2 adsorption. The appearance of the peak at 2478 eV in the exposed samples can be attributed to the formation of sulfide species SO_3^{-2} [124]. This provides additional support to the observations made earlier in the DRIFTs section.

5.6 Summary

The SO_2 adsorption on concrete was studied to understand the formation of different sulfur species on the concrete surface. Concrete samples were prepared with different components (cement and water with additions of fine and coarse aggregates respective) to understand the effect of each constituent during adsorption of SO_2. These samples were exposed to SO_2 for 8 hours and then examined using various analytical instruments. The data from these experiments shows that SO_2 adsorbs on the concrete surface and forms sulfate and sulfide species. This is confirmed by both DRIFTs and XANES spectra.

Chapter 6

Introduction to Membranes Filtration

6.1 Membranes for Water Filtration

Membranes emerged as a viable means of water purification in the 1960s with the development of high performance synthetic membranes [126]. Implementation of membranes for water treatment has progressed using more advanced membranes made from new materials and employed in various configurations. An increasing scarcity in fresh water sources fueled a push towards alternative resources such as ocean water. In the 1970s, exploration began into using membranes for water desalination [127]. Proving successful at producing purified water from salt water, membranes became a viable alternative to evaporation-based technologies in the water treatment market. Over the years, purified water standards have become more stringent, and a plethora of new applications have appeared [128]. However, new advancements in membrane technology in the last decade has seen improvements in performance, efficiency and cost and membranes continue to be one of the leading approaches in the filtration segment [129].

Widely recognized as the technology of choice for superior water and wastewater treatment, membranes provide a physical barrier that effectively removes solids, viruses, bacteria and other unwanted molecules. Different types of membranes are used for softening, disinfection, organic removal, and desalination of water and wastewater and these can be installed in compact, automated, modular units. Membrane filtration units can also be installed in relatively small facilities and can be fully automated to significantly reduce the required amount of operator attention. Recent advances in technology have significantly reduced the cost of membrane-based systems [130]. With advances in membrane technology, installation costs have decreased over the previous years as membrane systems don’t require large buildings or as much

land as conventional systems. Operating costs have also decreased as modern membranes have higher water output and remove more impurities while using less energy [131]. In the United States, regulations such as the Safe Drinking Water Act and the Long Term 2 Enhanced Surface Water Treatment Rule have had a significant impact on municipal water treatment. This, in addition to increasingly stringent wastewater discharge regulations, has promoted dramatic growth in the implementation of membrane technology.

Filtration in general can be defined as the separation of two or more components from a fluid stream based primarily on size differences as shown in Figure 6.1. The fluid stream here can either be liquid or gas phase and the other components could be any combination of the three phase. Further, the separation of dissolved solutes in liquid streams and separation of gas mixtures is also achieved by membrane filtration. In this thesis, filtration explicitly refers to the separation of solid immiscible particles from liquid streams.

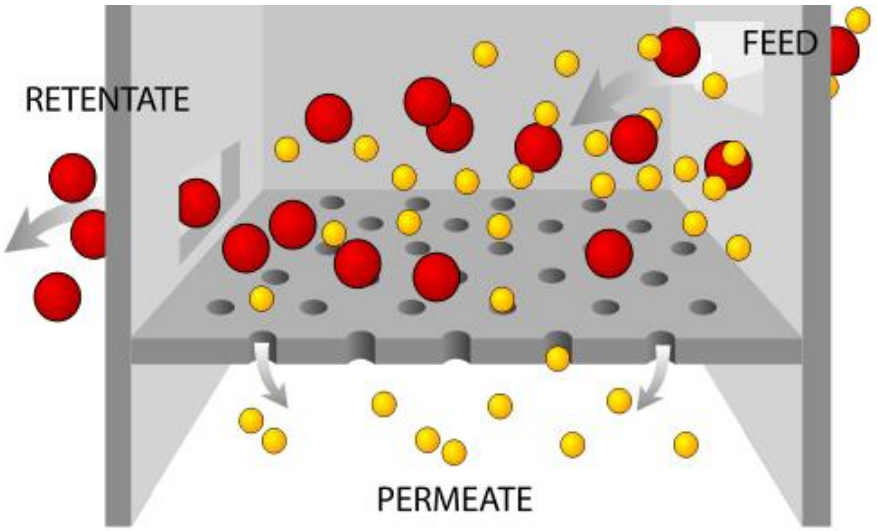

Figure 6.1: Overview of membrane separation process (Koros et al, 1996)

The primary role of a membrane is to act as a selective barrier. It should permit passage of certain components while retaining the remaining components of a mixture. By implication, either the permeating stream or the retained phase should be enriched in one or more components. In its broadest sense a membrane could be defined as "a region of discontinuity interposed between two phases", or as a "phase that acts as a barrier to prevent mass movement but allows restricted and/or regulated passage of one or more species through it" [132]. According to these definitions, a membrane can be gaseous, liquid, or solid or combinations of these. Membranes can be further classified by (a) nature of the membrane: natural versus synthetic; (b) structure of the membrane: porous versus nonporous, (c) application of the membrane: gaseous phase separations, gas-liquid, liquid-liquid, etc.; (d) mechanism of membrane action: adsorptive versus diffusive, ion-exchange, osmotic, or nonselective (inert) membranes.

Membranes can also physically or chemically modify the permeating species (as with ion-exchange or biofunctional membranes), conduct electric current, prevent permeation (e.g., in packaging or coating applications), or regulate the rate of permeation (as in controlled release technology). Thus, membranes may be either passive or reactive, depending on the membrane's ability to alter the chemical nature of the permeating species [133]. Ionogenic groups and pores in the membrane confer properties such as permselectivity and semipermeability.

In terms of versatility for separations, centrifugation is perhaps the only method to match membrane technology. However, an absolute requirement for centrifugal processes is the existence of a suitable density difference between the two phases that are to be separated, in addition to the two phases being immiscible. Membrane separation processes have no such

requirement. Furthermore, as membrane processes can separate from the molecular level all the way up to the macro scale level where particles can be seen, they are able meet a large number of filtration needs across various applications and industries. Another advantage of membrane processes is that they generally do not require a change in phase of permeating species to achieve separation (except for pervaporation). Thus the requirements for energy are generally very low. These power requirements only increase if there is a need to increase the feed pressure in order to drive the permeating component(s) across the membrane. Membrane separations, in theory, are very straightforward to implement. There are no moving parts (except for pumps or compressors), no complex control schemes, and little ancillary equipment compared to many other processes. As such, they can offer a simple, easy-to-operate, low maintenance process option as compared to other alternatives.

There are, however, some limitations to membrane processes. Membranes cannot remove water from solutes and are generally limited in their upper solids limit, i.e. very high particle concentration [134]. Older generation of membranes were plagued with problems such as fouling, difficulty in cleaning, limited operating conditions have actually been overcome through the development of superior membrane materials and improved module design. In this thesis, membranes and membrane processes discussed are strictly restricted to separation of immiscible solids from water.

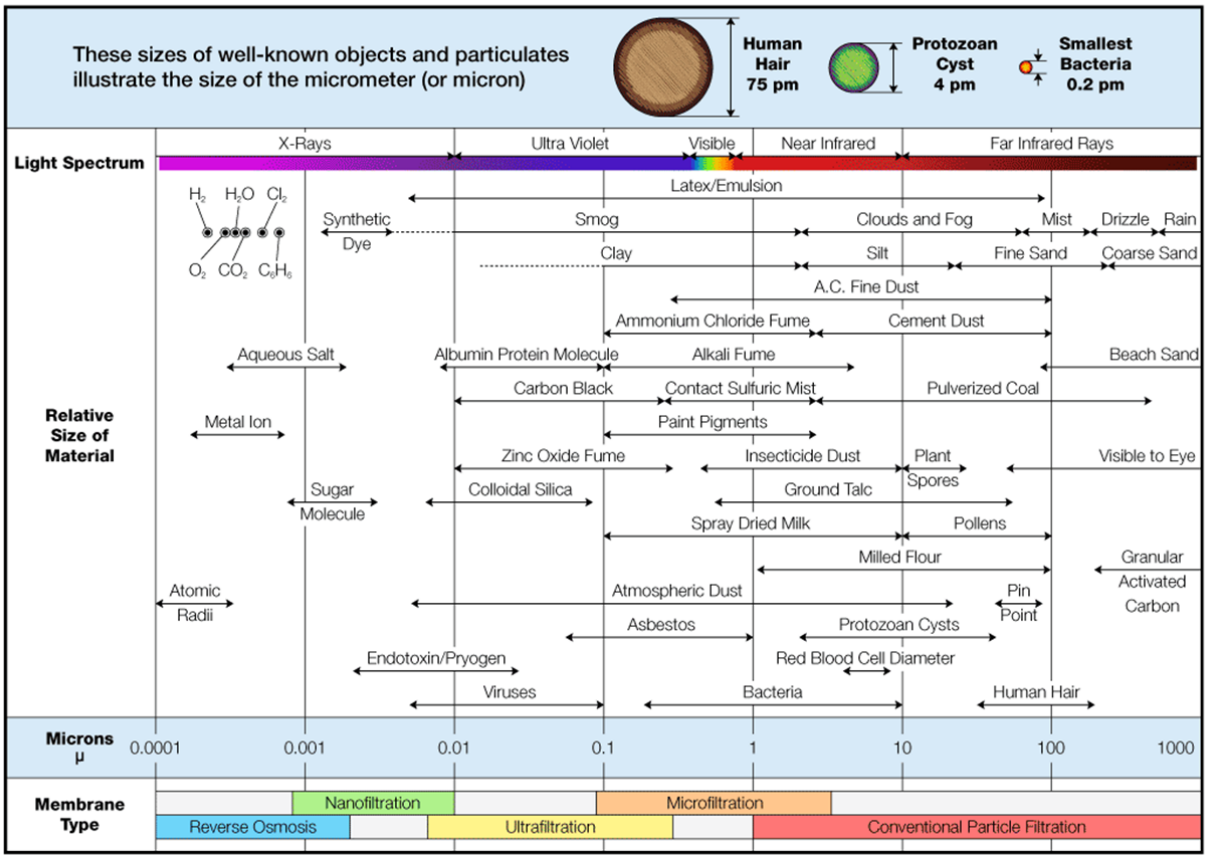

Figure 6.2: Filtration spectrum - Particle size chart for filtration applications (Water Processing, 3rd ed.)

Amongst all membrane applications, water treatment has become one of the most leading applications of membranes and membrane processes [135]. These treatment processes employ several types of membranes, depending on the material, configuration, application and size selectivity of the contaminant [136]. The most basic way to differentiate membranes process is according to the contaminant size selectivity of the membrane. As shown in Figure 6.2 these can be broadly described as microfiltration (MF), ultrafiltration (UF), reverse osmosis (RO), and nanofiltration (NF) membranes. Membranes with pore sizes in the micron range are called MF membranes. These have the largest pore size and typically reject large particles and various microorganisms. The pore size of UF membranes being smaller than the MF membranes, allows

them to additionally filter out bacteria and protein molecules along with large particles and microorganisms. RO membranes are generally considered non porous and tend to reject everything from particulate matter all the way down to low molar mass salt ions and organics. The relatively new segment of membrane processes is called NF membranes, as their operating range is between UF and RO membranes. These NF membranes are nano-porous with average pore size in the order of tens of angstroms. These processes are further elaborated and expanded upon in the next section.

6.2 Types of Membrane Processes

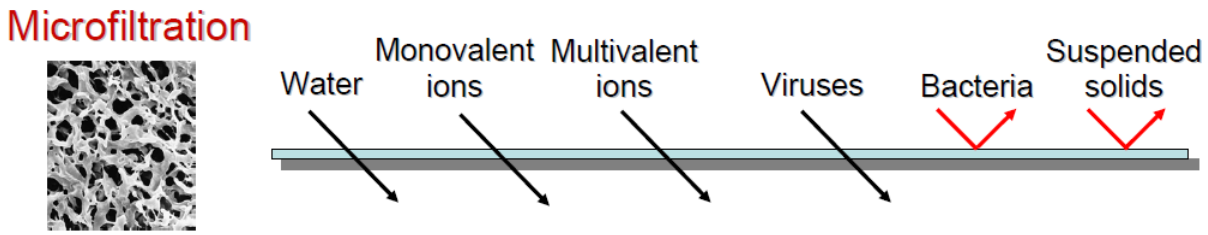

Figure 6.3: Schematic representation of microfiltration (Source: Membrane Technology and Research)

The Micro-Filtration (MF) process involves passing source fluids through a microporous membrane filter which removes particulate or biological matter in the range of 0.025 µm to 10.0µm (Figure 6.3). While depth filters or non-membrane type filters can be used to remove micron size particles, quantitative removal of contaminants requires the use of membranes with precisely defined pore size. MF membranes can be used for both pre-filtration or for final filtration stages in a filtration process plant depending on the requirement and the application. A

depth filter is usually employed in applications where a requirement for quantitative retention is not present or as a pre-filter to extend the life of a downstream filter. However, MF membranes can be used in conjunction with depth filters in filtration processes where they complement each other.

MF membranes are also used as analytical tools to validate the integrity and measure the efficiency of the system. For example, the bacteria captured on the surface of the membrane after clarification or sterilization process can be used for subsequent culture and analysis. MF membranes can also be used to remove undamaged cells from lysate during sample preparation. The pore size cut offs for MF membranes are typically in the range of 0.05µm to 1.0µm.

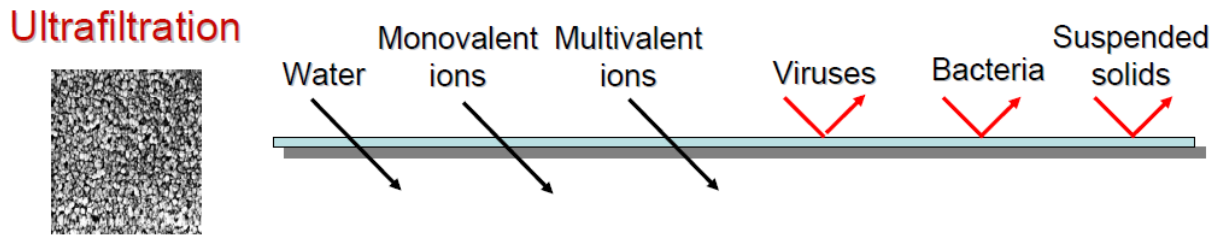

Figure 6.4: Schematic representation of ultrafiltration (Membrane Technology and Research)

Ultra-Filtration (UF) is a filtration process with membranes having pore sizes in the range of 0.1 to 0.001 micron. Typically, UF membranes will remove high molecular-weight substances, colloidal materials, and organic and inorganic polymeric molecules (Figure 6.4). Low molecular-weight organics and ions such as sodium, calcium, magnesium chloride, and sulfate are not removed by UF Membranes. Because only high-molecular weight species are removed, the osmotic pressure differential across the UF Membrane surface is negligible. Low applied pressures are therefore sufficient to achieve high flux rates from an UF membrane. The

primary basis for separation is molecular size, although in all filtration applications, the permeability of a filter medium can be affected by the chemical, molecular or electrostatic properties of the sample. UF can only separate molecules which differ by at least an order of magnitude in size. Molecules of similar size cannot be separated by ultrafiltration. Particulates ranging in size from 1kDa to 1000kDa molecular weight (MW) [132] are retained by certain UF membranes, while salts and water will pass through. Colloidal and particulate matter can also be retained. UF membranes can be used both to purify material passing through the filter and also to collect material retained by the filter. Materials significantly smaller than the pore size rating pass through the filter and can be depyrogenated, clarified and separated from high molecular weight contaminants. Materials larger than the pore size rating are retained by the filter and can be concentrated or separated from low molecular weight contaminants. UF membrane is typically used to separate proteins from buffer components for buffer exchange, desalting, or concentration. UF membranes are also ideal for removal or exchange of sugars, non-aqueous solvents, the separation of free from protein bound ligands, the removal of materials of low molecular weight, or the rapid change of ionic and/or pH environment. Depending on the protein to be retained, the most frequently used membranes have a nominal molecular weight limit (NMWL) of 3 kDa to 100 kDa. UF is more efficient because it can simultaneously concentrate and desalinate solutes. It does not require a phase change, which often denatures labile species, and UF can be performed either at room temperature or in at lower temperatures.

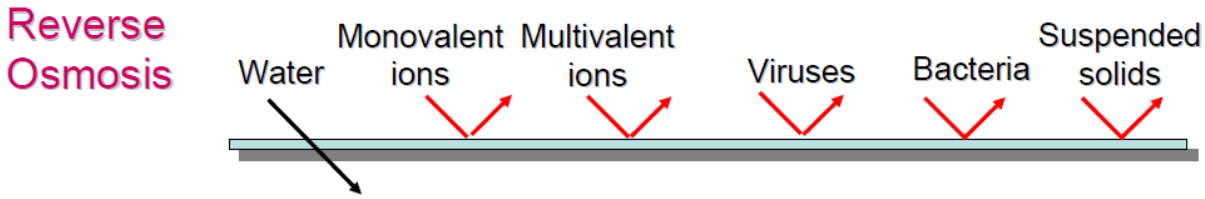

Figure 6.5: Schematic representation of reverse osmosis (Membrane Technology and Research)

The Reverse Osmosis (RO) process separates salts and small molecules from low molecular weight solutes (typically less than 100 daltons) at relatively high pressures using membranes with NMWLs of 1 kDa or lower (Figure 6.5). These membranes are generally rated by their retention of sodium chloride, while UF membranes are characterized according to the molecular weight of retained solutes. For example, Millipore water purification systems employ both RO membranes as well as UF membranes. RO systems are primarily used to purify tap water to purities that exceed distilled water 2 quality [137]. When there are two fluids having varying concentrations of dissolved solids coming into contact with each other, they will mix until equilibrium is attained and the concentration is uniform. When these two fluids are separated by a semi permeable membrane (which lets the fluid flow through, while dissolved solids stay behind), a fluid containing a lower concentration will move through the membrane into the fluids containing a higher concentration of dissolved solids.

After a while, the water level will be higher on one side of the membrane. The difference in height is called the osmotic pressure. By applying pressure which exceeds the osmotic pressure upon the fluid column, there will be a reversed effect. The fluid is pressed back through the membrane, while dissolved solids stay behind in the column. Using this technique, a larger part the salt content in the water can be removed.

This technique is mainly used for drinking water preparation. Other applications include the production of ultrapure water and boiler feed water. RO is also widely used in the food and beverage sector (concentration of fruit juice, sugar and coffee), in the galvanic industry (concentration of wastewater) and in the dairy industry (concentration of milk for cheese production).

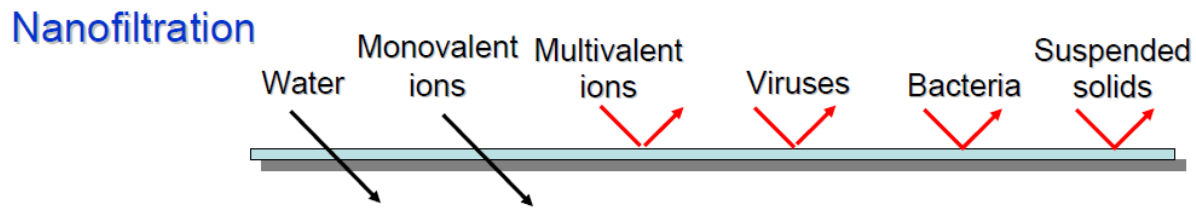

Figure 6.6: Schematic representation of nanofiltration (Source: Membrane Technology and Research)

Nano-Filtration (NF) process is a fairly new membrane filtration process. It is most often used low total dissolved solids water such as surface water and fresh groundwater (Figure 6.6). The main purpose of this is to soften the water and remove disinfection byproducts precursors such as natural organic matter and synthetic organic matter [138]. It is also gaining popularity in the food and beverage processing for applications like concurrent concentration and partial demineralization, especially in the dairy industry. NF is a membrane filtration-based method that uses nanometer sized cylindrical through-pores that pass through the membrane at 90°. NF membranes have pore sizes from 1-10 nanometers, smaller than that used in MF and UF, but just larger than that in RO. Membranes used are predominantly created from polymer thin films. Materials that are commonly used include polyethylene terephthalate or metals such as aluminum [139]. Pore dimensions are controlled by pH, temperature and time during development with pore densities ranging from 1 to 106 pores per cm2. Membranes made from

polyethylene terephthalate and other similar materials, are referred to as “track-etch” membranes, named after the way the pores on the membranes are made[140]. “Tracking” involves bombarding the polymer thin film with high energy particles. This results in making tracks that are chemically developed into the membrane, or “etched” into the membrane, which are the pores. Membranes created from metal such as alumina membranes, are made by electrochemically growing a thin layer of aluminum oxide from aluminum metal in an acidic medium.

6.3 Membrane Classification

As mentioned earlier, there are many ways to classify membranes. Presented below are additional criteria for membrane classifications.

6.3.1 According to membrane material

Polymeric Membranes

Polymeric membranes are the current market leaders in the membrane separation industry as they are extremely competitive in performance and economics [141]. A large number of polymers are available to make filtration membranes, however the choice of membrane polymer is not a trivial job. A polymer has to have relevant traits for the intended application [142] The polymer sometimes has to present a low binding affinity for separated molecules (as in the case of biotechnology applications), and has to withstand the severe cleaning conditions. It has to be compatible with selected membrane fabrication method [143]. The polymer has to have

appropriate properties to its chains rigidity, chain interactions, stereo-regularity, and polarity of its functional groups. The polymers can form amorphous and semi-crystalline structures (can also have varying glass transition temperatures), influencing the membrane performance characteristics. The polymer has to be available and cost effective to satisfy the low cost criteria of membrane separation process. Many membrane polymers are grafted, custom-modified, or fabricated as copolymers to improve their properties [142]. The most typical polymers in membrane synthesis are cellulose acetate, Nitrocellulose, and cellulose esters (CA, CN, and CE), polysulfone (PS), polyether sulfone(PES), polyacrilonitrile (PAN), polyamide, polyimide, polyethylene and polypropylene (PE and PP), polytetrafluoroethylene (PTFE), polyvinylidene fluoride (PVDF), polyvinylchloride (PVC).

Ceramic Membranes

Ceramic membranes today are produced using materials ranging from alumina to zirconia such that spectrum spans from A to Z in terms of materials. The most typical membranes are made of Al, Si, Ti or Zr oxides, with Ti and Zr being more stable than Al or Si oxides [144]. In a few uncommon cases, Sn or Hf are used as base elements. It should be noted that each oxide has a different surface charge in solution. Further different membranes can be composed of mixed oxides of two of the earlier mentioned elements, or are prepared by some added compounds present in smaller concentration.

6.3.2 According to membrane configuration

There are four basic membrane configurations i.e. tubular, spiral, hollow fiber, and flat sheet illustrated below in Figure 6.7. They differ both in packaging and in the type of material used. Each of these configuration has its own advantages and is used to address a range of physical characteristics according to the process fluids.

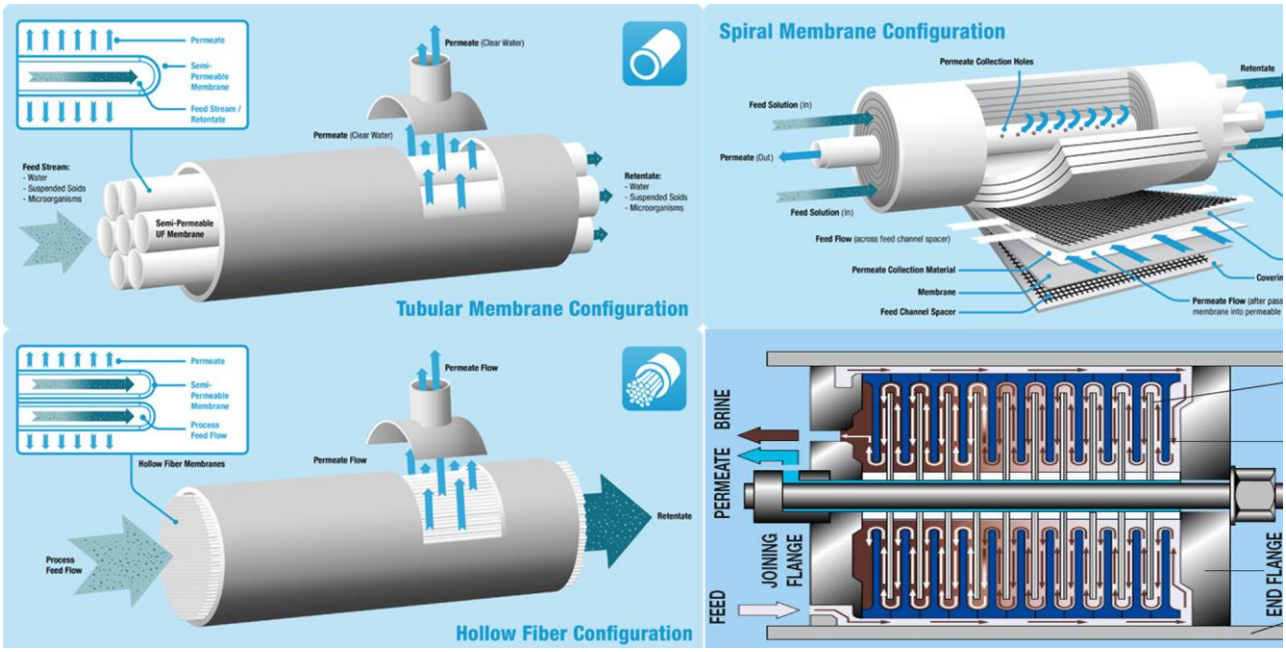

Figure 6.7: Different types of membrane configurations available today. Clockwise from top left (Tubular membranes, Spiral wound membranes, Plate and frame membranes, and Hollow Fiber membranes) (Koch Membrane Systems, Pall Corp.)

Spiral Wound

Spirals were not an early entry in UF or MF, they were invented in the early days of RO [147] and found unsuitable for general UF. The unsatisfactory features were gradually designed out of the spiral, while the attractive attributes; compactness, ease and economy of manufacture

and ease of replacement; were maintained. The truly successful UF spiral required over a decade of constant improvement. Success inspires imitation, and there are now a number of manufacturers of spiral membranes offering a wide variety of membrane types, resulting in a competitive market for replacements and a decline in user's costs. For almost any new application, the spiral design must be inadequate in order for another design to prevail.

Hollow Fiber/Capillary

Capillary devices, designed so that the process fluid flows inside the hollow fiber with the permeate flowing through the wall into a module housing are ideal for process applications, but difficulties in the manufacture of modules plagued them for years. Their primary market niche today for these membranes is in preparation of ultrapure water using UF, where the open path for permeate is an advantage. Capillaries are used in many other applications. In addition to the large volume capillary modules, there are two special variants. One, sold by Memtec (Australia), feeds the process stream on the shell side of the module with permeate exiting in the hollow fiber. This turns general design logic on its head, but it succeeds because of the innovation of pushing off the boundary layer accumulation of solids every few minutes with a blast of air pushed backwards through the membrane. The other variant (Mitsubishi Rayon Engg.) lets the fibers flop in the process stream because only the two ends are potted leaving numerous hairpin shaped membranes free to move in the fluid as it passes by.

Plate and Frame

Plate and frame devices are used in several applications. For most equipment, almost any fiat sheet stock may be fit into a plate and frame device, which can have a favorable influence on the economics of membrane replacement.

Tubular/Cartridges

For the applications where dead-end flow is appropriate, pleated cartridges are the usual answer though a strong movement towards compact and energy-efficient design is becoming apparent. Economics dictate that membrane equipment be compact to reduce the "footprint" on expensive industrial floor space, and improvements in design and membrane reliability make that possible.

6.3.3 According to filtration setup

Dead-end Filtration

The most basic form of filtration is dead-end filtration. The complete feed flow is forced through the membrane and the filtered matter is accumulated on the surface of the membrane (Figure 6.8 a). The dead-end filtration is a batch process, as accumulated matter on the filter decreases the filtration capacity, due to clogging. A next process step to remove the accumulated matter is required. Dead-end filtration can be a very useful technique for concentrating compounds.

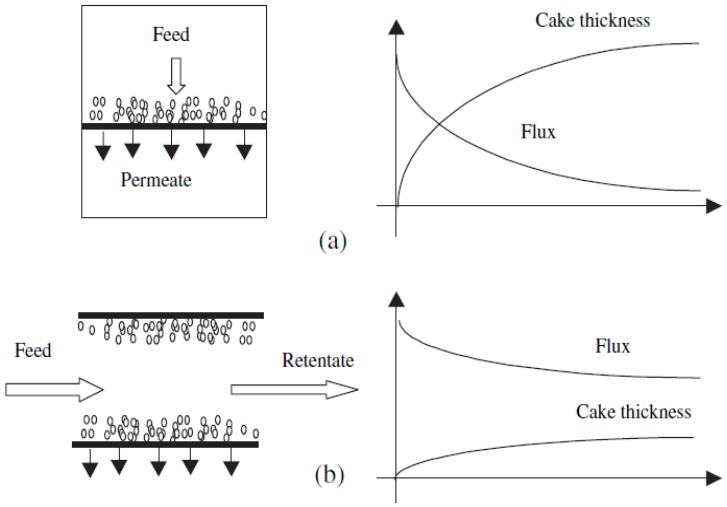

Figure 6.8: Schematic of filtration processes (a) dead end vs (b) cross flow (Ceramic Membranes for Separation and Reaction, Kang Li)

Cross-flow Filtration

With cross-flow filtration a constant turbulent flow along the membrane surface prevents the accumulation of matter on the membrane surface. The membranes used in this process are commonly tubes with a membrane layer on the inside wall of the tube (Figure 6.8 b). The feed flow through the membrane tube has an elevated pressure as driving force for the filtration process, and a high flow speed to create turbulent conditions. The process is referred to as "cross-flow", because the feed flow and filtration flow direction have a 90 degrees angle. Cross-flow filtration is an excellent way to filter liquids with a high concentration of filterable matter.

Hybrid-flow Filtration

The hybrid flow process combines the dead-end and the cross-flow principles. As in the cross-flow filtration tubular membranes are with the filtration layer on the inside wall are used. The filtration process has two phases: the production phase and the flushing phase. During the

production phase, the tubes are closed on one side and a dead-end filtration is performed. During the flushing phase, the tube is open on both sides and the fraction that did not pass through the membranes is removed in order to clean the membrane surface as in cross-flow filtration. This filtration technique is especially suitable for treating water streams containing suspended solids in low concentrations i.e. polishing.

Submerged Filtration

With submerged membrane filtration the membranes are submerged in the liquid that has to be filtered. The filtration is performed from the outside to the inside of the membrane (filtering layer is on the outer side of the tube or plate). Sheer forces along the membrane surface are created by a flow of air bubbles along the surface. In some cases the airflow also results in a liquid flow created by the airlift principle. The driving force is a vacuum applied on the inner side of the membrane.

6.4 Traditional Methods of Ceramic Membranes Preparation

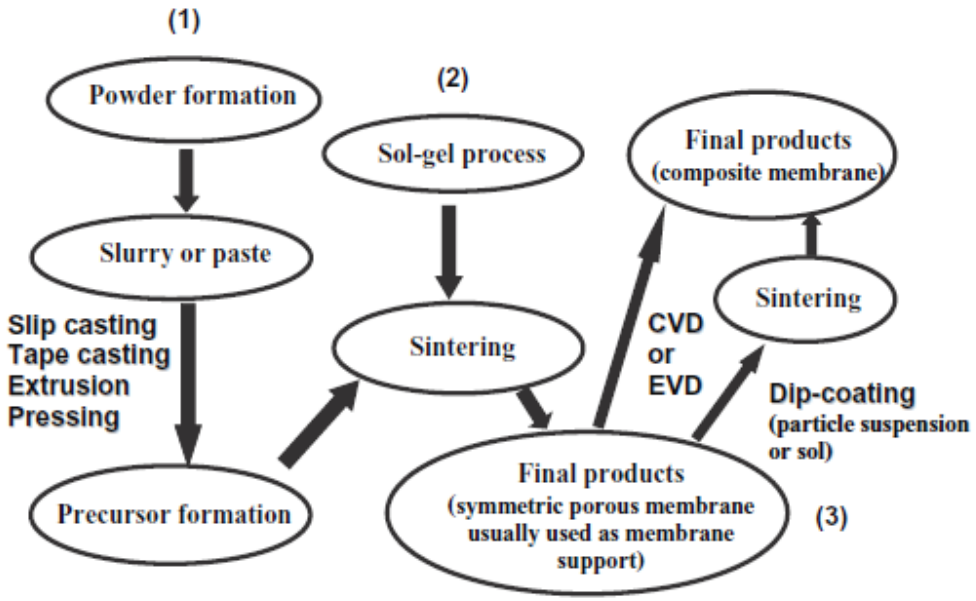

Figure 6.9: A generalized flow sheet for preparation of ceramic membranes using various conventional methods (Ceramic Membranes for Separation and Reaction, Kang Li)

Usually, ceramic membranes are prepared over several steps preparation of ceramic membranes involves several steps: (1) formation of particle suspensions; (2) shaping the membrane precursor i.e. flat sheet, tubular or monolithic and (3) sintering the shaped membrane precursor. A simplified diagram for preparation of symmetric and composite ceramic membranes is shown in Figure 6.9. The different methods listed here turn a slurry or paste into the membrane precursor which is then sintered to form the final membrane. The Figure 6.9 further demonstrates that every single traditional membrane manufacturing technique involving ceramics requires the

final sintering step to obtain finished membranes. Lastly, multi-layer or composite membranes need be repeatedly sintered after each layer to form the final membrane. Using the thermal spray technique for preparation of membranes presents a clear advantage as it does not involve the sintering process. Further, multi-layer membranes can be prepared concurrently without the need for repeated sintering.

6.4.1 Tape Casting/Rolling

This is one of the first methods used for large scale production of metallic membranes in the form of plates and sheets. The steps involved in this process are illustrated in the Figure 6.10. Here, ingots of the membrane precursor material are prepared by melting it at a high temperature. These ingots then undergo high temperature homogenization after which they are subjected to either hot and cold forging or pressing. Finally, the material goes through a repeated sequence of alternate cold rolling and annealing till it acquires the desired thickness. Palladium alloy tubes with a thickness of 50 μm and an outside diameter of 0.6 mm have been made commercially in Russia by seamless tube drawing [148]. The control of impurities at various processing stages becomes extremely critical when the metal foil becomes thinner. These impurities greatly affect the performance of the finished membranes,

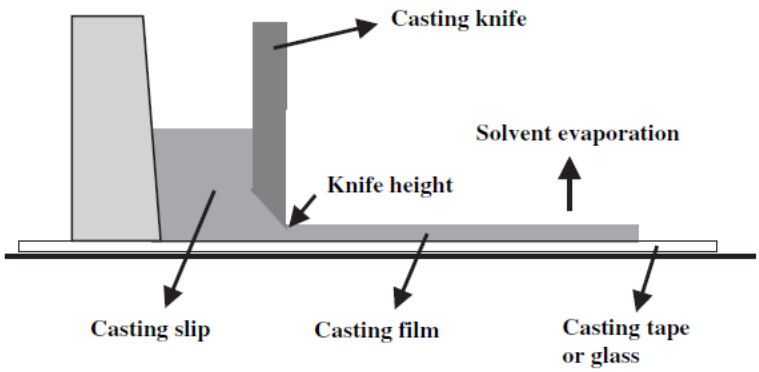

Figure 6.10: Tape casting process of membrane production (Ceramic Membranes for Separation and Reaction, Kang Li)

The inclusion of trace elements like (C, S, Si, Cl and O) or foreign particles or gases may render the membrane unusable by collection both sides of the membrane. Traces of certain materials (such and inclusion of foreign particles or gases may connect both sides of the membrane (with a thickness of 10 µm or less) and thus render it unsuitable for separation purposes. Aluminum foils have been made down to a thickness of 10 µm and special fabrication methods can be used to produce palladium (or its alloys) foils with a thickness under 1 µm [149].

6.4.2 Vapor Deposition

Dense membranes have been prepared using both chemical and physical vapor deposition (CVD and PVD) techniques. For PVD method, the membrane material is deposited via physical means (i.e. thermal evaporation or sputtering) whereas for CVD process it is done by chemical reactions.

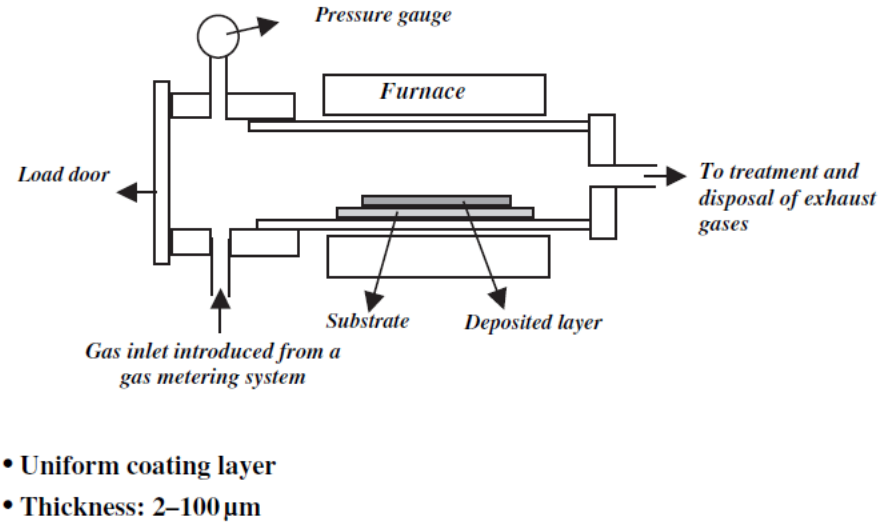

Figure 6.11: Vapor deposition process (Ceramic Membranes for Separation and Reaction, Kang Li)

During physical vapor deposition (also called thermal evaporation), a solid material is first vaporized by heating at a sufficiently high temperature followed by depositing a thin film onto a cooler substrate by condensation of the vapor (Figure 6.11). This process is usually conducted under high vacuum (approximately 10~5 torr). Conventional resistive heating of the metal to be deposited can be used as the evaporation energy source, but the issue of potential contamination of the metal with the crucible or lining materials can be serious. Other evaporation schemes such as electron gun, laser beam or flash evaporation do not require direct contact of the metal with the crucible and are also more energy efficient. Thin films of Pt, Ag, Au and Al have been deposited on porous supports by physical vapor deposition [150]. Due to the different partial pressures and evaporation rates of the metal components in an alloy melt, physical vapor deposition processes suffer from the shortcoming that direct deposition from solid alloys cannot be well controlled. Instead, dense alloy membranes may be produced by simultaneous or

sequential evaporation from separate sources of pure metals with the resulting compositions determined by the relative evaporation rates of the constituent metals.

Another kind of physical vapor deposition technique that can handle alloy deposition in a more controllable fashion is sputtering. The rates of evaporation for various metals using this method are similar. It does not involve thermal evaporation, instead, the method entails the use of rapid ion bombardment with an inert gas such as argon to dislodge atoms of a selected solid material and then deposit them onto a nearby target substrate. Its rate of deposition is in general lower than those of thermal evaporation processes. For comparison, the deposition rates for the resistive heating and the sputtering methods are approximately > 1 μm/min and < 0.1 μm/min, respectively. Films of Pd and Pd-Ag alloys as thin as 30 to 60 nm have been prepared by several researchers according to this technique [149]. Thin dense metal membranes on porous supports have been widely studied in recent years to impart a high permselectivity and a relatively high flux at the same time. Two parameters are found to be most critical to the synthesis of gastight and mechanically strong composite membranes by sputter deposition: the surface roughness of the support and the deposition temperature [151]. Fine pore supports result in better quality membranes than coarse-pore supports. The optimal deposition temperature appears to be about 400°C for coating an alumina support with thin palladium membranes (less than 500 nm thick).

6.4.3 Extrusion

A number of metal oxide powders can be mixed with certain organic additives to form a paste, called slip, for fabrication of dense ceramic membranes of a tubular or rod form by plastic extrusion. The slip generally has sufficient plasticity for ease of processing, or is added with

plasticizers such as glycerol or rubber solution in an organic solvent to be formed into various shapes, and yet is strong enough to maintain the physical integrity of the molded shape at its green state (i.e., before firing or calcining/sintering). The organic additives usually consist of solvents, dispersants, binders, plasticizers, viscosity modifiers, etc. The composition of the additives required depends on the characteristics of the ceramic powders, such as size distribution and morphology, and the forming conditions.

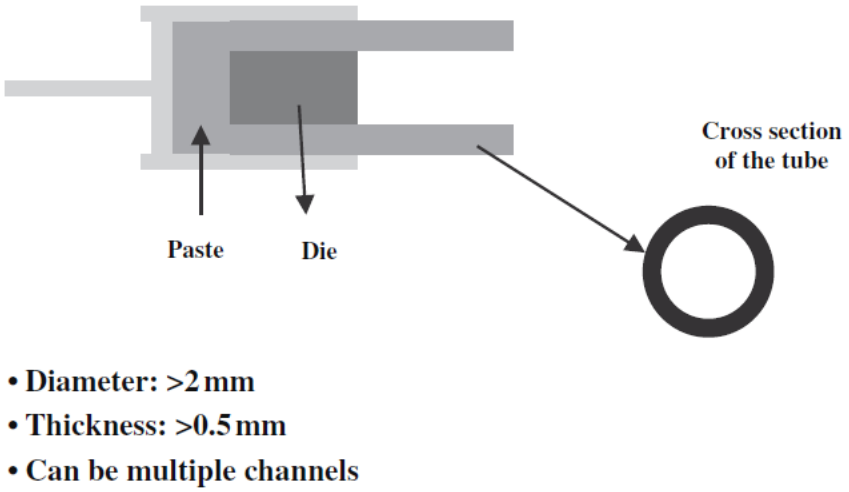

Figure 6.12: Extrusion method (Ceramic Membranes for Separation and Reaction, Kang Li)

The plastic mass of the slip is then forced through an extrusion die at high pressure to produce tubes or multichannel, honeycomb structures (Figure 6.12). The extruded shapes are typically heat treated slowly in the lower temperature range to remove gases from the decomposition of the organic additives. The heating rate is then escalated to the sintering range. For example, [152] describes the above procedures for making ceramic membrane tubes from perovskite-type oxides. They prepared ceramic powders of La-Sr-Fe-Co-0 perovskites by solid-state reaction of the constituent carbonates and nitrates. The powders are mixed and milled in

methanol with zirconia media for 15 hours, then dried and calcined in air at 850°C for 16 hours followed by further grinding. The resultant powders are then made into a slip by mixing with organic additives which facilitate shaping and maintaining green strength of the slip. The slip is extruded into tubes of an outside diameter of 6.5 mm and up to 0.3 m long at an extrusion die pressure of approximately 20 MPa. The tubes are then heated in air slowly at 5°C/h around 150-400°C range and then faster at 60°C/h to reach and stay at a high sintering temperature of 1200°C for 5 to l0 hours. The final composition and phase structure of the dense solid electrolyte membrane can be strongly influenced by the oxygen partial pressure employed during the sintering step. Sintering temperature or rate can depend on a number of factors. Slow densification of the membrane may be attributed to a low cation diffusion rate. For the ZrO2-CaO solid electrolyte, the maximum densification occurs at the lowest CaO content required for stabilization [153]. The sintering temperature should be high enough but not too high that the ion permselective properties are lost. The material can undergo substantial volume expansion as a result of phase transition, thus potentially leading to destruction of the physical integrity.

6.4.4 Pressing/sintering

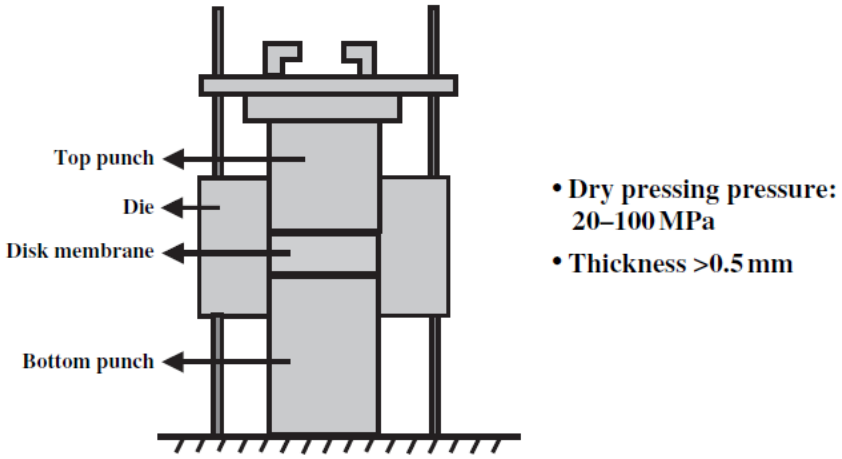

Figure 6.13: Pressing method (Ceramic Membranes for Separation and Reaction, Kang Li)

Disk and plate membranes can also be formed using conventional cold or isostatic pressing methods. Cold pressing technique requires pressures between 2000 to 100,000 psi. Isostatic pressing methods applies uniformly distributed hydrostatic pressure from all directions to improve the overall density of the membrane. Sometimes partially sintered compact is subject to the isostatic pressing. Typically some solvent such as water and some binders (e.g., poly vinyl alcohol, zirconium oxychloride or wax) and lubricants (e.g., carbowax) are used [153]. These organic binders are volatilized during the sintering process and burn out at temperatures above 300° C.

Similar to the extrusion method, pressing technique also requires the precursor particles (i.e. alumina, zirconia etc.) to be mixed or reacted with an inorganic cementing material. Generally, the cementing materials are preferred to have permselective properties comparable to the precursor particles. Adhesive materials like phosphates of zirconium, titanium and zinc are

common examples of such cements although other materials such as calcium aluminate and calcium aluminosilicates can also be considered as potentialcandidates as well [154]. Lastly, for these cementing materials to be effective, the metal oxides must be only partially hydrated so that they are reactive with the bonding compounds. As earlier, the final step in this method is the sintering process.

6.4.5 Slip casting/sintering

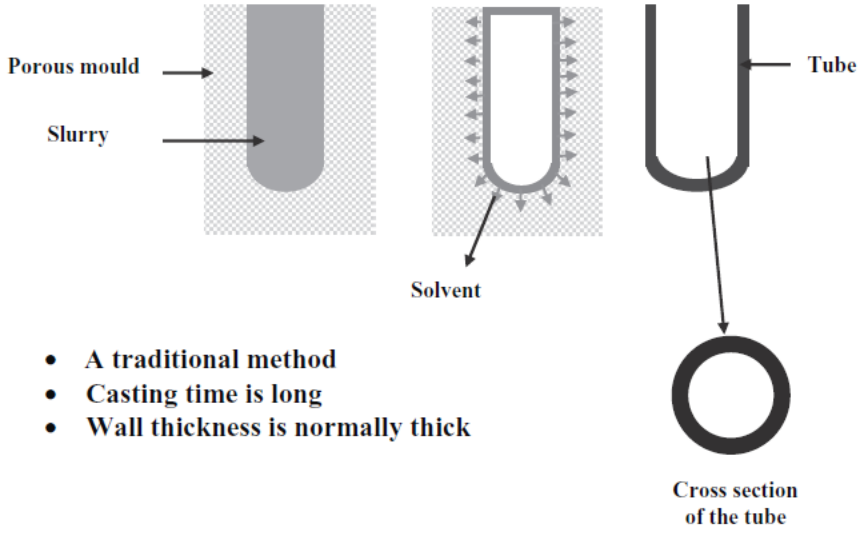

Figure 6.14: Slip casting method (Ceramic Membranes for Separation and Reaction, Kang Li)

Tubular membranes can also be produced using the slip casting method. In the slip casting process tubes can be slip cast in plaster molds using the so called slip prepared from the stabilized powders and a binder such as polyvinyl alcohol as shown in Figure 6.14. The slip is maintained at a pH level of 3-4 and is degassed prior to fabrication in order to remove any

entrapped air. Dosage of the binders dictates the rheological behavior of the slip. Further, viscosity modifiers are sometimes added to control the rheology for ease of processing.

Ceramic membranes with mixed ion and electronic conducting materials (e.g., yttria-stabilized zirconia doped with titania or ceria) can be slip cast into a tubular form from the pastes containing the constituent oxides in an appropriate proportion. These cast tubes are then subject to sintering at 1,200 to l,500°C [155].

6.4.6 Sol-Gel Method

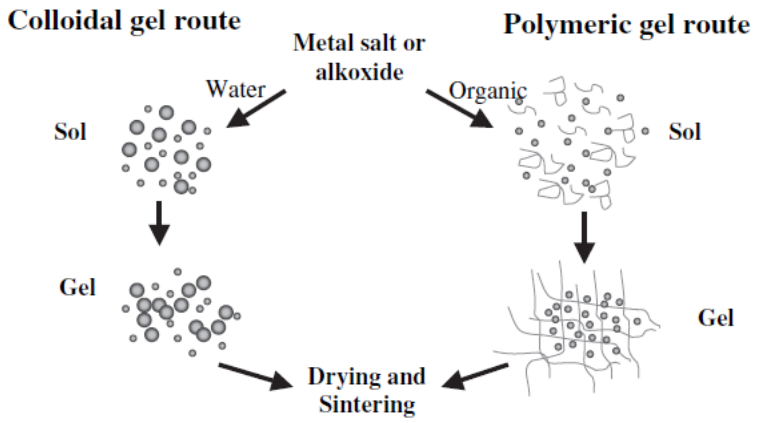

Figure 6.15: Sol-Gel method (Ceramic Membranes for Separation and Reaction, Kang Li)

The sol-gel method was first applied for development of ceramic UF membranes by Leenaars et al. [156-158]. This technique was said to be one of the most significant methods for fabrication of ceramic membranes. It was believed as one of the most important techniques in fabrication of ceramic membranes. A more comprehensive description of this technology can be found in the literature [96, 159-162]. Sol-gel method offers the key advantage of being able to

accurately control the desired pore size of the membrane. This is especially true when it comes to membranes with small pores. The Figure 6.15 shows the two major ways the membrane is prepared using the sol-gel technique:

(1) The colloidal route, in which a metal salt is mixed with water to form a sol. The sol is coated on a membrane support, where it forms a colloidal gel.

(2) The polymer route, in which metal–organic precursors are mixed with organic solvent to form a sol, which is then coated on a membrane support, where it forms a polymer gel.

Colloidal sols are the colloidal solutions of dense oxide particles such as Al_2O_3, SiO_2, TiO_2 or ZrO_2. Leenaars et al. developed g-alumina membranes with pore diameters of 4–10 nm from a bohemite sol [156]. As the pore sizes of these membranes are in the UF range, they have been used in separation of colloidal particles and large molecular weight solutes, or have been used as a membrane support where smaller pore size membranes can be further developed. For gas separation based on molecular sieving effects, ceramic membranes with pore sizes less than 1 nm must be employed. In this case, the membrane can be prepared through the polymer sol route using the g-alumina membrane prepared from the above colloidal sol as a support. It should be noted that in the polymer sol route, the pore size of the membrane prepared is determined by the degree of branching of the inorganic polymer. As can be seen, a low degree of branching would result in a narrower pore system. Polymeric sols of SiO_2 with low branched clusters have been prepared using acidic hydrolysis with the corresponding Si alkoxides [163, 164]. These sol-gel membranes show high selectivities in gas separation [163].

Since sols of very small particles are prepared through hydrolysis and condensation of their corresponding alkoxides, the partial charges of the metal in the alkoxides influence the hydrolysis behavior. Transition metals such as Ti or Zr in the alkoxides carry much higher partial charges than the Si in tetraethylorthosilicate. Transition metal alkoxides hydrolyse much faster than Si alkoxides. In addition, the properties of the type of R ligands in the alkoxide, the degree of oligomerization of the starting alkoxide, the possibility of a coordination expansion of the metal during the hydrolysis and the pH influence the hydrolysis behavior. In the drying process of the coated sol, gelation takes place. After thermal treatment, the gel particles become sintered and the membranes are produced through the sol-gel technique.

6.4.7 Dip Coating

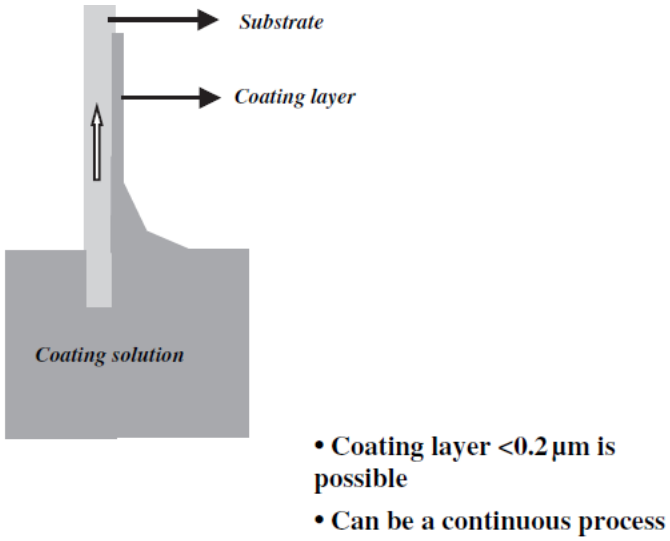

Figure 6.16: Dip coating method (Ceramic Membranes for Separation and Reaction, Kang Li)

The process of producing membranes via the dip coating technique is show in the illustration Figure 6.16. The critical factors that affect dip coating are a) the viscosity of the

particle suspension and b) the coating speed or time. Here, the drying starts simultaneously with the dip coating. This is especially true when the substrate is in contact with an atmosphere having relative humidity below 100 %. For a multi-layer or multi step membrane, the complete dip coating procedure i.e. dipping, drying and calcination is repeated after the first layer is calcined. Alumina membranes have been prepared with nominal pore size of 100nm using commercially available sub-micron alumina power with d=500nm [165].

6.5 Need for scalable membranes

A membrane system is built from components and assembled into modules which, in turn, form the complete system. The-single components consist of a (usually ceramic) supporting system and the final (usually ceramic) separation layer. The supporting system can be a single plate, tube, hollow fiber or monolithic multichannel or honeycomb structure. The final separation layer can be porous or dense and single phase or composite. A hierarchic system can be built from a sandwich of macro-, meso-, microporous layers, which can be tailor-made by changing the chemical or physical nature of the pore system. Each step (product) in the manufacturing process can be used for specific applications. The quality of the underlying support (system) determines, to a high degree, the properties and quality of the final top layer and the number of steps necessary in a multi-step coating process to obtain a defect-free final separation layer. The support system must also fulfil strict quality standards and requirements and must be compatible with other components of the membrane module and system.

Before a membrane system is accepted by users in applications on a commercial scale, many requirements must be fulfilled. The main requirements are related to a large number of technological problems to be solved and/or a variety of possibilities for realization.

On the membrane market, polymeric membranes are used extensively while inorganic membranes are mainly used in special cases, where polymeric membranes cannot be used. In the inorganic membrane markets ceramic membrane materials are dominant, especially alumina membranes which are widely used. Ceramic membranes are especially suitable for processes with high temperatures and harsh chemical environments or for processes where sterilizability of the membrane is important. Because of this, the ceramic membranes have found many applications in the food, beverage, biotechnological and pharmaceutical industries as well as in the petrochemical industry, environmental control, electronic industry, gas separation and other process industries. In 1986, the market of membrane industry worldwide was about $1 billion. In 1989, the market of inorganic membranes was about $32 million and of ceramic membranes $19 million. Nowadays, the worldwide market of the membrane filtration industry is over $10 Billion USD per year. The share of ceramic membranes in this market has gone from a few million USD to almost $3 Billion USD as of 2014 and is expected to increase to $5.1 Billion USD by 2020 [166]. In food, beverage, and biotechnology applications inorganic membranes constitute 12% of the market. The main usage (80%) of inorganic membranes is in the dairy industry [167, 168].

A major disadvantage is the large pumping capacity is required for almost all inorganic membranes in order to operate them at the recommended velocities of 26 m/sec. A single USFilter 37P19-40 module containing 37 Membralox elements, each 102 cm long with 19 of the 4-mm diameter channels, would have a membrane area of about 8.9 m^2 (95 ft^2) and require a

cross-flow rate of 700 gallons per minute (gpm) or 160 m^3 per hour (As per Pall Corp. website). The pressure drop with water would be 0.5-1.5 bar. In general, one should choose the smallest channel size available that can handle the feed. Not only will it require less pumping, but it will also lower the unit cost of the membrane, since more area will be available in the element with smaller channels.

Lastly, the expensive nature of ceramic membranes is probably the biggest limitation of ceramic membranes. For example, in 1996, polymeric spiral-wound membrane elements cost \$50-100/m^2 in the United States. Inorganic membranes cost \$250-400/m^2 this makes it economically infeasible to use ceramic membranes over polymeric membranes despite the performance advantages. This thesis aims to provide the first step in the production and scale up of cheap ceramic membranes for use in micro and ultrafiltration processes.

Chapter 7

Thermal Sprayed Membranes for Water Filtration

7.1 Introduction to Thermal Spray Technique

Ceramic membranes are heavily used in filtration processes which not only demand high chemical and thermal stability but also extended durability. However, applications of these membranes are limited by a few major drawbacks, resulting in a much smaller market share as compared to that for polymeric membranes. These drawbacks as explained in the previous chapter include high manufacturing cost, stemming from expensive fabrication methods, complex processing, and higher operating costs [165]. Traditionally produced ceramic membranes via sol-gel, extrusion, and/or sintering methods are time consuming to manufacture and expensive [167]. While many methods have been explored to reduce the fabrication costs of the ceramic membranes [171], low scalability of membrane's dimensions remains an issue to overcome. Therefore, in order to expand the market for inorganic membranes, cost effective and scalable manufacturing methods need to be developed.

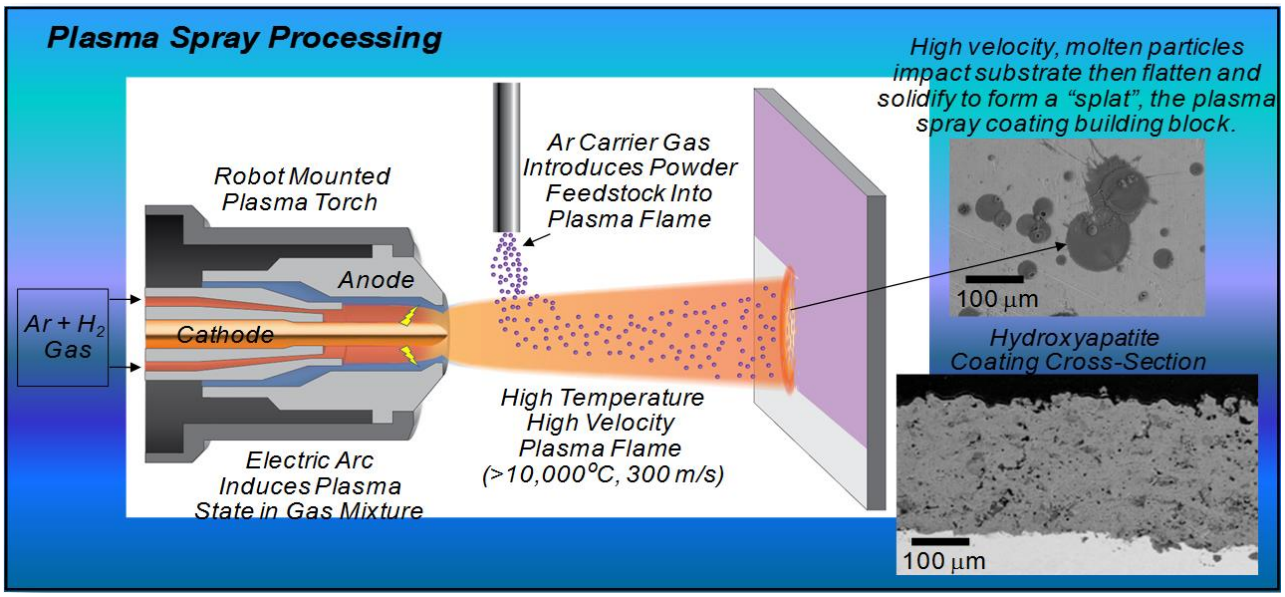

Figure 7.1: Schematic diagram showing the plasma spray process (CTSR, Stony Brook University)

Thermal spray (TS) is a well-established technique for producing protective coatings which are extensively used in industries requiring thermal or surface protection of components, such as gas turbine, heavy machinery, etc. The process requires use of a high temperature and high velocity flame, such as plasma jet and oxy-fuel jet to melt the feedstock material and to deposit it onto a substrate surface (Figure 7.1). The coating formation occurs with successive impingement of molten material in droplet forms on the substrate surface [172]. Due to layer-by-layer assemblage of individual particles, also referred to as 'splats', these coatings contain a myriad array of various kinds of defects, such as macro pores, interlamellar pores, microcracks, oxide inclusion etc. (Figure 7.2) [173]. The process can coat almost any non-volatile material including metals, ceramics and even polymers. There are several variants of this process, such as combustion flame spray (CFS), atmospheric plasma spray (APS), vacuum plasma spray (VPS), high-velocity oxygen fuel (HVOF) and others [174]. Among these methods, APS and CFS are

the simplest and the most cost effective processes. For example, in such applications as fuel cells, APS provides significant cost and performance advantages as compared to that for the conventional wet casting process [175]. Given that the main focus of TS technology is to produce protective coatings, it would be also extremely encouraging to produce high quality porous membranes using a technique that is traditionally reserved for fabrication of coatings for thermal insulation. Over the last decade there have been several attempts to produce porous coatings using TS APS method with a primary focus on such applications as gas separation and fuel cell electrodes [176]. However, there have been only a few attempts to use this technique to manufacture porous ceramic membranes for water filtration [177-179]. These attempts produced low porosity membranes, which exhibited limited water permeability. However, these published results for the water filtration membranes did not include optimization of the membrane performance. In this dissertation, a systematic study of membrane performance is presented by exploring the effects of different TS processes and process conditions as well as different types of feedstock materials on membranes permeability. For a given set of process parameters, the coating thickness was correlated to water flux and rejection. In addition to performance measurements, the membranes were characterized by XRD, EDX, SEM and pore size analysis.

7.2 Advantages of Thermal Spray over Conventional Methods

Although many methods have been proposed for fabricating porous inorganic membranes, the inorganic media comprised only 7.9% of the total membrane market volume in

2003. This number is only expected to grow to 9.2% in 2008 [168]. The main barriers for the growth of market volume of inorganic membranes are process complexity, time constraints, difficulty in welding materials and high manufacturing costs of the available methods. Therefore, new manufacture methods to fabricate cost-effective inorganic membranes with sufficient tensile strength have the potential to increase the growth rate and thus the market volume.

While sol–gel and slip casting processes are still utilized for membrane production, the potential of plasma spray technology to develop these structures is explored here. Unique advantages of this process include high throughput manufacturing, high speed deposition capability, minimal heat input into the substrate, in-situ rapid application and applicability of a wide range of substrate, conformal shapes and environments, along with improved cost-effectiveness. In fact, thermal spray has been used for a number of years in the production of both electrodes and interconnects in solid oxide fuel cell (SOFC) manufacture. With further process optimization it is possible to produce ultra-thin, multi material, multi-layer membranes with tunable pores and surface chemistries and high selectivity for a wide range of applications.

7.3 Material Selection and Process Parameters

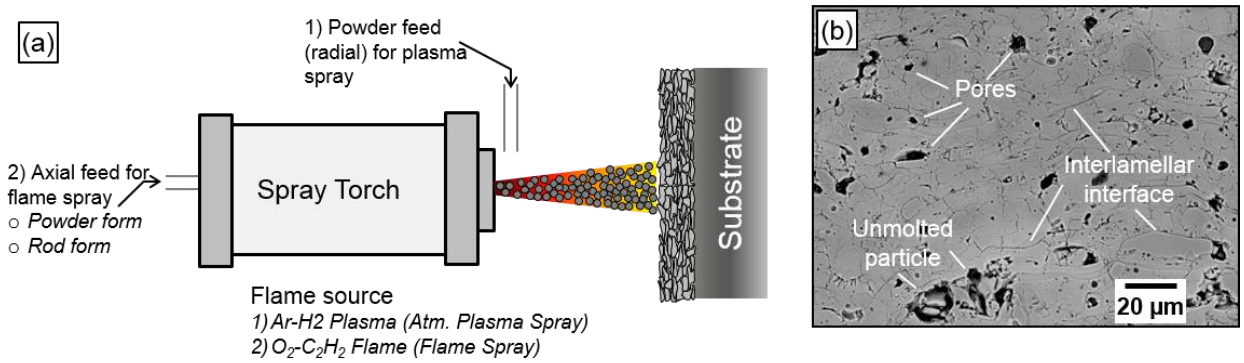

Figure 7.2: Schematic of the (a) plasma spray process (b) SEM image of spray cross section showing various features

Alumina is one of the most widely used and well-studied material in both thermal spray and the ceramic membrane field. It was one of the first materials to be thermal sprayed and has been well characterized under numerous spray conditions [180-183]. Further it is one of the most commonly used materials for preparation of ceramic membranes with its application is many filtration segments [184-186]. It is also extremely safe to use for filtering fluids that are for human consumption like dairy and beverages. Hence alumina was selected as the material of choice for preparing the thermal sprayed membrane because of its versatility and its well characterized nature. The Al_2O_3 ceramic membranes were prepared using APS (Ar-H_2 plasma, F4 MB, Oerlikon Metco, Westbury, NY, USA) and CFS (oxy-acetylene, TeraDyn^{TM} 3000, and Rokide^{TM}, Saint Gobain, Worcester, MA, USA) spray processes. The feedstock introduction into the spray plume was radial and axial for APS and CFS process, respectively. Two types of alumina feedstock were used- powder (Micron abrasive, Westfield, MA, USA) and rod type (Saint Gobain Ceramic Materials, Worcester, MA, USA). The powders were used for both APS

and CFS processes, while the rod feedstock was used only for CFS process. When introduced to a flame, powder feedstock materials produced a higher degree of porosity as compared to that for rod feedstock due to significant number of unmolten particles trapped in the coating. While in rod-based CFS process, the feedstock is introduced axially to the plume and is melted locally in the hottest section of plume. The molten zone is then subjected to a high pressure N_2 jet, which first fragments and then carries out the molten particles to a substrate. This process fabricates a coating with almost no unmolten particle and relatively denser microstructure as compared to the powder type feedstock, since only fully molten particles can be carried out by N_2 jet. The process parameters details for the thermal spray processes are summarized in Table 7.1.

Spray parameters	Plasma spray	Flame spray
Argon (slpm) / Oxygen (slph)	30 & 47.5	40
H_2 (slpm) / Acetylene (slph)	2 & 6	40
Current (A)	450	-
Plasma Power (kW)	24 & 34	-
Feedstock	Powder	Powder & Rod
Spray distance (cm)	10 & 15	15
Raster speed (mm/s)	500	500
Mean Particle Size (μm)	50	50
Feed Rate (gm/min)	30	30

Table 7.1: Processing conditions for the thermal spray samples

All the membranes were deposited on 100 x 25 mm porous stainless steel substrates of 2mm thickness, procured from Mott Corp., Farmington, CT, USA, with an average pore size of 10 µm. In order to investigate the effect of membrane thickness on infiltration performance, three different thicknesses (~100, 200 and 300 µm) were sprayed for each set of process and corresponding processing condition. The deposited membranes were cut in to multiple pieces 25mm x 25mm, using high speed saw, (Buehler Inc., Chicago, IL, USA). These specimens were evaluated for clean water flux and rejection rate in a dead-end filtration module setup under 4.5 bar pressure in the ambient conditions. The schematic of test method and an image of test cell is show in the Figure 7.3. Rejection rate was measured using 1 µm polystyrene spheres (Fisher Scientific Inc., Pittsburg, PA, USA). At least three measurements per specimens were measured.

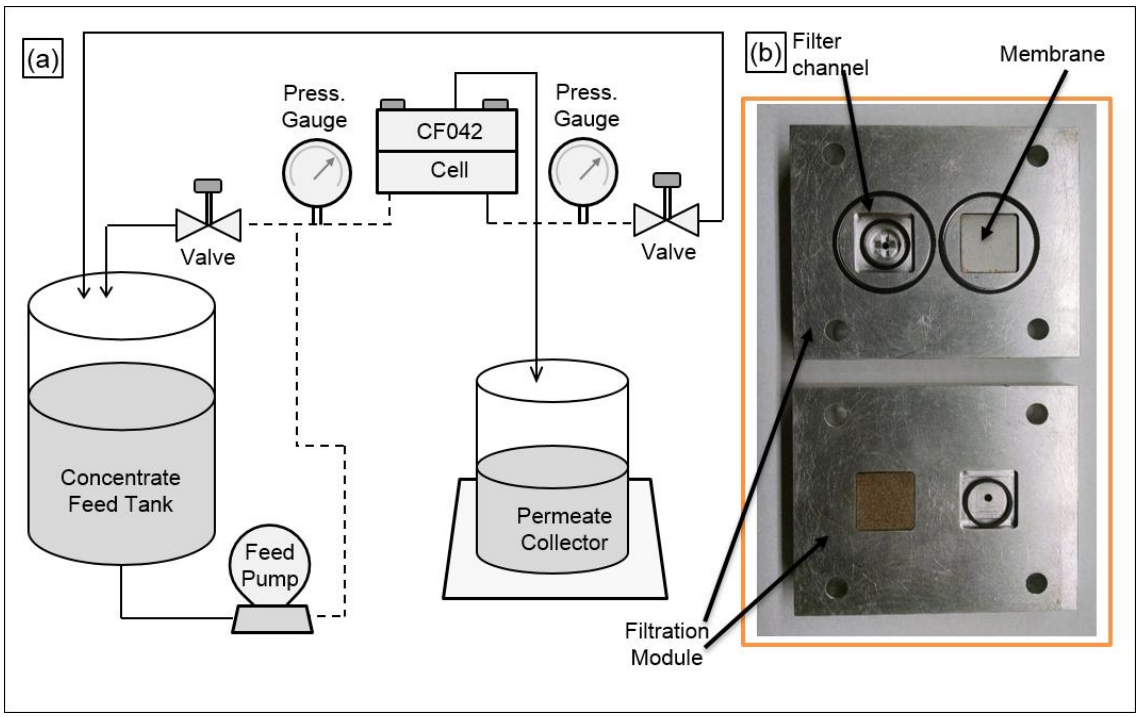

Figure 7.3: (a) Schematic of the filtration system showing the filtration cell (b) Photo of the actual cell and one of the prepared membranes

7.4 Sample Preparation and Characterization

Since TS process involves melting and rapid solidification of material, there is always a possibility of phase change of material during the deposition process. Therefore, to ensure the presence of appropriate phases, the membranes were analyzed by XRD ((Philips PW 1720, Philips Analytical Systems, Mahwah, NJ, USA) with the following settings: working voltage and current of 35 kV and 25 mA, step size of 0.02° and scan 2-theta range from 20 to 70°. SEM (Hitachi TM3000, Angstrom Scientific Inc., Ramsey, NJ, USA) was used to obtain microstructures of polished cross-section of membranes under back-scattered electron mode. Standard image analysis (ImageJ software using Otsu algorithm) procedure was used to determine overall porosity of the membranes [187]. Pore size analysis was done using gray scale SEM images. Each of the membrane samples was sliced at the same depth before polishing and imaging to maintain consistency across the samples. Thickness measurements were done using a digital micrometer and verified using the image analysis software mentioned above. The flame sprayed membranes were designated as F1 and F2 based on the rod and powder feed stocks respectively. Likewise, plasma sprayed membranes were labeled based on the changes in the plasma power and spray distance with P1, P2 and P3, corresponding to 24 kW and 10 cm, 24kW and 15 cm and 34kW and 15 cm spray distance. Although a direct coating adhesion test (ASTM C-633) was not performed, the range for thermal sprayed ceramics can be from 10 MPa to 50 MPa, depending on substrate and coating material, substrate roughness and on processing conditions.

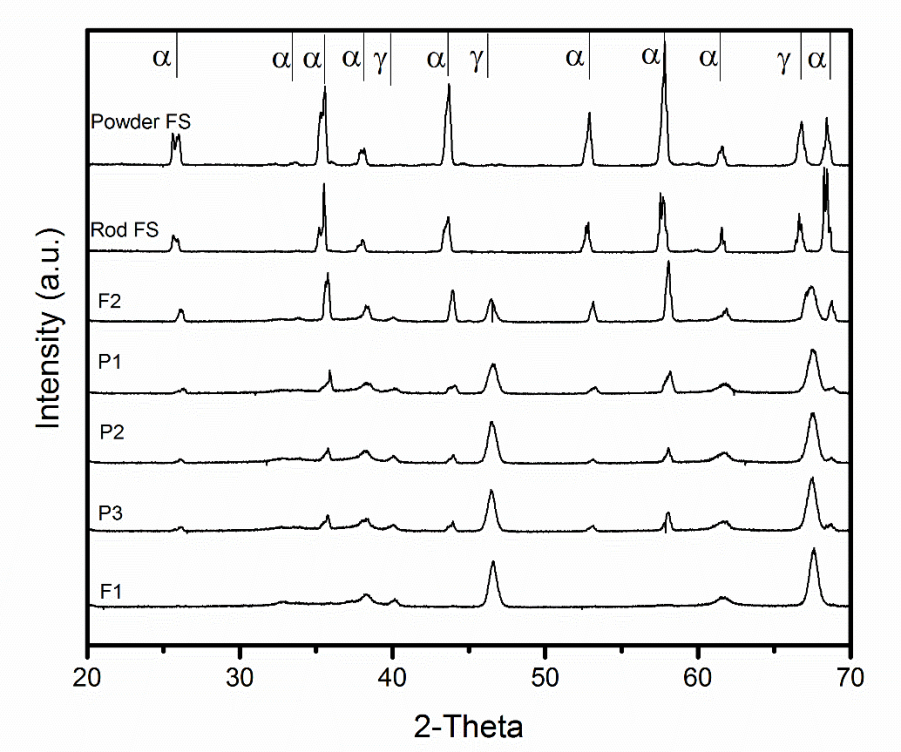

Figure 7.4: XRD spectra of the prepared membranes (α - Gamma Alumina (JCPDS 50-741), γ - Alpha Alumina (JCPDS 46-1212)

The sprayed membranes were analyzed under XRD for phase transformations that could potentially occur during spray and cooling process. The diffraction patterns obtained from the surfaces of the five membranes are shown in Figure 7.4. The two group of membranes, sprayed using powder (F2, P1-3), and rod (F1) feedstock display presence of similar phases associated to their individual feedstock. There are clear differences between the two starting feedstock. The rod feed stock and the corresponding coating shows lesser peaks of α-Al_2O_3 than the powder feedstock and their coatings. These differences can primarily be attributed to the processing of feedstock material. Since the primary purpose of this study is to produce TS membranes at low cost, only commercially grade materials were used for deposition. It is also important to mention

that the spraying process parameters affect the final composition of membranes. Compared to the initial feedstock materials, the sprayed membranes from both (APS and CFS) processes resulted in significant reduction of α-Al_2O_3 phase as shown in Figure 7.4. Similar observations have been reported by other researchers, and have been explained by rapid quenching phenomenon of particles, which limits the formation of thermodynamically stable α-Al_2O_3 phase [188]. Further, coatings sprayed with APS process show more intense peaks attributed to γ-Al_2O_3 phase as compared to those sprayed with CFS process. This can attributed to the higher temperature of plasma in APS as compared to the flame temperature in CFS, resulting in greater melting and faster cooling of particles forming metastable γ-Al_2O_3 phase [189]. It is important to mention that there was no significant difference among the diffraction patterns of the three APS membranes was observed. The EDX (Energy Dispersive X-ray Spectroscopy) results as seen in Figure 7.5 for the prepared membranes generally showed presence of aluminum and oxygen elements with no impurities.

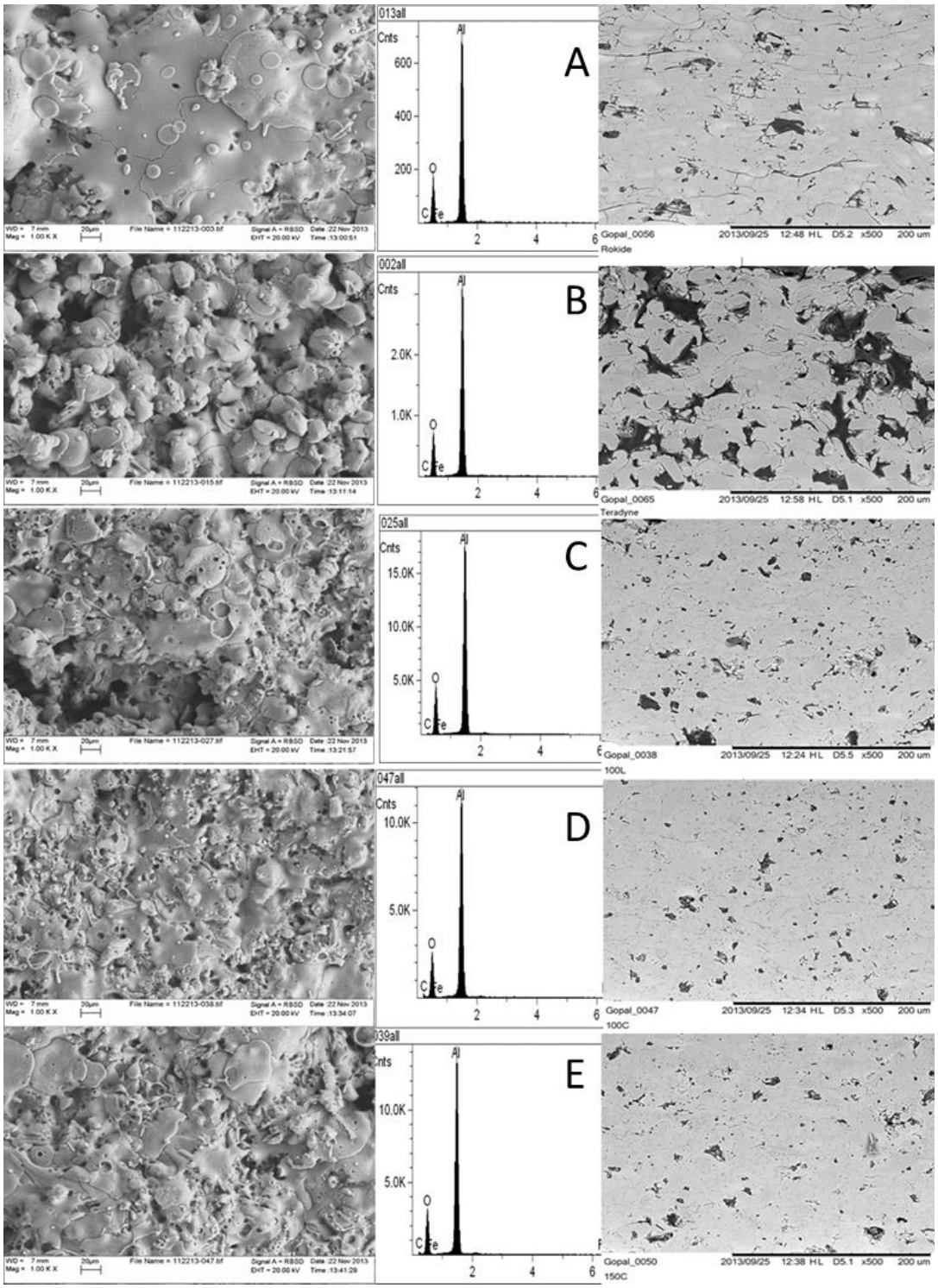

Figure 7.5: Surface morphology, EDAX Spectra and Cross Section SEM of the prepared membranes. The images on the left show the surface morphology while the ones on the right show the cross section areas.

The graphs in the middle show the EDAX spectra. A) Flame spray rod sample membrane [F1] B) Flame Sprayed powder sample membrane [F2] C) Plasma sprayed membrane [P1] D) Plasma sprayed membrane [P2] and E) Plasma sprayed membrane [P3]. All membranes imaged are of 300 µm thickness.

7.5 Morphology and Porosity Analysis

Figure 7.6 shows the cross section SEM image of various 300 µm thickness membranes used in this study. The membranes exhibited variable morphology due to both different spray parameters as well as spray processes. For comparison, the micrograph of porous substrate (Figure 7.6a) is also included, which reveals that all the membranes were much less porous than the substrate material.

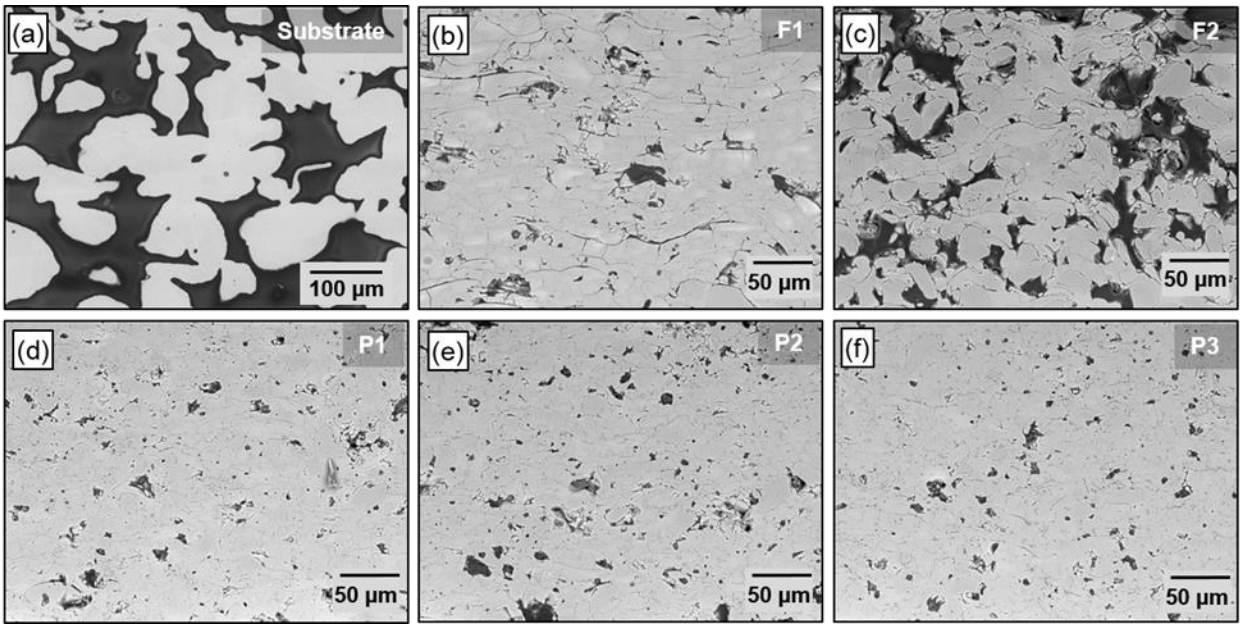

Figure 7.6: SEM images of the as prepared 300 µm thick membranes

Based on these SEM characterization images, the membrane microstructures can be categorized in three types. First, with moderate porosity and large inter-splat interfaces (F1, Figure 7.6 b), second with large globular types pores (F2, Figure 7.6 c) which also have the largest porosity, and third with relatively denser microstructures and almost no inter-splat boundaries (P1-3, Figure 7.6 d-f [190]. Although, detailed discussion on individual coating microstructure is out of the scope of this study, the differences among these categories are simply associated with the process and/or feedstock selection. As described earlier, the APS coatings or membranes are generally denser primarily due to greater (almost complete) melting of particles, while the powder-CFS membranes are significantly porous due to poor melting and formation of large voids (globular pores). On the other hand, due to assemblage of individual molten particle, the rod-CFS membranes tend to achieve density level similar to APS coatings, however they form large inter-lamellar interfaces due to lower particle impact velocities compared to those obtained in APS processes. Comparing the three APS membranes, variation between the processing conditions, such as spray distance (10 cm (P2) vs 15 cm (P3)) and plasma power (24 kW (P1) vs 34 kW (P2)) doesn't appear to be as significant in terms of microstructure. Although, these processing condition variations are significant, one reason for APS process sensitivity towards these membranes could be lower melting temperature of Al_2O_3 resulting in nearly complete melting of particles for all the cases.

7.6 Summary

In this chapter the concept of thermal spray process and its advantages over traditional membrane manufacturing techniques was introduced. Further, the material selection, sample preparation and process parameters involved was described. These samples were then characterized using various methods and analyzed for phase transformation, morphology, porosity and pore structure. The observed microstructural analysis provides insight into the membrane formation dynamics associated with each processing condition, which can be utilized to understand the performance results of the various membranes, such as flux and rejection rates, discussed in the next chapter.

Chapter 8

Optimization of Process Parameters

8.1 Thermal Spray Process Parameters

Thermal spray process parameters can be defined in a number of ways. In fact there are various accounts of the different number of variables with regards to thermal spray process some ranging from a few to others stating hundreds of parameters [191-197]. The possible combinations of parameters that can produce coating according to specification are quite numerous [198]. Process manipulations aside parameters can be streamlined into those that affect mass, time and temperature. These parameters directly affect the coating characteristics and to stabilize a thermal spray process, manipulation, time, temperature, and mass must all be held constant [172, 174]. A few of these variables are listed below.

Manipulation of variables such as standoff distance, surface speed, pitch and angle of increment change the characteristics of the final spray product [199]. These are defined as given below.

1. Standoff distance: the distance from the face of the gun to the part being coated
2. Surface speed: the relative velocity between the gun and the part
3. Pitch or increment: the distance that the gun moved with each subsequent stroke of the gun manipulation or revolution of the part
4. Angle of impingement: the variation of the spray stream from normal or 90° to the surface of the part

The time variable is controlled in part by:

1. Gun design (e.g., bore geometry and exit diameter)
2. Total arc/flame gas flow, that is, primary plus secondary gas flows (fuel-to-oxygen ratio being a significant parameter in flame spray processes)
3. Arc gas characteristics
4. Available energy, electrical or chemical, acting upon the arc/flame gases

Temperature is controlled in part by:

1. The same gas issues as for time, above
2. The available energy acting upon the system

Mass of the feedstock particles is a complex variable, and perhaps the most significant one, in the sense that beyond specifications, it is the most difficult to control because feedstock is usually a purchased commodity [200-202]. The mass of spray material supplied to the gun has several important characteristics. Variables common to all feedstock include chemistry, melting point, thermos-physical properties, and coefficient of thermal expansion. Further, each type of feedstock has its own set of parameters that affect the final coating. In case of rod the characteristic parameters include Diameter, Circularity, Straightness, and Porosity. Whereas for powder feedstock the important characteristics are Particle size, Particle shape/morphology, which affects a powder's feedability, Particle size distribution, Method of manufacture and apparent density [203-206].

Lastly, it was important understand the effect of all these parameters on the two thermal spray processes used in this thesis. The flame spray process uses the energy available in the

chemical bonds of fuel gases. In these combustion processes, the melting and expansion power of the flame jet is produced by breaking molecular bonds in the fuel gas and the number of bonds broken per unit time (higher fuel gas flow rates). Plasma, on the other hand, utilizes the energy of an electric arc, the power of which is directly related to the voltage drop across and the current flow through the arc. In most plasma systems, power is calculated as the product of the voltage and the current supplied by the system. Depending on losses to the water cooling, the electrical to thermal conversion efficiency of a plasma spray gun ranges from 42 to 65% of the power input to the gun [204, 207]. The heating power is measured by the specific gas enthalpy, which is the energy per unit mass of gas, for example, J/L or kW/scfh.

In this dissertation manipulation characteristic standoff distance was varied, the gun design parameter available energy or input energy, the feedstock type between powder and rod and finally the coating thickness. Before testing the membranes for filtration efficiency it is necessary to understand the basics behind the filtration process. The dead end filtration testing performed on these thermal sprayed membranes are evaluated based on the dead end filtration theory.

8.2 Evaluation of membranes' performance

The ceramic membrane samples produced using thermal spray techniques were evaluated for filtration efficiency using a dead-end filtration cell. In dead-end filtration as shown in Figure 8.1 the flow direction is perpendicular to the filter surface and the particles retained rapidly coagulate on the surface of the filter. This forms a cake which reduces the overall performance of the filter. As the pores of the filter get clogged by the cake, the filtration performance is considerably reduced in a very short period time [169, 170].

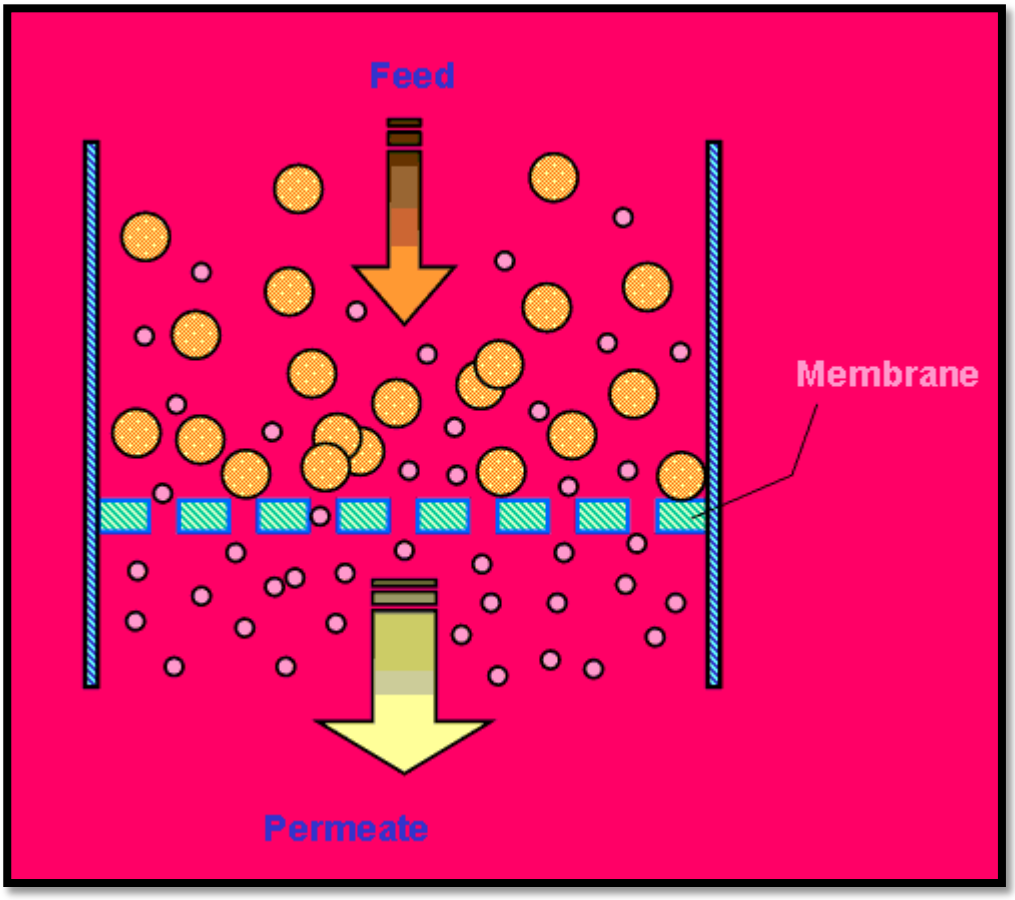

Figure 8.1: Visual representation of dead-end filtration process (Source: Separationprocesses.com)

The filter cell used for experiments described in the thesis was machined from Delrin sheet (Polyoxymethlene) and the rated for pressure up to 100 psi as shown below Figure 8.2. It is a simple pressurized dead end filtration cell with the membrane sealed using 2 O-rings to avoid pressure loss and leakage. There is no stirrer for removing the cake formation and membrane is supported by a porous backing.

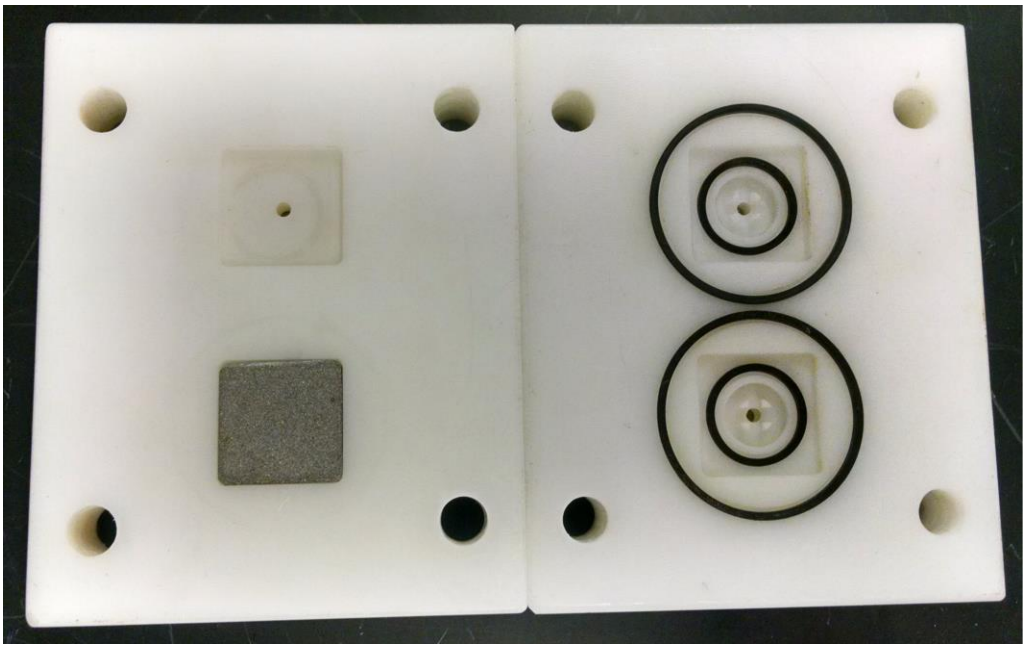

Figure 8.2: Dead-end filtration cell used for the experiments described in this thesis

8.3 Dead-end Filtration Theory

This section gives a brief overview of the theory on the basis of which filtration testing of the prepared membranes was performed [144]. The dead end filtration is the one where the flow of water is perpendicular to the membrane surface. The water is pushed through the membrane by pressure. All the water that is introduced in the dead-end-cell passes through as permeate, in

other words, there is no rejected water. In dead end filtration, the retained particles build up with time on the membrane surface or within the membrane. In either case, the particle builds results in an increased resistance to filtration and causes the permeate flux to decline, as a result dead end filtration requires the stopping of filtration in order to clean or replace the membrane. Therefore this type of filtration is also called batch filtration.

There are two types of filtration which can be employed in a dead end cell unit; dead-end microfiltration with constant flux and dead end microfiltration with constant pressure drop. The dead end microfiltration with constant flux ensures that the permeate flux through the filter remains constant, this filtration can be achieved by positive displacement pump. As the cake build-up increases with time, the pressure drop must be increased to maintain constant flux. In dead end microfiltration with constant pressure, as the cake builds-up with time the permeate flux decreases.

Membranes provide absolute barrier to particles greater than their pore size. A membrane process requires two bulk phases physically separated by a third phase, the membrane. The membrane phase interposed between the two-bulk phases controls the exchange of mass between the two bulk phases in a membrane process. The process allows the selective and controlled transfer of a certain species from one bulk phase to another bulk phase separated by the membrane. In this thesis the dead end filtration with constant pressure drop was used.

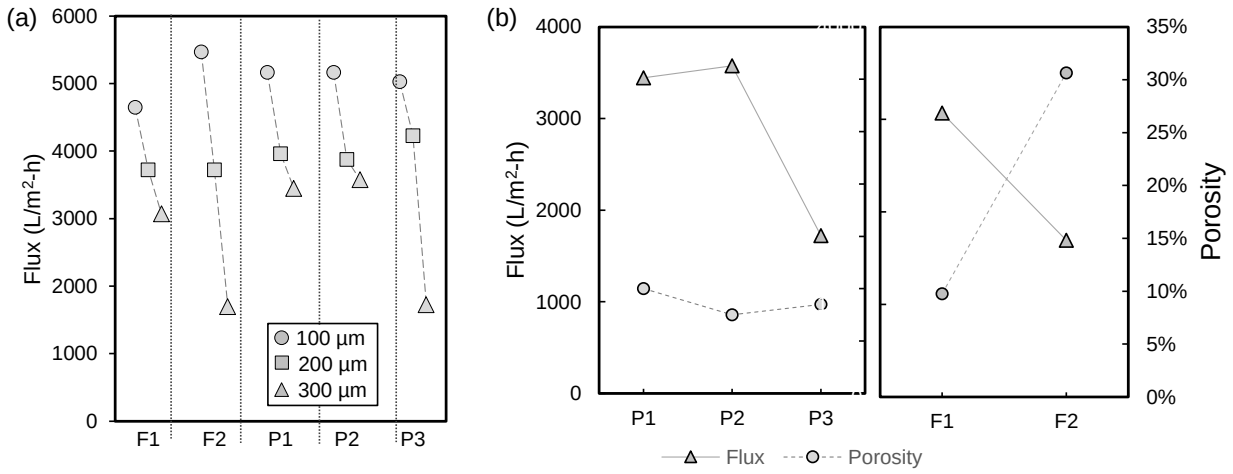

Figure 8.3: Clean water flux vs thickness for the prepared membranes (a) F1-2 being the flame sprayed membranes and P1-3 being the plasma sprayed membranes. (b) Graph showing the variation of the porosity with respect to the flux for the various membranes.I) Compares the flux and porosity for the Plasma sprayed membranes and II) compares the flux and porosity between the flame sprayed membranes.

The results from flux measurement conducted on the various membranes are presented in above figure. The Figure 8.3a shows the effect of varying the thickness of the membrane on the clean water flux. The flux drop was seen for all the membranes irrespectively of the type of feedstock material, spray distance or plasma power. The overall trend for the samples tested showed that the flux drops rapidly as the membrane thickness increases. The figure also suggests that there is a thickness threshold [179] below which the effect of membrane thickness on flux is not noticeable. Another interesting observation is that all of the 100 µm thick membranes had clean water flux ranging from around 4500-5500 LMH, which is comparable to commercially available ceramic membranes [177]. It should be noted that these membranes were compared

against other plasma sprayed ceramic membranes that exhibited similar flux characteristics but had a different porosity attributes.

As mentioned earlier, two different spray techniques, CFS vs. APS, were employed and will consider each technique separately in the following discussion. The 100 μm thickness membranes produced by the solid rod feedstock (F1) exhibited a relatively high flux of 4650 LMH accompanied by smaller drop in flux as the thickness of membrane increased when compared to membranes produced from powder feedstock. This might be due a complete melting of the particles producing a much more linear dependence of flux as a function of thickness as compared to fairly heterogeneous nature of partially molten particles in case of powder feedstock. The samples produced using the powder feedstock showed very high flux (~5500 LMH) at lower thickness followed by a dramatic flux drop at higher thickness. Several effects might be in play here, the high flux at lower thicknesses could be attributed to the high porosity (30%) while the reduction in overall permeability could be due to the development of high proportion of dead end pores as the membrane thickness increases. It is important to note that the water flux for this membrane is significantly higher than that for the membrane of the same thickness produced from the rod feedstock (F1). This shows that the feedstock as well as the spray method greatly influences the membrane performance. When comparing the flux and porosity together (Figure 8.3 b) the solid feedstock (F1) produces a more uniform lamellar coating with more through pores/channels whereas the sample produced from powder feedstock (F2) had larger void spaces and higher proportion of dead end pores, as mentioned in the previous section, leading to a greater drop in overall flux. It should be noted that the ratio of dead

end pores in these samples is very difficult to quantify and the assumptions here are based on the extensively literature available for the well-studied field of thermal spray process.

For the plasma sprayed P1, P2 and P3 membranes, the flux at the lower (100 µm) thickness range was nearly the same with all 3 membranes despite the fact that several spray parameters (plasma power and/or spray distance) were varied during the spray process illustrating the possibility of a thickness threshold mentioned earlier [208]. For the 200 µm thick P3 sample the increase in the spray distance could explain the slight increase in water flux when compared to the other plasma sprayed samples with the same thickness. This is due to longer distance between the substrate and the plasma jet which correlates with loss in kinetic energy alongside greater degree of melting of the spray particles and generally higher porosity of the coating [209] as confirmed by the image analysis of microstructure shown in Table 8.1. However, it must be noted that the change in porosity does not linearly correlate to change in flux as seen by a drastic drop in the flux for the 300 µm thick P3 membrane, which could due to the conversion of pass-through/interconnected pores into dead-end pores. Further, an inverse correlation between plasma power and porosity (Figure 8.3 b P1 and P2) was observed, due to the fact that an increase in plasma power results in fully molten droplets that leads to better interactions between splats and substrate and/or other splats [210] thereby reducing the overall void spaces between splats. However, any observable trends cannot be discerned when considering the effect of plasma power on both flux and porosity. This could be either due the presence of dead end pores in the membrane with higher porosity (P1) or the presence of defects in the membrane with lower porosity (P2), either of which would partly nullify the effect of increasing the plasma power.

8.4 Effect of process parameters

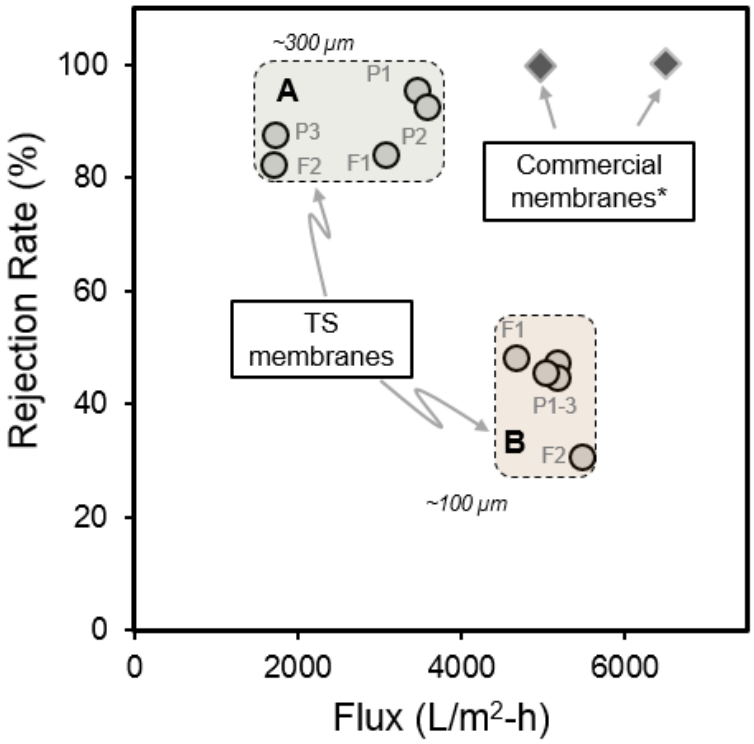

*Figure 8.4: Flux vs Rejection rate group (A) shows the 300 µm thick membranes and group (B) shows all of the 100 µm thick membrane (*As compared with 0.1-0.5 µm pore size SiC LiqTech membranes).*

In order to analyze the reasons for variation in the membrane and to ultimately design better membranes it is important to correlate spray type, processing conditions and resulting morphologies to both rejection rates and water flux. Figure 8.4 shows the results of size exclusion tests on the membranes with Groups A and B representing membrane thickness of 300 µm and 100 µm respectively. In terms of performance, Group A has intermediate flux and the highest rejection rate, whereas Group B has the largest flux and the lowest rejection rate. One important parameter which can explain the performance is the membrane thickness. This

analysis leads to a rather predictable conclusion that thinner membranes (Group B) are relatively ineffective in filtering 1 μm latex spheres as compared to the thicker membranes (Group A). A closer examination of this trend within group B indicates that the flame spray membranes showed either enhanced flux or increased rejection rate but not both. If one sets up the criteria of the best performance based on large water flux and high rejection rate, the performance of the flame spray membranes cannot be considered as the optimal one. In contrast, the plasma sprayed membranes showed a better performance based on above criteria. Understanding the performance of thicker membranes is a much more difficult task. Some of the membranes in this group show excellent rejection rate (F1, P1 and P2) while simultaneously maintaining significant flux. In contrast there are other membranes (F2 and P3) that also have a lower flux with relatively lower rejection rates. It is possible to explain these differences based on membranes' morphologies.

Within Group A, F1, P1 and P2 membranes had similar lamellar dense microstructures as described earlier and displayed similar rejection rates. However, it is also important to mention that there are also subtle morphological differences originating from different spray technique, feedstock and processing parameters in each of these membranes. As a result of these differences, the plasma sprayed membranes, which exhibited a more compact microstructure with greater proportion of inter lamellar pores' connectivity and smaller average pore sizes, gave the optimal flux and rejection rate as compared to all the other membranes. Further, the membranes F2 and P3 show similar value of flux and rejection rate, despite being produced by quite different spray techniques. This could due to a combination of increase in the dead-end pores with the increase in thickness for flame spray membrane (F2) and the increase in tortuosity

in the plasma spray membrane (P3) due to increase in the spray distance causing a drop in the kinetic energy creating a less compact [209]. Also, there was the possibility of the thinner membrane having inherent imperfections such as cracks, uncoated substrate or delaminated coating, all of which might explain the high flux, low rejection at lower thicknesses as seen in Figure 8.4. However, further investigation is required to clarify these observations.

Material	F1	F2	P1	P2	P3	Substrate
Porosity	9.8%	30.7%	10.0%	7.5%	8.5%	39.6%
Avg. pore size (µm)	1.43	2.57	1.03	0.82	0.84	10
Spray distance (cm)	15	15	10	10	15	
Plasma power (kW)	-	-	24	34	34	

Table 8.1: Porosity and Pore size variation across prepared 300 µm thick membranes

From the point of view of practical applications, the measurements (Table 8.1) suggest that the plasma spray membranes P1 and P2) can provide the highest rejection with acceptable porosity, alongside a high degree of water flux as compared to all the other membranes. However, there is a substantial decrease in the flux as the membrane thickness increases, possibly due to various factors mentioned earlier. Further investigation is required to evaluate contributions of these factors to water flux decrease and to improve the size exclusion characteristics of the membrane.

8.5 Summary

In this chapter the process parameters associated with the thermal spray technique were briefly explained. The filtration efficiency of the thermal sprayed membranes using a dead end filtration cell were tested and the results were analyzed. From the observed data, the thinner thermal spray membranes have better permeability while the thicker membranes have better rejection rate characteristics. A comparison of the membranes prepared in this project with commercial membranes shows that the thicker membranes are comparable to commercial ones in terms of rejection rate although they still need to be optimized in terms of the overall flux.

Chapter 9

Concluding remarks and future work

9.1 Concluding Remarks

Air quality in urban areas across the globe is rapidly deteriorating, creating hazardous living and environmental conditions for more than fifty percent of the world's population. Criteria pollutants in these regions, like NO_X and SO_X, are responsible for adverse health conditions like emphysema, lung damage and respiratory diseases. These pollutants are also one of the leading causes for acid rain, smog and ground level ozone in such populated areas. Air pollution is a complex and difficult problem to tackle as it is affected by a number of variables from weather to geographic location. As a result, the emphasis has generally been more on air quality control rather than pollution mitigation. Further, the policy decisions on air quality control are governed by factors like economic, political and social contexts that vary greatly across the world. Pollution mitigation in most cases has been done through the use of adsorbents. However, using adsorbents in urban regions can be prohibitively expensive and logistically unviable when considering the costs and quantities required. As an alternative this research proposes the use of concrete which is one of the widely used materials especially in urban areas. Further, concrete from construction and demolition waste is generally available in large quantities which can be easily transported within urban locations for use as adsorbents. This thesis discusses and proves the merits of using concrete as an efficient adsorbent for removing the priority air pollutants mentioned above.

The research found that though aged concrete has a substantially lower NO_2 uptake when compared to a fresh concrete there is still a considerable amount of NO_2 removal capacity (approx. 60%), even for a 12 year old concrete. It means that despite the drop in adsorption

capacity with the concretes' age it can still be considered as a viable adsorbent. In addition, spectroscopic evidence suggest nitrate and nitrite species formation due to NO_2 exposure, indicating that chemical neutralization occurs between NO_2 and surface alkaline species, such as those attributed to calcium hydroxide. Supplementary experiments with active phase of concrete, such as portlandite, provided further support of this hypothesis. Similarly, results for SO_X adsorption showed that concrete is highly effective in removing it and forms sulfate and sulfite surface species due to reactions with calcium hydroxide. These results show that concrete both fresh and old can be used as an adsorbent especially in urban areas.

The second part of this thesis demonstrates the use of thermal spray process to produce highly scalable and cost effective ceramic membranes. The development of these inexpensive membranes especially important for emergent nations like India and China where low cost filtration can help in providing clean water for impoverished population.. One of the primary reasons for the lack of widespread adoption of ceramic membranes is due to their substantial manufacturing costs and energy needed for manufacturing of these materials. The thermal spray technique provides a scalable and cost effective method to produce economically viable ceramic membranes. Furthermore, this technique offers a possibility to tune the membrane's properties according to specific application requirements.

The membranes are prepared in this study by two different spray techniques (flame spray and plasma spray), and were characterized and tested for porosity, elemental analysis, morphology, flux and rejection rate. The results show that these membranes provide excellent water permeability comparable to that of commercial membranes especially at low membrane thicknesses. Further, the size exclusion test showed that these membranes are able to reject up to

96% of the particulates. While some of the trends described here require more detailed investigation, it is clear that the thermal spray can be used for the production of ceramic membranes. Optimizing the spray parameters and material combinations would lead to substantial improvements in the flux and filtration performance of these membranes allowing for its use in the commercial space especially in the micro and ultrafiltration regimes

9.2 Future Challenges

This thesis provides a basis for the use of concrete as an adsorbent for urban air pollution remediation. However, there are several issues that need to be addressed before it can be implemented effectively. One of the most important challenges is to accurately identify the underlying adsorption mechanism for each of the criteria pollutants. The mechanism will define the way in which each of these pollutants interact with the concrete and determine its adsorptive capacity. The reaction mechanisms will also signify how concrete would react when exposed to a mixture of gases. This can be extended to focus on quantitative understanding of the adsorption by concrete. Further, it is also essential to clarify the influence of various environmental factors on adsorption capacity of concrete. There is anecdotal evidence that suggests a drastic change in the reaction mechanisms with changes in temperature, humidity and presence of surface organics. A thorough understanding of the effects these factors have on concrete would greatly help in determining where it can be best used as an adsorbent. For example, in cement manufacturing plants and power generation units, the flue gases have temperatures ranging from 200 to 500 °C and consist of a mixture NO_X and SO_X. The adsorption characteristics of concrete

in such conditions would be vastly different. Understanding the effect of the elevated temperatures and the competitive nitrate and sulfate reactions would help in predicting not only the effectiveness but also the quantity of the adsorbent required for a specified period of time. Lastly, the research done in this thesis suggests the possibility of using exhausted pollutant adsorbed concrete be incorporated back into fresh concrete as a beneficial additive, thereby, providing enhanced mechanical and chemical properties. It is already known that Calcium Nitrate $Ca(NO_3)_2$, one of the components formed when NO_2 is adsorbed by concrete, can be used as an admixture to impart additional anticorrosion properties to reinforced concrete. This would improve the overall sustainability of concrete and provide a possible alternative to recycle concrete instead of landfilling it.

The research presented here clearly shows that thermal spray can be an effective manufacturing technique for the large scale production of ceramic filtration membranes. This, however, requires further understanding of how the process parameters and material selection affect the membrane morphology, thereby, affecting the performance characteristics. A comprehensive understanding of the average pore size, porosity and overall morphology of these membranes can be obtained using advanced characterization techniques. Also, the membranes can be tested using water containing various environmentally relevant contaminants such as bacteria to improve membrane filtration performance. With further investigation and systematic optimization of the various spray parameters, it is possible to produce scalable and economic ultrafiltration and nanofiltration ceramic membranes. Finally, due the versatility of the thermal spray process it is extremely easy to produce multi-layer, multi-material composite membranes which can be tuned to filter specific contaminants.

Bibliography

[1] G. Ramakrishnan, R.J. Moon, A. Orlov, Development of novel inexpensive adsorbents from waste concrete to mitigate SOx emissions. *(In Preparation)*, Cement & Concrete Research, (2015).

[2] G. Ramakrishnan, G. Dwivedi, S. Sampath, A. Orlov, Development and optimization of thermal sprayed ceramic microfiltration membranes, J Membrane Sci, 489 (2015) 106-111.

[3] G. Ramakrishnan, A. Orlov, Development of novel inexpensive adsorbents from waste concrete to mitigate NOx emissions, Build Environ, 72 (2014) 28-33.

[4] G. Ramakrishnan, S. Zhao, W.Q. Han, A. Orlov, Simultaneous observation of gas phase and surface species in photocatalytic reactions on nanosize Au modified TiO2: The next generation of DRIFTS systems, Chem Eng J, 170 (2011) 445-450.

[5] S. Zhao, G. Ramakrishnan, D. Su, R. Rieger, A. Koller, A. Orlov, Novel photocatalytic applications of sub-nanometer gold particles for environmental liquid and gas phase reactions, Appl Catal B-Environ, 104 (2011) 239-244.

[6] M. Uchimiya, A. Orlov, G. Ramakrishnan, K. Sistani, In situ and ex situ spectroscopic monitoring of biochar's surface functional groups, J Anal Appl Pyrol, 102 (2013) 53-59.

[7] K. Jones, M. Uchimiya, A. Orlov, G. Ramakrishnan, M.J. Castaldi, J. LeBlanc, S. Hiradate, Enrichment of Carboxyl Surface Functional Groups on Low Pyrolysis Temperature Pecan Shell Biochars (In Preparation), Energy & Fuels, (2015).

[8] K. Jones, G. Ramakrishnan, M. Uchimiya, A. Orlov, New Applications of X-ray Tomography in Pyrolysis of Biomass: Biochar Imaging, Energy & Fuels, 29 (2015) 1628-1634.

[9] J. Ging, R. Tejerina-Anton, G. Ramakrishnan, M. Nielsen, K. Murphy, J.M. Gorham, T. Nguyen, A. Orlov, Development of a conceptual framework for evaluation of nanomaterials release from nanocomposites: Environmental and toxicological implications, Sci Total Environ, 473 (2014) 9-19.

[10] A. Orlov, G. Ramakrishnan, J. Ging, A. Hubert, P. Feka, C. Korach, Evaluating safety and stability of CNT nanocomposites exposed to environmental conditions, Proceedings of the Technical Proceedings of the 2012 NSTI Nanotechnology Conference and Expo, Santa Clara, CA, (2012) 335-337.

[11] G. Ramakrishnan, G. Dwivedi, S. Sampath, A. Orlov, Innovative Application of Plasma Spray Process: Manufacture of Economic and Scalable Ceramic Microfiltration Membranes, Abstracts of Papers of the American Chemical Society, (2014).

[12] G. Ramakrishnan, A. Orlov, Studies of gas phase NO2 removal using fresh and recycled concrete, Abstracts of Papers of the American Chemical Society, 246 (2013).

[13] G. Ramakrishnan, S. Peethamparan, A. Orlov, Utilizing demolished concrete as efficient NO2 adsorbent and beneficial concrete admixture, Abstracts of Papers of the American Chemical Society, 245 (2013).

[14] G. Ramakrishnan, S. Zhao, A. Orlov, Simultaneous observation of gas phase and surface species in photocatalytic reactions: The next generation of DRIFTS applications, Abstracts of Papers of the American Chemical Society, 240 (2010).

[15] R.B. Heimann, Classic and advanced ceramics: from fundamentals to applications, John Wiley & Sons, 2010.

[16] K.G. Budinski, M.K. Budinski, Engineering materials, Nature, 25 (2009) 28.

[17] Ceramics: Market Shares, Strategies, and Forecasts, Worldwide, 2014 to 2020.

[18] J.S. Reed, J.S. Reed, Principles of ceramics processing, 2nd ed., Wiley, New York, 1995.

[19] R.C. Buchanan, Ceramic materials for electronics, CRC press, 2004.

[20] J. Rodel, A.B.N. Kounga, M. Weissenberger-Eibl, D. Koch, A. Bierwisch, W. Rossner, M.J. Hoffmann, R. Danzer, G. Schneider, Development of a roadmap for advanced ceramics: 2010-2025, J Eur Ceram Soc, 29 (2009) 1549-1560.

[21] P.K. Mehta, P.J. Monteiro, Concrete: microstructure, properties, and materials, McGraw-Hill New York, 2006.

[22] V. Smil, Making the modern world : materials and dematerialization, Wiley, Chichester, West Sussex, United Kingdom, 2014.

[23] World Cement - Demand and Sales Forecasts, Market Share, Market Size, Market Leaders, (2013).

[24] N. Narayanan, K. Ramamurthy, Structure and properties of aerated concrete: a review, Cement & Concrete Composites, 22 (2000) 321-329.

[25] J.G. MacGregor, J.K. Wight, S. Teng, P. Irawan, Reinforced concrete: Mechanics and design, Prentice Hall Upper Saddle River, NJ, 1997.

[26] A. C150, Standard Specification of Portland Cement, in, ASTM International West Conshohocken, PA, 2012.

[27] V.M. Malhotra, Global Warming, and Role of Supplementary Cementing Materials and Superplasticizers in Reducing Greenhouse Gas Emissions from the Manufacturing of Portland Cement, Advances in Concrete Structural Durability, Proceedings of Icdcs2008, Vols 1 and 2, (2008) 24-35.

[28] I. Enting, T. Wigley, M. Heimann, Intergovernmental Panel on Climate Change (IPCC), Working Group 1, 1994: Modelling results relating future atmospheric CO 2 concentrations to industrial emissions, ORNL/CDIAC DB1009. Oak Ridge, Tennessee: Carbon Dioxide Information Analysis Center, US Department of Energy, Oak Ridge National Laboratory, (1995).

[29] N. Mahasenan, S. Smith, K. Humphreys, The cement industry and global climate change: Current and potential future cement industry CO2 emissions, Greenhouse Gas Control Technologies, Vols I and Ii, Proceedings, (2003) 995-1000.

[30] C. Chen, G. Habert, Y. Bouzidi, A. Jullien, Environmental impact of cement production: detail of the different processes and cement plant variability evaluation, Journal of Cleaner Production, 18 (2010) 478-485.

[31] B.M. Al Smadi, K.K. Al-Zboon, K.M. Shatnawi, Assessment of air pollutants emissions from a cement plant: A case study in Jordan, Jordan Journal of Civil Engineering, 3 (2009).

[32] M. Abu-Allaban, H. Abu-Qudais, Impact assessment of ambient air quality by cement industry: A case study in Jordan, Aerosol and Air Quality Resarch, 11 (2011) 802-810.

[33] M. Schuhmacher, J.L. Domingo, J. Garreta, Pollutants emitted by a cement plant: health risks for the population living in the neighborhood, Environmental research, 95 (2004) 198-206.

[34] A.R. Nielsen, M.B. Larsen, P. Glarborg, K. Dam-Johansen, High-Temperature Release of SO2 from Calcined Cement Raw Materials, Energy & Fuels, 25 (2011) 2917-2926.

[35] D.P. Rall, Review of the health effects of sulfur oxides, Environmental health perspectives, 8 (1974) 97-121.

[36] J.D. Spengler, B.G. Ferris, D.W. Dockery, F.E. Speizer, Sulfur-Dioxide and Nitrogen-Dioxide Levels inside and Outside Homes and the Implications on Health-Effects Research, Environmental Science & Technology, 13 (1979) 1276-1280.

[37] J.H. Ware, B.G. Ferris, D.W. Dockery, J.D. Spengler, D.O. Stram, F.E. Speizer, Effects of Ambient Sulfur-Oxides and Suspended Particles on Respiratory Health of Preadolescent Children, Am Rev Respir Dis, 133 (1986) 834-842.

[38] L.S. Jensen, NOx from cement production-Reduction by Primary Measures, 1999.

[39] C.A. Hendriks, E. Worrell, D. De Jager, K. Blok, P. Riemer, Emission reduction of greenhouse gases from the cement industry, in: Proceedings of the fourth international conference on greenhouse gas control technologies, 1998, pp. 939-944.

[40] D.L. Mauzerall, B. Sultan, N. Kim, D.F. Bradford, NOx emissions from large point sources: variability in ozone production, resulting health damages and economic costs, Atmos. Environ., 39 (2005) 2851-2866.

[41] M. Lippmann, Health-Effects of Ozone - a Critical-Review, Japca J Air Waste Ma, 39 (1989) 672-695.

[42] M. Kampa, E. Castanas, Human health effects of air pollution, Environ Pollut, 151 (2008) 362-367.

[43] Global Environment Outlook: environment for development (GEO-4), in, UNEP, 2007, pp. 572.

[44] M.L. Bell, F. Dominici, J.M. Samet, A meta-analysis of time-series studies of ozone and mortality with comparison to the national morbidity, mortality, and air pollution study, Epidemiology, 16 (2005) 436-445.

[45] M.L. Bell, A. McDermott, S.L. Zeger, J.M. Samet, F. Dominici, Ozone and short-term mortality in 95 US urban communities, 1987-2000, Jama-Journal of the American Medical Association, 292 (2004) 2372-2378.

[46] J.B. Ruidavets, M. Cournot, S. Cassadou, M. Giroux, M. Meybeck, J. Ferrieres, Ozone air pollution is associated with acute myocardial infarction, Circulation, 111 (2005) 563-569.

[47] A. Gryparis, B. Forsberg, K. Katsouyanni, A. Analitis, G. Touloumi, J. Schwartz, E. Samoli, S. Medina, H.R. Anderson, E.M. Niciu, H.E. Wichmann, B. Kriz, M. Kosnik, J. Skorkovsky, J.M. Vonk, Z. Dortbudak, Acute effects of ozone on mortality from the "Air pollution and health: A European approach" project, American Journal of Respiratory and Critical Care Medicine, 170 (2004) 1080-1087.

[48] A. Gryparis, E. Samoli, G. Toulomi, B. Forsberg, K. Katsouyanni, A. project, Ozone effects on total mortality results from the APHEA2 project, Epidemiology, 12 (2001) 372.

[49] Asian air pollution online, J Environ Monitor, 10 (2008) 918-918.

[50] K.B. He, H. Huo, Q. Zhang, Urban air pollution in China: Current status, characteristics, and progress, Annu Rev Energ Env, 27 (2002) 397-431.

[51] J. Watts, China: the air pollution capital of the world, Lancet, 366 (2005) 1761-1762.

[52] M.G. Badami, Transport and urban air pollution in India, Environ Manage, 36 (2005) 195-204.

[53] EPA, NOx Control Technologies for the Cement Industry: Final Report, in, EPA, 2000.

[54] EPA, Alternative Control Techniques Document Update – NOx Emissions from New Cement Kilns, in, 2007.

[55] M. Horgnies, I. Dubois-Brugger, E.M. Gartner, NOx de-pollution by hardened concrete and the influence of activated charcoal additions, Cement and Concrete Research, 42 (2012) 1348-1355.

[56] I. Galan, C. Andrade, P. Mora, M.A. Sanjuan, Sequestration of CO2 by Concrete Carbonation (vol 44, pg 3181, 2010), Environmental Science & Technology, 44 (2010) 4830-4830.

[57] C.S. Poon, E. Cheung, NO removal efficiency of photocatalytic paving blocks prepared with recycled materials, Construction and Building Materials, 21 (2007) 1746-1753.

[58] G. Husken, M. Hunger, H.J.H. Brouwers, Experimental study of photocatalytic concrete products for air purification, Build Environ, 44 (2009) 2463-2474.

[59] S.H. Shen, M. Burton, B. Jobson, L. Haselbach, Pervious concrete with titanium dioxide as a photocatalyst compound for a greener urban road environment, Construction and Building Materials, 35 (2012) 874-883.

[60] A. Folli, C. Pade, T.B. Hansen, T. De Marco, D.E. Macphee, TiO2 photocatalysis in cementitious systems: Insights into self-cleaning and depollution chemistry, Cement and Concrete Research, 42 (2012) 539-548.

[61] H. Dylla, M.M. Hassan, M. Schmitt, T. Rupnow, L.N. Mohammad, Laboratory Investigation of the Effect of Mixed Nitrogen Dioxide and Nitrogen Oxide Gases on Titanium Dioxide Photocatalytic Efficiency in Concrete Pavements, Journal of Materials in Civil Engineering, 23 (2011) 1087-1093.

[62] M. Chen, J.-W. Chu, NOx photocatalytic degradation on active concrete road surface - from experiment to real-scale application, Journal of Cleaner Production, 19 (2011) 1266-1272.

[63] M.M. Ballari, H.J.H. Brouwers, Full scale demonstration of air-purifying pavement, Journal of Hazardous Materials, 254 (2013) 406-414.

[64] L. Senff, D.M. Tobaldi, S. Lucas, D. Hotza, V.M. Ferreira, J.A. Labrincha, Formulation of mortars with nano-SiO2 and nano-TiO2 for degradation of pollutants in buildings, Composites Part B-Engineering, 44 (2013) 40-47.

[65] S.S. Lucas, V.M. Ferreira, J.L. Barroso de Aguiar, Incorporation of titanium dioxide nanoparticles in mortars - Influence of microstructure in the hardened state properties and photocatalytic activity, Cement and Concrete Research, 43 (2013) 112-120.

[66] V. Matejka, P. Matejkova, P. Kovar, J. Vlcek, J. Prikryl, P. Cervenka, Z. Lacny, J. Kukutschova, Metakaolinite/TiO2 composite: Photoactive admixture for building materials based on Portland cement binder, Construction and Building Materials, 35 (2012) 38-44.

[67] J. Chen, S.-c. Kou, C.-s. Poon, Photocatalytic cement-based materials: Comparison of nitrogen oxides and toluene removal potentials and evaluation of self-cleaning performance, Build Environ, 46 (2011) 1827-1833.

[68] M.M. Ballari, Q.L. Yu, H.J.H. Brouwers, Experimental study of the NO and NO2 degradation by photocatalytically active concrete, Catalysis Today, 161 (2011) 175-180.

[69] L. Cassar, Photocatalysis of cementitious materials: Clean buildings and clean air, Mrs Bull, 29 (2004) 328-331.

[70] M. Hunger, G. Huesken, J. Brouwers, Photocatalysis applied to concrete products - Part 1: Principles and test procedure, Zkg International, 61 (2008) 77-85.

[71] J. Kolarik, J. Toftum, The impact of a photocatalytic paint on indoor air pollutants: Sensory assessments, Build Environ, 57 (2012) 396-402.

[72] J.V.S. de Melo, G. Triches, Evaluation of the influence of environmental conditions on the efficiency of photocatalytic coatings in the degradation of nitrogen oxides (NOx), Build Environ, 49 (2012) 117-123.

[73] S. Kundu, A.K. Gupta, Analysis and modeling of fixed bed column operations on As(V) removal by adsorption onto iron oxide-coated cement (IOCC), Journal of Colloid and Interface Science, 290 (2005) 52-60.

[74] S. Kundu, A.K. Gupta, As(III) removal from aqueous medium in fixed bed using iron oxide-coated cement (IOCC): Experimental and modeling studies, Chem Eng J, 129 (2007) 123-131.

[75] A. Licata, The Application of Activated Carbon Enhanced Lime for Controlling Acid Gases, Mercury, and Dioxins from MWCS, in, Yonkers, NY.

[76] M. Heng, K. Murata, Aging of concrete buildings and determining the pH value on the surface of concrete by using a handy semi-conductive pH meter, Analytical Sciences, 20 (2004) 1087-1090.

[77] M.F. Bertos, X. Li, S.J.R. Simons, C.D. Hills, P.J. Carey, Investigation of accelerated carbonation for the stabilisation of MSW incinerator ashes and the sequestration of CO2, Green Chem., 6 (2004) 428-436.

[78] M.B. Mercader, Reactivity of acid gas pollutants with $Ca(OH)_2$ at low temperature in the presence of water vapor, in: Facultat de Química, Departament d'Enginyeria Química i Metallúrgia, Universitat de Barcelona, 2005.

[79] M. Balonis, The Influence of Inorganic Chemical Accelerators and Corrosion Inhibitors on the Mineralogy of Hydrated Portland Cement Systems, in, University of Aberdeen,, Aberdeen, 2010.

[80] M. Ahmaruzzaman, A review on the utilization of fly ash, Progress in Energy and Combustion Science, 36 (2010) 327-363.

[81] L. Evangelista, J. de Brito, Mechanical behaviour of concrete made with fine recycled concrete aggregates, Cement & Concrete Composites, 29 (2007) 397-401.

[82] I.B. Topcu, S. Sengel, Properties of concretes produced with waste concrete aggregate, Cement and Concrete Research, 34 (2004) 1307-1312.

[83] L. Haselbach, A. Thomas, Carbon sequestration in concrete sidewalk samples, Construction and Building Materials, 54 (2014) 47-52.

[84] S. Kashef-Haghighi, S. Ghoshal, Physico-Chemical Processes Limiting CO2 Uptake in Concrete during Accelerated Carbonation Curing, Industrial & Engineering Chemistry Research, 52 (2013) 5529-5537.

[85] A.M. Ramirez, K. Demeestere, N. De Belie, T. Mantyla, E. Levanen, Titanium dioxide coated cementitious materials for air purifying purposes: Preparation, characterization and toluene removal potential, Build Environ, 45 (2010) 832-838.

[86] U.S. Environmental Protection Agency, http://www.epa.gov/airquality/nitrogenoxides/.

[87] M.S. Marano, G., Estimating SCR Installation Costs, Power, (2006).

[88] B. Hoskins, Uniqueness of SCR Retrofits Translates Into Broad Cost Variations, Power Engineering.

[89] B.J. Finlayson-Pitts, J.N. Pitts, Chemistry of the upper and lower atmosphere: theory, experiments and applications, Academic Press: San Diego, Calif., London, 2000.

[90] Y.F. Elshorbany, J. Kleffmann, R. Kurtenbach, M. Rubio, E. Lissi, G. Villena, E. Gramsch, A.R. Rickard, M.J. Pilling, P. Wiesen, Summertime photochemical ozone formation in Santiago, Chile, Atmos. Environ., 43 (2009) 6398-6407.

[91] W.O. Milligan, A Review of the Application of X-Ray and Electron Diffraction Methods to Contact Catalysis, Phys Rev, 67 (1945) 197-197.

[92] M.A. Bollinger, M.A. Vannice, A kinetic and DRIFTS study of low-temperature carbon monoxide oxidation over Au-TiO2 catalysts, Appl Catal B-Environ, 8 (1996) 417-443.

[93] D.M. Byler, H. Susi, Examination of the Secondary Structure of Proteins by Deconvolved Ftir Spectra, Biopolymers, 25 (1986) 469-487.

[94] G.J. Millar, M.L. Nelson, P.J.R. Uwins, In situ imaging of catalytic etching on silver during methanol oxidation conditions by environmental scanning electron microscopy, J Catal, 169 (1997) 143-156.

[95] M. Vrinat, L. Demourgues, Study of Unsupported Sulfided Co-Mo Catalysts - Scanning Electron-Microscopy and Catalytic Activity in Hydrodesulfurization, Cr Acad Sci Ii, 293 (1981) 1045-1048.

[96] M.J. Gieselmann, M.A. Anderson, M.D. Moosemiller, C.G. Hill, Physicochemical Properties of Supported and Unsupported Gamma-Al2o3 and Tio2 Ceramic Membranes, Separ Sci Technol, 23 (1988) 1695-1714.

[97] A. Bianconi, Surface X-Ray Absorption-Spectroscopy - Surface Exafs and Surface Xanes, Appl Surf Sci, 6 (1980) 392-418.

[98] L. Que, Physical methods in bioinorganic chemistry : spectroscopy and magnetism, University Science Books, Sausalito, Calif., 2000.

[99] M. Bausach Mercader, Reactivity of acid gas pollutants with Ca(OH)2 at low temperature in the presence of water vapour, in: F. Cunill Garcia, F. Izquierdo Torres (Eds.), Universitat de Barcelona. Departament d'Enginyeria Química i Metal·lúrgia, 2005.

[100] G.Q. Chen, J.H. Gao, J.M. Gao, Q.A. Du, X.L. Fu, Y.J. Yin, Y.K. Qin, Simultaneous Removal of SO2 and NOx by Calcium Hydroxide at Low Temperature: Effect of SO2 Absorption on NO2 Removal, Industrial & Engineering Chemistry Research, 49 (2010) 12140-12147.

[101] Y.C. Du, Q. Meng, R.Q. Hou, J. Yan, H.X. Dai, T. Zhang, Fabrication of nano-sized Ca(OH)(2) with excellent adsorption ability for N2O4, Particuology, 10 (2012) 737-743.

[102] J.H. Gao, G.Q. Chen, J.X. Liu, X.L. Fu, J.M. Gao, Q.A. Du, Y.K. Qin, Simultaneous Removal of SO2 and NOx by Calcium Hydroxide at Low Temperature: Evolution of the Absorbent Surface Structure, Energy & Fuels, 24 (2010) 5454-5463.

[103] R. Hill, K. Daugherty, The interaction of calcium nitrate and a Class C fly ash during hydration, Cement and Concrete Research, 26 (1996) 1131-1143.

[104] R. Kumar, B. Bhattacharjee, Porosity, pore size distribution and in situ strength of concrete, Cement and Concrete Research, 33 (2003) 155-164.

[105] F. Vodak, K. Trtik, O. Kapickova, S. Hoskova, P. Demo, The effect of temperature on strength-porosity relationship for concrete, Construction and Building Materials, 18 (2004) 529-534.

[106] B. Freedman, Environmental ecology: the ecological effects of pollution, disturbance, and other stresses, Academic Press, 1995.

[107] A. Rabl, J.V. Spadaro, Public health impact of air pollution and implications for the energy system, Annu Rev Energ Env, 25 (2000) 601-627.

[108] R. Álvarez-Rodríguez, C. Clemente-Jul, Hot gas desulphurisation with dolomite sorbent in coal gasification, Fuel, 87 (2008) 3513-3521.

[109] G.T. Amrhein, S.J. Vecci, J.M. Rackley, Furnace ammonia and limestone injection with dry scrubbing for improved simultaneous SOX and NOX removal, in, Google Patents, 1993.

[110] N. Gandhi, V. Mary Priyanka, D. Sirisha, Controlling SO2 by Using Low Cost Adsorbents, Environmental Research, Engineering and Management, 62 (2012) 53-56.

[111] J.S. Buchanan, M.F. Mathias, J.F. Sodomin III, G.J. Teitman, Removing SOx, NOX and CO from flue gases, in, Google Patents, 1996.

[112] P. Chu, G.T. Rochelle, Removal of SO2 and NOx from stack gas by reaction with calcium hydroxide solids, JAPCA, 39 (1989) 175-179.

[113] S.B. Ghorishi, C.F. Singer, W.S. Jozewicz, C.B. Sedman, R.K. Srivastava, Simultaneous control of Hg0, SO2, and NOx by novel oxidized calcium-based sorbents, Journal of the Air & Waste Management Association, 52 (2002) 273-278.

[114] J.H. Gao, G.Q. Chen, X.L. Fu, Y.J. Yin, S.H. Wu, Y.K. Qin, Enhancement mechanism of SO2 removal with calcium hydroxide in the presence of NO2, Korean J Chem Eng, 29 (2012) 263-269.

[115] K.T. Lee, S. Bhatia, A.R. Mohamed, Removal of sulfur dioxide using absorbent synthesized from coal fly ash: Role of oxygen and nitrogen oxide in the desulfurization reaction, Chem Eng Sci, 60 (2005) 3419-3423.

[116] A. Vairavamurthy, B. Manowitz, G.W. Luther, Y. Jeon, Oxidation-State of Sulfur in Thiosulfate and Implications for Anaerobic Energy-Metabolism, Geochim Cosmochim Ac, 57 (1993) 1619-1623.

[117] M.J. Morra, S.E. Fendorf, P.D. Brown, Speciation of sulfur in humic and fulvic acids using X-ray absorption near-edge structure (XANES) spectroscopy, Geochim Cosmochim Ac, 61 (1997) 683-688.

[118] K. Xia, F. Weesner, W.F. Bleam, P.R. Bloom, U.L. Skyllberg, P.A. Helmke, XANES studies of oxidation states of sulfur in aquatic and soil humic substances, Soil Sci Soc Am J, 62 (1998) 1240-1246.

[119] G. Sarret, J. Connan, M. Kasrai, G.M. Bancroft, A. Charrie-Duhaut, S. Lemoine, P. Adam, P. Albrecht, L. Eybert-Berard, Chemical forms of sulfur in geological and archeological asphaltenes from Middle East, France, and Spain determined by sulfur K- and L-edge X-ray absorption near-edge structure spectroscopy, Geochim Cosmochim Ac, 63 (1999) 3767-3779.

[120] M.D. Jackson, S.R. Chae, S.R. Mulcahy, C. Meral, R. Taylor, P.H. Li, A.H. Emwas, J. Moon, S. Yoon, G. Vola, H.R. Wenk, P.J.M. Monteiro, Unlocking the secrets of Al-tobermorite in Roman seawater concrete, Am Mineral, 98 (2013) 1669-1687.

[121] M.D. Jackson, J. Moon, E. Gotti, R. Taylor, S.R. Chae, M. Kunz, A.H. Emwas, C. Meral, P. Guttmann, P. Levitz, H.R. Wenk, P.J.M. Monteiro, Material and Elastic Properties of Al-Tobermorite in Ancient Roman Seawater Concrete, J Am Ceram Soc, 96 (2013) 2598-2606.

[122] S.R. Chae, J. Moon, S. Yoon, S. Bae, P. Levitz, R. Winarski, P.J.M. Monteiro, Advanced Nanoscale Characterization of Cement Based Materials Using X-Ray Synchrotron Radiation: A Review, Int J Concr Struct M, 7 (2013) 95-110.

[123] M.L. Gorbaty, G.N. George, S.R. Kelemen, Direct Determination and Quantification of Sulfur Forms in Heavy Petroleum and Coals .2. The Sulfur-K Edge X-Ray Absorption-Spectroscopy Approach, Fuel, 69 (1990) 945-949.

[124] F. Farges, H. Keppler, A.M. Flank, P. Lagarde, Sulfur K-edge XANES study of S sorbed onto volcanic ashes, J Phys Conf Ser, 190 (2009).

[125] T.P. Da Silva, M.O. Figueiredo, More about the energy intelligent behaviour of secondary iron sulphates in AMD, Geochim Cosmochim Ac, 72 (2008) A736-A736.

[126] L. SIDNEY, S. SRINIVASA, Sea water demineralization by means of an osmotic membrane, 1963.

[127] H. Strathmann, K. Kock, P. Amar, R. Baker, The formation mechanism of asymmetric membranes, Desalination, 16 (1975) 179-203.

[128] H. Lonsdale, The growth of membrane technology, J Membrane Sci, 10 (1982) 81-181.

[129] F. Meng, S.-R. Chae, A. Drews, M. Kraume, H.-S. Shin, F. Yang, Recent advances in membrane bioreactors (MBRs): membrane fouling and membrane material, Water research, 43 (2009) 1489-1512.

[130] A. Basile, Advances in membrane technologies for water treatment, Elsevier, Boston, MA, 2015.

[131] S. Al-Obaidani, E. Curcio, F. Macedonio, G. Di Profio, H. Al-Hinai, E. Drioli, Potential of membrane distillation in seawater desalination: thermal efficiency, sensitivity study and cost estimation, J Membrane Sci, 323 (2008) 85-98.

[132] M. Cheryan, M. Cheryan, Ultrafiltration and microfiltration handbook, Technomic Pub. Co., Lancaster, Pa., 1998.

[133] G. Saracco, V. Specchia, Catalytic inorganic-membrane reactors: present experience and future opportunities, Catalysis Reviews—Science and Engineering, 36 (1994) 305-384.

[134] H. Strathmann, L. Giorno, E. Drioli, Introduction to membrane science and technology.

[135] J. Mallevialle, P.E. Odendaal, M.R. Wiesner, Water treatment membrane processes, American Water Works Association, 1996.

[136] R.W. Baker, Membrane technology and applications, 3rd ed., John Wiley & Sons, Chichester, West Sussex ; Hoboken, 2012.

[137] R.D. Noble, S.A. Stern, Membrane separations technology: principles and applications, Elsevier, 1995.

[138] A.I. Schäfer, A.G. Fane, T.D. Waite, Nanofiltration: principles and applications, Elsevier, 2005.

[139] Nanotechnology in Biology and Medicine: Methods, Devices, and Applications, Nanotechnology in Biology and Medicine: Methods, Devices, and Applications, (2007) 1-746.

[140] P.Y. Apel, I.V. Blonskaya, S.N. Dmitriev, O.L. Orelovitch, B. Sartowska, Structure of polycarbonate track-etch membranes: Origin of the "paradoxical" pore shape, J Membrane Sci, 282 (2006) 393-400.

[141] R. Hughes, Industrial membrane separation technology, Springer Science & Business Media, 1996.

[142] R. Steiner, Microfiltration and Ultrafiltration-Principles and Applications. LJ ZEMAN, AL ZYDNEY Marcel Dekker, New York, 1996, 648 Seiten, Zahlr. Abb. u. tab., geb., $185,-, ISBN 0-8247-9735-3, Chemie Ingenieur Technik, 69 (1997) 1479-1479.

[143] B.S. Lalia, V. Kochkodan, R. Hashaikeh, N. Hilal, A review on membrane fabrication: Structure, properties and performance relationship, Desalination, 326 (2013) 77-95.

[144] K. Li, Ceramic membranes for separation and reaction, John Wiley, Chichester, England ; Hoboken, NJ, 2007.

[145] A. Julbe, D. Farrusseng, C. Guizard, Porous ceramic membranes for catalytic reactors - overview and new ideas, J Membrane Sci, 181 (2001) 3-20.

[146] J. Coronas, J. Santamaria, Catalytic reactors based on porous ceramic membranes, Catalysis Today, 51 (1999) 377-389.

[147] D.T. Bray, D.H. Hopkins, Spiral wound membrane, in, Google Patents, 1989.

[148] V.M. Gryaznov, O.S. Serebryannikova, Y.M. Serov, M.M. Ermilova, A.N. Karavanov, A.P. Mischenko, N.V. Orekhova, Preparation and Catalysis over Palladium Composite Membranes, Appl Catal a-Gen, 96 (1993) 15-23.

[149] J. Shu, B.P.A. Grandjean, A. Vanneste, S. Kaliaguine, Catalytic Palladium-Based Membrane Reactors - a Review, Can J Chem Eng, 69 (1991) 1036-1060.

[150] S. Ilias, R. Govind, Development of high temperature membranes for membrane reactor: an overview, in: AIChE Symp. Ser, 1989, pp. 18.

[151] V. Jayaraman, Y.S. Lin, M. Pakala, R.Y. Lin, Fabrication of Ultrathin Metallic Membranes on Ceramic Supports by Sputter-Deposition, J Membrane Sci, 99 (1995) 89-100.

[152] U. Balachandran, J.T. Dusek, M.S. Kleefisch, T.P. Kobylinski, Functionally gradient material for membrane reactors to convert methane gas into value-added products, in, Google Patents, 1996.

[153] E. Subbarao, Solid electrolytes and their applications, Springer Science & Business Media, 2012.

[154] B. Carl, Preparation of hydrous metal oxide membranes and acid salts thereof, in, Google Patents, 1969.

[155] E.A. Hazbun, Ceramic membrane for hydrocarbon conversion, in, Google Patents, 1988.

[156] A.F.M. Leenaars, K. Keizer, A.J. Burggraaf, Structure, Permeability, and Separation Characteristics of Porous Alumina Membranes, Acs Sym Ser, 281 (1985) 57-68.

[157] A.F.M. Leenaars, A.J. Burggraaf, The Preparation and Characterization of Alumina Membranes with Ultra-Fine Pores .4. Ultrafiltration and Hyperfiltration Experiments, J Membrane Sci, 24 (1985) 261-270.

[158] A.F.M. Leenaars, A.J. Burggraaf, The Preparation and Characterization of Alumina Membranes with Ultra-Fine Pores .3. The Permeability for Pure Liquids, J Membrane Sci, 24 (1985) 245-260.

[159] M.D. Moosemiller, C.G. Hill, M.A. Anderson, Physicochemical Properties of Supported Gamma-Al2o3 and Tio2 Ceramic Membranes, Separ Sci Technol, 24 (1989) 641-657.

[160] M.A. Anderson, M.J. Gieselmann, Q.Y. Xu, Titania and Alumina Ceramic Membranes, J Membrane Sci, 39 (1988) 243-258.

[161] L.C. Klein, D. Gallagher, Pore Structures of Sol-Gel Silica Membranes, J Membrane Sci, 39 (1988) 213-220.

[162] A. Larbot, A. Julbe, C. Guizard, L. Cot, Silica Membranes by the Sol-Gel Process, J Membrane Sci, 44 (1989) 289-303.

[163] R.M. de Vos, H. Verweij, Improved performance of silica membranes for gas separation, J Membrane Sci, 143 (1998) 37-51.

[164] W.J. Elferink, B.N. Nair, R.M. DeVos, K. Keizer, H. Verweij, Sol-gel synthesis and characterization of microporous silica membranes .2. Tailor-making porosity, Journal of Colloid and Interface Science, 180 (1996) 127-134.

[165] A.J. Burggraaf, L. Cot, Fundamentals of inorganic membrane science and technology, Elsevier, Amsterdam ; New York, 1996.

[166] Ceramic Membrane Market by Material (Titania, Alumina, Zirconium Oxide), by Application (Water and Wastewater Technology, Pharmaceuticals, Food and Beverage, Chemical Processing, Biotechnology), by Technology (Ultrafiltration, Microfiltration, Nanofiltration), by Region - Global Trends & Forecasts to 2020, (2015).

[167] H.P. Hsieh, Inorganic Membranes for Separation and Reaction, Elsevier Sci. B.V., (1996).

[168] R. Mallada, M. Menendez, VOLUME 13 MEMBRANE SCIENCE AND TECHNOLOGY SERIES Inorganic Membranes: Synthesis, Characterization and Applications PREFACE, Membr Sci Tech Ser, 13 (2008) Xiii-Xv.

[169] A.S. Kim, E.M.V. Hoek, Cake structure in dead-end membrane filtration: Monte Carlo simulations, Environ Eng Sci, 19 (2002) 373-386.

[170] A. Grenier, M. Meireles, P. Aimar, P. Carvin, Analysing flux decline in dead-end filtration, Chem Eng Res Des, 86 (2008) 1281-1293.

[171] S. K., Profile of the International Membrane Industry - Market Prospects to 2008 3rd Ed, Elsevier Ltd., (2003) 50-51.

[172] R.B. Heimann, Plasma-Spray Coating – Principles and applications, VCH, (1996).

[173] P. Bengtsson, T. Johannesson, Characterization of Microstructural Defects in Plasma-Sprayed Thermal Barrier Coatings, J Therm Spray Techn, 4 (1995) 245-251.

[174] L. Pawłowski, The science and engineering of thermal spray coatings, 2nd ed., Wiley, Chichester, England ; Hoboken, NJ, 2008.

[175] R. Hui, Z.W. Wang, O. Kesler, L. Rose, J. Jankovic, S. Yick, R. Maric, D. Ghosh, Thermal plasma spraying for SOFCs: Applications, potential advantages, and challenges, J Power Sources, 170 (2007) 308-323.

[176] A.A. Kulkarni, S. Sampath, A. Goland, H. Herman, A.J. Allen, J. Ilavsky, W.Q. Gong, S. Gopalan, Plasma spray coatings for producing next-generation supported membranes, Top Catal, 32 (2005) 241-249.

[177] K.L. Tung, C.C. Hsiung, T.C. Ling, K.S. Chang, T.T. Wu, Y.L. Li, C.H. Kang, W.Y. Chen, D. Nanda, Preparation and characterization of aluminum oxide cermet microfiltration membrane using atmospheric plasma spraying, Desalination, 245 (2009) 408-421.

[178] Y.F. Lin, K.L. Tung, Y.S. Tzeng, J.H. Chen, K.S. Chang, Rapid atmospheric plasma spray coating preparation and photocatalytic activity of macroporous titania nanocrystalline membranes, J Membrane Sci, 389 (2012) 83-90.

[179] S.S. Madaeni, M.E. Aalami-Aleagha, P. Daraei, Preparation and characterization of metallic membrane using wire arc spraying, J Membrane Sci, 320 (2008) 541-548.

[180] R.A. Miller, Thermal barrier coatings for aircraft engines: History and directions, J Therm Spray Techn, 6 (1997) 35-42.

[181] D.R. Clarke, C.G. Levi, Materials design for the next generation thermal barrier coatings, Annu Rev Mater Res, 33 (2003) 383-417.

[182] M.J. Stiger, N.M. Yanar, M.G. Topping, F.S. Pettit, G.H. Meier, Thermal barrier coatings for the 21st century, Z Metallkd, 90 (1999) 1069-1078.

[183] X.Q. Cao, R. Vassen, D. Stoever, Ceramic materials for thermal barrier coatings, J Eur Ceram Soc, 24 (2004) 1-10.

[184] W.F. Maier, I.C. Tilgner, M. Wiedorn, H.C. Ko, A. Ziehfreund, R. Sell, Microporous Inorganic Membranes - Preparation, Characterization and Separation Properties, Adv Mater, 5 (1993) 730-735.

[185] Y.S. Lin, I. Kumakiri, B.N. Nair, H. Alsyouri, Microporous inorganic membranes, Separ Purif Method, 31 (2002) 229-379.

[186] Y.S. Lin, Microporous and dense inorganic membranes: current status and prospective, Sep Purif Technol, 25 (2001) 39-55.

[187] N. Otsu, A Threshold Selection Method from Gray-Level Histograms, Systems, Man and Cybernetics, IEEE Transactions on, 9 (1979) 62-66.

[188] P. Chraska, J. Dubsky, K. Neufuss, J. Pisacka, Alumina-base plasma-sprayed materials .1. Phase stability of alumina and alumina-chromia, J Therm Spray Techn, 6 (1997) 320-326.

[189] M.I.F. Macedo, C.A. Bertran, C.C. Osawa, Kinetics of the gamma ->alpha-alumina phase transformation by quantitative X-ray diffraction, J Mater Sci, 42 (2007) 2830-2836.

[190] L.C. Erickson, H.M. Hawthorne, T. Troczynski, Correlations between microstructural parameters, micromechanical properties and wear resistance of plasma sprayed ceramic coatings, Wear, 250 (2001) 569-575.

[191] J.R. Mawdsley, Y.J. Su, K.T. Faber, T.F. Bernecki, Optimization of small-particle plasma-sprayed alumina coatings using designed experiments, Mat Sci Eng a-Struct, 308 (2001) 189-199.

[192] K. Ramachandran, V. Selvarajan, P.V. Ananthapadmanabhan, K.P. Sreekumar, Microstructure, adhesion, microhardness, abrasive wear resistance and electrical resistivity of the plasma sprayed alumina and alumina-titania coatings, Thin Solid Films, 315 (1998) 144-152.

[193] P. Saravanan, V. Selvarajan, D.S. Rao, S.V. Joshi, G. Sundararajan, Influence of process variables on the quality of detonation gun sprayed alumina coatings, Surf Coat Tech, 123 (2000) 44-54.

[194] S. Guessasma, G. Montavon, C. Coddet, Modeling of the APS plasma spray process using artificial neural networks: basis, requirements and an example, Comp Mater Sci, 29 (2004) 315-333.

[195] H. Herman, S. Sampath, R. McCune, Thermal spray: Current status and future trends, Mrs Bull, 25 (2000) 17-25.

[196] R. Westergard, L.C. Erickson, N. Axen, H.M. Hawthorne, S. Hogmark, The erosion and abrasion characteristics of alumina coatings plasma sprayed under different spraying conditions, Tribol Int, 31 (1998) 271-279.

[197] V.S. Ramachandran, J.J. Beaudoin, Handbook of analytic techniques in concrete science and technology, 1st edition ed., Noyes Publications, Park Ridge, New Jersey, USA, 2001.

[198] P. Fauchais, M. Fukumoto, A. Vardelle, M. Vardelle, Knowledge concerning splat formation: An invited review, J Therm Spray Techn, 13 (2004) 337-360.

[199] Asm Handbook, Volume 5a: Thermal Spray Technology, Adv Mater Process, 173 (2015) 40-40.

[200] H. Chen, S.W. Lee, H. Du, C.X. Ding, C.H. Choi, Influence of feedstock and spraying parameters on the depositing efficiency and microhardness of plasma-sprayed zirconia coatings, Mater Lett, 58 (2004) 1241-1245.

[201] P. Cheang, K.A. Khor, Thermal Spraying of Hydroxyapatite (Ha) Coatings - Effects of Powder Feedstock, J Mater Process Tech, 48 (1995) 429-436.

[202] P. Fauchais, G. Montavon, G. Bertrand, From Powders to Thermally Sprayed Coatings, J Therm Spray Techn, 19 (2010) 56-80.

[203] S. Sampath, X.Y. Jiang, J. Matejicek, L. Prchlik, A. Kulkarni, A. Vaidya, Role of thermal spray processing method on the microstructure, residual stress and properties of coatings: an integrated study for Ni-5 wt.%Al bond coats, Mat Sci Eng a-Struct, 364 (2004) 216-231.

[204] L.L. Shaw, D. Goberman, R.M. Ren, M. Gell, S. Jiang, Y. Wang, T.D. Xiao, P.R. Strutt, The dependency of microstructure and properties of nanostructured coatings on plasma spray conditions, Surf Coat Tech, 130 (2000) 1-8.

[205] M.H. Li, P.D. Christofides, Modeling and analysis of HVOF thermal spray process accounting for powder size distribution, Chem Eng Sci, 58 (2003) 849-857.

[206] M. Vardelle, A. Vardelle, A.C. Leger, P. Fauchais, D. Gobin, Influence of Particle Parameters at Impact on Splat Formation and Solidification in Plasma Spraying Processes, J Therm Spray Techn, 4 (1995) 50-58.

[207] P. Fauchais, Understanding plasma spraying, J Phys D Appl Phys, 37 (2004) R86-R108.

[208] M.E. Aalami-Aleagha, S.S. Madaeni, P. Daraei, A New Application of Thermal Spray in Preparation of Metallic Membrane for Concentration of Glucose Solution, J Therm Spray Techn, 18 (2009) 519-524.

[209] O. Sarikaya, Effect of some parameters on microstructure and hardness of alumina coatings prepared by the air plasma spraying process, Surf Coat Tech, 190 (2005) 388-393.

[210] C.J. Li, A. Ohmori, Relationships between the microstructure and properties of thermally sprayed deposits (vol 11, pg 370, 2002), J Therm Spray Techn, 12 (2003) 6-6.